RF SENSING AND PROCESSING METHODS FOR NONINVASIVE HEALTH MONITORING

A Dissertation

presented to

the Faculty of the Graduate School

at the University of Missouri-Columbia

In Partial Fulfillment

of the Requirements for the Degree

Doctor of Philosophy

---

by

RESULI NUERZATI

Dr. Marjorie Skubic, Dissertation Supervisor

DECEMBER 2021

The undersigned, appointed by the dean of the Graduate School, have examined the Dissertation entitled

RF SENSING AND PROCESSING METHODS FOR NONINVASIVE HEALTH MONITORING

presented by Resuli Nuerzati,

a candidate for the degree of Doctor of Philosophy, and hereby certify that, in their opinion, it is worthy of acceptance.

Professor Marjorie Skubic

Professor Scott Kovaleski

Professor Justin Legarsky

Professor Laurel Despins

Dedicated with love and appreciation to

my parents and everyone who supported me in this journey with their ideas.

THANK YOU!

ACKNOWLEDGMENTS

I would like to thank my advisor Prof. Skubic for her tremendous guidance and astonishing knowledge. I consider myself to be extremely fortunate to be a part of the Eldercare and Rehabilitation Technology Lab at University of Missouri-Columbia. Prof. Skubic not only shared her unique perspective on the research with me, but also gave me a direction to be a good researcher, to solve the difficult problem in the world, to help the people who need help, and to make the world a better place where everyone can get the help, the support and the hope.

I also would like to thank Prof. Kovaleski for his valuable suggestions, his time and countless insights on Learning Room Structure and Activity Patterns Using RF Sensing for In-Home Monitoring of Older Adults research project. I really appreciated all my committee members, Noah Marchal, Dan Fischbach, RuHan Yi whose help and suggestions encouraged me in going further. Thank you to all my friends and colleagues at Mizzou.

Finally, I am grateful to my parents. Without their support, I couldn't finish my PhD.

Contents

List of Symbols

X_{TX}	Transmitted Signal
X_{RX}	Received Signal
X_{IF}	Intermediate Frequency Signal
c	Speed of Light
S	Slope of chirp
B	Bandwidth of RF
T_c	Chirp Duration Time
T_f	Frame Time
f_{start}	Carrier Frequency
f_c	Carrier Frequency
f_b	Beat frequency
$\mathbf{F_s}$	Sample Frequency
R_{max}	Maximum Range which can be detected by RF
R_{target}	Target Distance

$\boldsymbol{r}$	Range Resolution of RF
$\boldsymbol{v_{target}}$	Target Velocity
$\boldsymbol{v_{res}}$	Velocity Resolution of RF
$\boldsymbol{\varphi(t)}$	Phase
$\boldsymbol{\theta_{res}}$	Angle Resolution of RF
$\boldsymbol{N_{ant}}$	Number of Antennas
$\boldsymbol{N_{chirp}}$	Number of chirp in per frame
$\boldsymbol{\lambda}$	Wave Length
$\boldsymbol{\theta}$	Angle of Arrival
$\boldsymbol{z}$	Coherently Combined Signal
$\odot$	Hadamard Product

List of Acronyms

The following acronyms are used through this dissertation:

AOA	Angle of Arrival
A/D	Analog – to - Digital
ADC	Analog – to – Digital Circuit
bmp	Breaths Per Minute
CW	Continuous Wave
CFAR	Constant False Alarm Rate
dB	Decibel
DC	Direct Current
DFT	Discrete Fourier Transform
DSP	Digital Signal Processing
FFT	Fast Fourier Transform
FM	Frequency Modulation
FMCW	Frequency Modulation Continuous Wave
FIR	Finite Impulse Response

FCM	Fuzzy C-Mean
IF	Intermediate Frequency
I	In - Phase
IFFT	Inverse Fast Fourier Transform
LNA	Low Noise Amplifier
MUSIC	The Multiple Signal Classification
Q	Quadrature
RF	Radio Frequency
RADAR	Radio Detection and Ranging
SAR	Synthetic Aperture Radar
SNR	Signal – to – Noise Ratio
VCO	Voltage Control Oscillator

List of Figures

List of Tables

Abstract

Vulnerable populations include groups of people with a higher risk of poor health as a result of the limitations due to illness or disability. The health issues of vulnerable populations include three categories: physical, psychological, and social. The people with physical issues include high-risk mothers and infants, older adults and others with chronic illnesses and people with disabilities. The psychological issues of vulnerable populations include chronic mental conditions, such as bipolar disorder, major depression, and hyperactivity disorder, as well as substance abuse and those who are suicidal. The social issues in vulnerable populations include those living in abusive families, the homeless, etc. This dissertation concentrates on methods for helping two groups of vulnerable populations, namely, frail older adults and psychiatric hospital patients, to monitor their activity level, respiration rate, sleeping quality, and restless time in bed.

In the first part of our work, we investigate a contactless monitoring system for psychiatric patients in a naturalistic hospital setting that can track their motion in bed, estimate the breathing rate of patients during their peaceful sleeping periods, and can be used to estimate a patient's restless time and sleep quality. Specifically, the contactless monitoring system uses a Vayyar Radar system with a carrier frequency of 6.014 GHz to capture all reflections by the FMCW (frequency modulation continuous waveform) signal. The Vayyar Radar system has been installed in a Psychiatric Center to capture 12 nights with over 135 hours of data from 7 patients. A depth camera and a thermal camera have also been installed and are used as the ground truth. The goal is to classify in bed and out of bed classes, quantify restlessness in bed, and determine the breathing rate while patients are lying in bed.

We have simulated the psychiatric hospital set-up in the lab, where a respiration belt is used for ground truth, and tested the system with body postures of patients observed in the psychiatric

hospital. We estimated respiration rate with different sleep postures, with the aim of investigating a contactless monitoring system for psychiatric patients in the hospital that can estimate the breathing rate of patients during typical sleeping postures, and find the torso area when the patients use other postures, such as reading books in bed or reversing the body on the bed.

In the second part of our work, we investigate two methods for learning the room structure via radio wave reflections for longitudinal health monitoring of older adults in a naturalistic home setting. The goal is to use these data as part of a monitoring system that can be easily installed in a home with minimal configuration, for the purpose of detecting very early signs of illness and functional decline. Two studies are conducted using RF (radio frequency) sensing. The first method learns the structure from the RF clutter patterns and uses the beat frequency of the maximum peak in each chirp to calculate the wall position. The second method learns the room structure from active movement patterns and uses the open space between the clusters of active movement patterns to estimate the possible wall locations. Comparing the two results from these methods provides a more robust wall location. In addition, a background filter is designed based on the wall position, and the activity level of people in different rooms is estimated using a fuzzy rule system applied to the RF motion data.

I. Introduction

1.1 Contactless Monitoring for Psychiatric (Psych) Center Patients

1.1.1 Motivation

Millions of people in the U.S are affected by mental illness each year. For instance, 51.5 million adults in the U.S experienced mental illness in 2019, 13.1million of U.S adults experienced serious illness in 2019, and those serious illness patients need 24-hour residential treatment [1]. With this situation, there has been considerable interest in monitoring psychiatric patients' status in the hospital, including respiration rate, sleeping quality, and restless time during treatment periods.

In the Psych Center environment, stringent requirements are in place to protect the patients' privacy and safety, to ensure that they are not harming themselves or others. Safety checks are conducted by the staff every 15 minutes, and each patient's status is manually recorded in a log, which includes the location of the patient as well as breathing and sleeping status. At night, staff will often enter the patient's room with a flashlight to perform these checks. Cameras are not permitted due to privacy requirements. The safety requirements also prevent the use of wearable sensors and other accessible sensors. For instance, a bed sensor positioned under the mattress is problematic if the hardware or wires are accessible to the patient. For patient safety, furniture in the Psych Center rooms are, in fact, bolted to the floor and cannot be moved. Thus, a contactless monitoring system that is not accessible to patients is essential in this setting. Our motivations are as follows:

1) Detect life signs in a naturalistic hospital setting of patients

2) Track movement patterns in bed of patient

3) Estimate patients' breathing rate during the sleeping period

4) Estimate restless time and sleeping quality

1.1.2 My Contribution

We investigate a contactless monitoring system for Psych Center patients in a naturalistic hospital setting that can track their motion in bed, estimate the breathing rate of patients during their peaceful sleeping periods, and can be used to estimate a patient's restless time and sleep quality. Specifically, the contactless monitoring system uses a Vayyar Radar system with a carrier frequency of 6.014 GHz to capture all reflections by the FMCW (frequency modulation continuous waveform) signal. The Vayyar Radar system has been installed in the Psych Center to capture 12 nights with over 135 hours of data from 7 patients. A depth camera and a thermal camera have also been installed and are used as the ground truth. The goal is to classify in bed and out of bed classes, quantify restlessness in bed, and determine the breathing rate while patients are lying in bed.

We explore different sleeping postures in a lab setting. In our current IRB-approved study in a Psychiatric Center, sensors were embedded into the area above the ceiling and mounted over the bed at a height of 2.3 m. We have simulated this set-up in the lab, where a respiration belt is used for ground truth, and tested the system with body postures of patients observed in the psychiatric hospital. We present work on respiration rate estimation with different sleep postures, with the aim of investigating a contactless monitoring system for psychiatric patients in the hospital that can estimate the breathing rate of patients during typical sleeping postures, and find the torso area when the patients use other postures, such as reading books in bed or reversing the body on the bed. Data

were collected from twelve healthy younger adults and two older adults in a controlled lab setting;

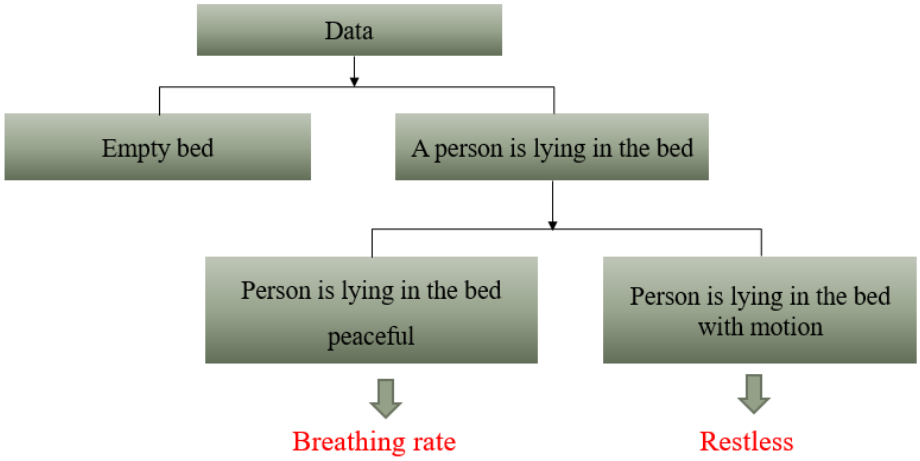

Fig.1 The flow diagram for the Psych Center data processing

1.2 Learning Room Structure and Activity Patterns Using RF Sensing for In-Home Monitoring of Older Adults

1.2.1 Motivation

In recent years, the number of older adults has increased substantially in the world. The global population aged 60 years or over numbered 962 million in 2017, more than twice as large as in 1980 [2]. The number of people aged 80 or over worldwide will increase more than threefold between 2017 and 2050, and adults rise from 137 million to 425 million. The number of older persons is expected to double again by 2050, when it is projected to reach nearly 2.1 billion [2]. With this demographic trend, there has been considerable interest in helping older adults to maintain their health and functionality as they age.

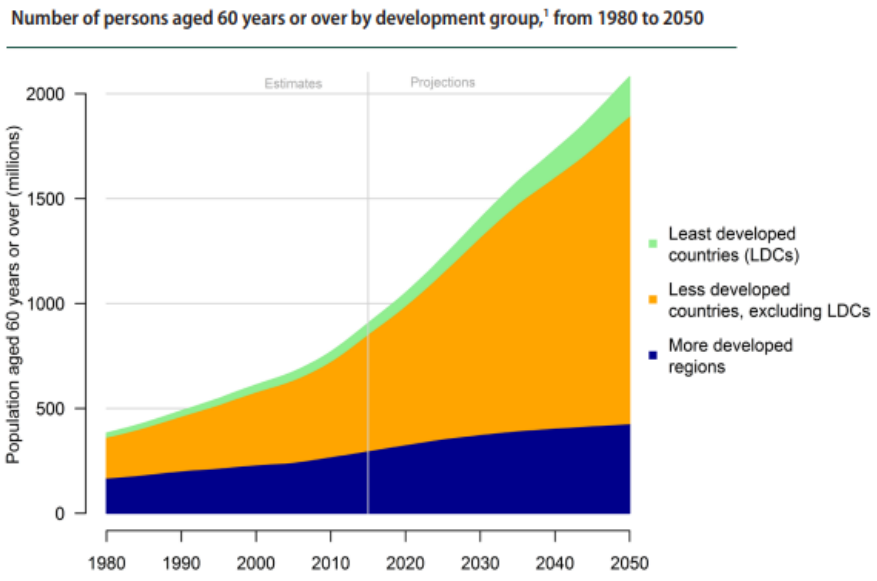

Fig.2 Number of persons aged 60 years or over by the development group from 1980 to 2050[2]

To support independent living for older adults, there has been much work using a variety of approaches. In our observations on monitoring older adults in the home, especially frail older adults, they are more willing to accept passive, non-wearable sensors mounted in the home, which do not require them to do anything special. PIR motion sensors are inexpensive and can easily be installed to get room-specific activity. However, current installation methods require manual configuration such that each address must be designated for a specific room. Also, batteries need to be replaced regularly for continued monitoring. We aim to address these limitations by exploring a different sensing method that would, ultimately, be a one-time set-up, in which someone hangs it on a wall and plugs it in. Our motivations are as follows:

1) Capture general movement patterns in home of older adults

2) Recognize pattern changes that relate to changing health

3) Support scalable deployments in real home settings

4) Support easy installation without requiring measurements including by consumers

5) Eliminate the need for replacing batteries

1.2.2 My Contribution

We present preliminary work on RF (radio frequency) sensing for longitudinal health monitoring of older adults in a naturalistic home setting, with the aim of detecting early changes in health status. Specifically, the RF sensor uses a frequency modulated continuous wave (FMCW) radar with center frequency 2.315 GHz to capture all reflections by radio signal, so older adults do not need to wear any sensor or do anything outside of their normal daily routines. Two methods are investigated in our work for learning the room structure in a naturalistic setting, which includes learning room structure via the RF clutter pattern and learning the room structure from active movement. The results from these two approaches are compared to get a more accurate wall position. Next, a background filter is designed based on the estimated wall position, which allows us to estimate the overall activity level in the different rooms. A system of fuzzy rules is then used to estimate activity density as part of the in-home behavior pattern.

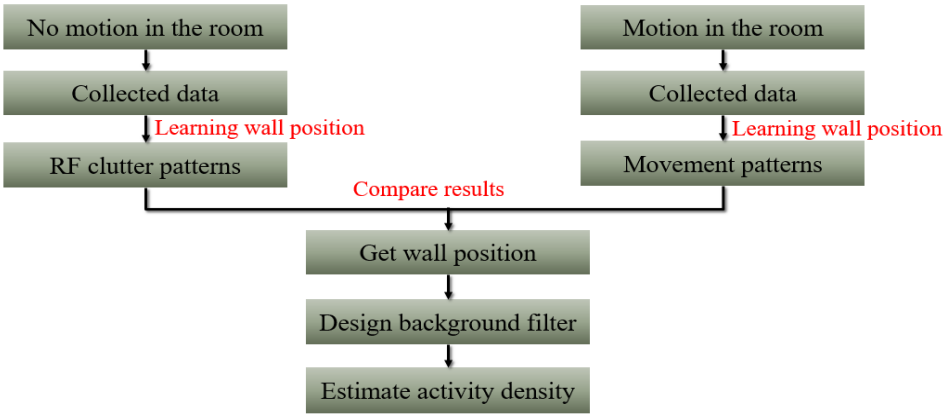

Fig.3 the flow diagram for the wall position estimation

1.3 Dissertation Organization

Chapter 2 provides an in-depth review of RF sensing, vital sign detection, learning room structure, and activity level estimation. It reviews the historical evolution of RF sensing, vital sign detection in different areas, such as in the lab setting, in the non-clinical environment, and in the clinical environment, different signal processing approaches, and in-home monitoring system for older adults.

Chapter 3 introduces all data sets in this dissertation: Psychiatric center data set (2019), Eldercare and Rehabilitation Technology Lab data set (2020), and Contactless Extraction of Heart and Respiratory Rate with Depth, Thermal and Radar Sensing Devices project (2018) data set.

Chapter 4 introduces the FMCW radar system in the Psychiatric center contactless monitoring system and analyzes its performance by the MATLAB simulation. Meanwhile, this chapter introduced the FMCW radar system of the Learning Room Structure and Activity Patterns Using RF Sensing for In-Home Monitoring of Older Adults project and analyzed its performance by MATLAB simulation.

Chapter 5 presents the RF signal processing, which is included in frame data processing, beamforming, angle of arrival, matched filter design, and target detection.

Chapter 6 presents the out of bed vs. in bed classification algorithm, which is included in data preprocessing, single patient's balanced data classification, and imbalanced data set classification.

Chapter 7 presents respiration rate estimation algorithms. We present work on respiration rate estimation with different sleep postures, with the aim of investigating a

contactless monitoring system for psychiatric patients in the hospital that can estimate the breathing rate of patients during typical sleeping postures and find the torso area when the patients use other postures, such as reading books in bed or reversing the body on the bed. This respiration rate estimation algorithm is applied to estimate the respiration rate of psych center patients. The restless time of psych center patients estimate by the restless time formula.

Chapter 8 presents a learning room structure and activity patterns project. We present preliminary work on RF (radio frequency) sensing for longitudinal health monitoring of older adults in a naturalistic home setting, with the aim of detecting early changes in health status. Two methods are investigated in our work for learning the room structure in a naturalistic setting, which includes learning room structure via the RF clutter pattern and learning the room structure from active movement. The results from these two approaches are compared to get a more accurate wall position. Next, a background filter is designed based on the estimated wall position, which allows us to estimate the overall activity level in the different rooms. A system of fuzzy rules is then used to estimate activity density as part of the in-home behavior pattern.

The conclusions are summarized in Chapter 9, and future work is discussed.

II. Background and Related Work

2.1 RF Sensing

The beginning of modern electromagnetic theory can be traced first to Hertz in 1886 who demonstrated reflection of radio waves, and in 1900 Tesla described a concept for electromagnetic detection and velocity measurement in an interview. In 1903 and 1904, the German engineer Hulsmeyer experimented with ship detection by radio wave reflection. In 1922, Guglielmo Marconi demonstrated the radio's ability of public broadcast. In the same year, Naval Research Laboratory (NRL) demonstrated ship detection and aircraft detection by radar. All of those substantial investigations led to a US patent for what would be called a continuous wave (CW) radar in 1934. The development of radar accelerated and spread in the middle and late 1930s. Most countries used radar for military applications including surveillance, navigation and weapon guidance for ground, sea, and air vehicles [3-5].

Radar is an electromagnetic system where the transmitting antenna emits electromagnetic radiation, the signal energy reradiated back by reflecting the target. The received antenna collects the returned signal. The received signal is processed by the digital signal processing part of the radar to extract target location, angular position and relative velocity. Radar is capable of sensing through the structure, darkness, haze, log, rain, and snow. Compared to other sensors, sensing through the environment is the most important attribute. Now radar enjoys an increasing range of application, including weather monitoring and prediction [6-7], traffic control [8-9], wind turbine design [10-11], soil surface level sensing [12], remote sensing [13-14] and clinical environments [15-16].

2.2 Contactless Monitoring for Psychiatric (Psych) Center Patients

In the Psych Center environment, stringent requirements are in place to protect the patients' privacy and safety, to ensure that they are not harming themselves or others, and to track each patient's status which includes the location of the patient as well as breathing and sleeping status. To minimize the risk of the patients' absences from the unit in the psychiatric center, there has been some work using radio frequency identification (RFID). The method of using an RFID-enabled solution monitored psychiatric patients from absconding, localized the patients in the unit, and generated an alert if the patients escaped from unit [17-18].

The vital signs such as respiration rates are important measurements of patients' status. In the clinical environment, the Respiration Inductance Plethysmography (RIP) strap and Electrical Impedance Tomography is used to monitor the respiration rate of patients, and those are accurate measurements for breathing. But RIP would cause considerable discomfort for requiring patients to wear a sensor during sleeping [19-20].

In non-clinical environments, a number of researchers have been investigating wearable sensors for monitoring respiration rate. Some wearable sensors use microphones that capture the patients' acoustic signal during breathing. The accelerometers embedded in wearable fitness trackers [21-22] have been used to estimate breathing rate by capturing mechanical movements of patient's chest expansion. The hydraulic bed sensors [23-25] have been used to monitor the respiration rate when the people are sleeping. The heath chair [26-27] has been used to monitor the respiration rate and heart rate when people were sitting on chairs.

To enable continuous and unobtrusive monitoring the respiration rate, there has been much work using wireless signals in lab environment settings. The contactless infant monitoring system [28] has been used to achieve motion detection and respiration monitoring by using white noise for sleeping infants in the life-like infant simulator environment. The ORiNOCO system [29] was developed with two wireless LAN PC cards, one as a transmitter and the other one as a receiver and is operated as 2.4 GHz microwave Doppler radar principle. The ORiNOCO system was used to obtain heart rate and respiration rate of the seating subject at the distance of 40cm. The Sleep Minder system [30] operates at 5.8 GHz pulsed-wave Doppler mode, and is placed facing the subject, in line with the chest at a distance of approximately 0.2 m and with an elevation of approximately 0.5 m from the edge of the bed, and facing towards the torso of the subject. The Sleep Minder has been used to measure respiration rate during a sleeping subject in a laboratory environment.

In order to reduce environmental factors, such as light, temperature, interference from other signals, and fading effect, the continuous wave (CW) radar has been used to monitor the vital signs in laboratory environments. In [31-33], the medical radar has been researched for remote monitoring of human cardiac and respiratory motion, which has transmitted a 0.5-18GHz continuous wave (CW) radio frequency measure heart rate of a person lying on his back with a bare chest and the radar antenna above the chest. In [34] the 2.4 GHz Doppler radar used to capture the abdomen's movement during breathing when the stationary subject was positioned 0.8m away from antennas where antennas were aligned to focus on the abdomen. The Fourier and wavelet transform approaches were used in extracting respiration rate.

Compared to CW radar, frequency modulated continuous wave (FMCW) radar can accurately measure the range and velocity of the target, since much work has used FMCW radar to monitor vital signs in laboratory settings, which operated at 24 GHz ,77GHz and 81 GHz facing the subject's chest area of the subject to capture chest movement caused by the breathing and heartbeat [35-36]. In [37-39], the FMCW radar has been used to monitor multiple users' vital signs simultaneously to separate the RF reflections arriving from different objects in laboratory settings.

To evaluate the capability of FMCW radar in estimating respiration rate in a natural home setting, WiBreath system was developed by the University of Washington, and used 2.4 GHz with single transmitter-receiver pair to capture the respiration rate at various line of sight and non-line of sight position in homes [40]. The DeepBreath system [41-42] was developed by MIT and monitors the respiration signals throughout night for people who share the same bed.

The theoretical signal processing analysis for FMCW radar has been presented in some papers [43-45]. The wavelet transform method was applied to separate the heart rate and respiration rate [46]. Adaptive cancellation of respiration harmonic was implemented for extracting heart rate signal [47]. The novel signal processing method was used to separate and recover respiration signals [48].

2.3 Learning Room Structure and Activity Patterns Using RF Sensing for In-Home Monitoring of Older Adults

To support independent living for older adults, there has been much work using a variety of approaches. For example, Honeywell developed the Independent LifeStyle Assistant (ILSA) system for passive monitoring (medication, mobility, sleep patterns, occupancy) [49]. Activities of Daily Living (ADL) have been captured by a variety of sensors including heat sensors, motion sensors, vibration sensors and electric current sensors [50]. Passive infrared (PIR) motion sensors have been used to capture activity in the home [51], [52]; motion density estimation based on motion sensors may provide indications of health change [53] - [55]. The combination of motion sensors, bed sensors, and door sensors has been used to detect cognitive changes [56]. Some monitoring systems have used a mixture model to analyze a person's behavioral patterns [57]. Walking gait in the home has also been investigated because of the link to both physical and cognitive health [58] - [62].

An alternative approach is to use wearable health monitoring devices. A number of researchers have been investigating wrist sensors for monitoring human rest/activity cycle [63]. Some of the wrist sensors use a model to measure the health condition of an individual [64]. In nursing homes, actigraphy sensors worn on the wrist have been used to monitor the circadian activity rhythm; also, daily maximum activity level may link to heart failure of a patient [65], [66]. An RFID-detecting glove has been used to recognize activities by analyzing proximity with objects [67]. While the wearable sensor has the advantage to collect data outside of the home, many seniors refuse to wear it because of discomfort, have difficulties charging the sensor, or forget to wear it. Thus, there are still challenges in using wearable sensors for continuous, long-term monitoring of older adults.

Additional research is also being performed on in-home monitoring systems based on Wi-Fi fingerprints. Researchers have been investigating the use of Wi-Fi fingerprints for localizing people. The advantage of this approach is that no additional hardware is needed, as the system just uses existing Wi-Fi signals, and people are localized according to the received signal strength indicator from the wireless access points. However, individuals are required to carry a smartphone with them for localization [68]-[71], and many older adults are unable or unwilling to use smartphones now.

To enable sensing through structure, a number of researchers have been investigating see-through-wall technology. In [72]-[73], the passive bistatic Wi-Fi radar has been attempting to detect people moving behind walls. In this system, the Wi-Fi access point (AP) was as the transmitter, and three nodes of multistatic netted radar operated at 2.4 GHz were as receivers. The wall reflection removed by quantitatively examines the difference between the signal of line sight node and the signal of the non-line sight node. The moving objects have been detected through a substantial multilayer wall structure which also contained an air gap.

In [74]-[77], the ultra-wide bandwidth (UWB) RF sensor with multiple GHz bandwidth used to localize and track the person behind the wall. In [78]-[79], the wall reflection was removed in the time domain by using a very short pulse, whereby the pulse reflected off the wall arrives earlier in time than that reflected off moving people behind the wall. In [80]-[81], the removing wall reflection was achieved in the frequency domain by using an analog filter. In this case, reflections off objects at different distances arrive with different frequencies, and the analog filter was designed based on the frequency of the wall. UWB has bigger bandwidth which gives higher resolution, the short wavelength with high signal-

noise ratio (SNR), and the higher resolution which is good for RF imaging processing. However, the cost of UWB is expensive.

Researchers have recognized the limitation of UWB and explored the less expensive narrowband RF system. Wi-Vi system [82] is a less expensive and simple RF system for localizing people's movement behind the wall. The system was constructed using an FMCW radar with three LP0965 directional antennas, two for the transmitting signal, and one for the receiving signal. Three USRP N210 software radios with SBX daughter boards were connected to the antennas. The Wi-Vi system employed at 2.4 GHz with 20MHz bandwidth which were close to the ISM Wi-Fi band, and the movement of people emulated an antenna array, which has been used to identify the moving direction with respect to the Wi-Vi system. The wall reflection was eliminated by subtracting the channel between the first transmit antenna and the receive antenna from the channel between the second transmit antenna and the receive antenna. The Wi-Vi can accurately track single person movement.

The Wi-Track system [83]-[84] is an advanced system of the Wi-Vi system and mounted on a foldable platform with ten WA5VJB directional antennas, five for transmit signal, and five for receiving signal. USEP2 with LFRX-LF daughterboard at the receive chain used to digitize signals. The wall reflection in Wi-Track was eliminated by subtracting the output of the time of flight (TOF) profile in a given sweep from the TOF profile of signal in the previous sweep due to the reflections of static objects maintained constant over time. The Wi-Track can localize multiple people and track 3D motion of an individual behind the wall.

III. Data Set

3.1 Psychiatric (Psych) Center Data Set (2019)

Most rooms in Psych Center are single patient rooms, and the furniture is bolted to the floor and cannot be moved for patient safety (Fig.5). They have one double room which can take two patients at the same time. We decided to use the double room to run an experiment because the patients in the double room are usually not as severely ill as the patients might be in a single room.

We installed a depth camera, a thermal camera and the Vayyar radar (14 TX, and 13 Rx.) system on ceiling over each bed in the double room. The depth camera data and the thermal camera data are used as the ground truth. Safety checks are conducted by the staff every 15 minutes, and each patient's status is manually recorded in a log which is used as another ground truth for the radar system.

Each night's data are collected from 9:00 pm to 6:00 am over 9 hours (32400 seconds). The total number of radar data frames for 9 hours is 372,504, where each frame has 34,034 data samples. The total required memory space for 9 hours is 95 GB. In the psych center, we have seven different subjects; The patient's information is shown in Table I. We have 6 male patients and one female patient, and their ages are from 19 to 49. All patients have some type of mental health problem and at times, poor sleeping quality during nighttime sleeping periods.

3.2 Eldercare and Rehabilitation Technology Lab Data Set (2021)

Data were collected from three healthy younger adults and two older adults in a controlled lab setting; see Table II for subject details. Subject 1 and subject 2 were asked

to lie on the bed in eleven different sleeping postures. Five subjects were asked to flip their head to the opposite side of bed Subjects 3-5 were asked to sit up in bed while reading. The RF sensor was installed over the bed in the same position and distance to bed as the patient room setting in the University of Missouri Psychiatric Center.

Table.I Patient Information for Psychiatric Center Study

patient ID	***sex***	***age***	***height(cm)***	***weight (kg)***	***BMI***
1	M	49	172.7	98.6	33
3	M	38	180.3	92.3	28
5	M	49	185.4	89.5	26
7	M	41	177.8	81.2	26
10	F	18	149.8	51.2	23
2	M	20	175.2	86.3	28
4	M	19	182.8	113	34

Table.II Subject Information for 2021 Lab Study

	sex	***age***	***height***	***weight***	***BMI***
Subject 1	F	34	166cm	53kg	19.3
Subject 2	M	26	170cm	66kg	22.8
Subject3	F	30	164cm	55kg	20.4
Subject 4	F	67	161cm	68kg	26
Subject 5	M	70	179cm	77kg	24

3.3 Contactless Extraction of Heart and Respiratory Rate with Depth, Thermal and Radar Sensing Devices Lab Data Set (2018)

As part of an earlier study in 2018, a depth camera, a thermal camera and the Vayyar radar (14 TX, and 13 Rx.) system was installed on the ceiling of the Center for Eldercare and Rehabilitation Technology lab. The respiration rate was collected by the depth camera, the thermal camera, respiration belt and the radar system. For the purpose of this dissertation, we are interested in the Vayyar radar data. The respiration belt is used as the ground truth for the radar data. Subjects (see Table III for subject details) were asked to lie on the bed in four different sleeping postures: back sleeping, left side sleeping, right side sleeping and stomach sleeping [85].

Table.III Subject Information for 2018 Lab Study

Subject	***sex***	***age***	***height (cm)***	***weight(kg)***	***BMI***
Subject2	M	25	179.3	78	24
Subject6	M	35	179.3	78	24
Subject8	M	29	179.3	85	26
Subject9	F	27	170	60	21
Subject10	F	27	160	55	21
Subject11	F	23	157	48	19
Subject12	F	24	162.5	61	23
Subject13	F	26	164	50	19
Subject15	F	24	162.5	54	20

IV. System

4.1 FMCW Radar System

The frequency modulated continuous wave (FMCW) radar is an ideal mode for short range radar system, and it has the advantages as follows [86]:

1) Ability to detect the target in very small range
2) Ability to measure simultaneous targets' range and velocity
3) Being more robust against noise. The information of received signal is stored in the phase of received signal in the frequency modulation, thus, FMCW radar is less affected by the noise in comparison to other radar systems.
4) The vital sign information is encoded in the phase of the received signal, therefore, FMCW radar is the best choice for detecting the breathing rate.

In the FMCW radar system, the slope, *S*, of the chirp (Fig.4) is defined by [87-88]

$$S = \frac{B}{2\,T_c} \tag{1}$$

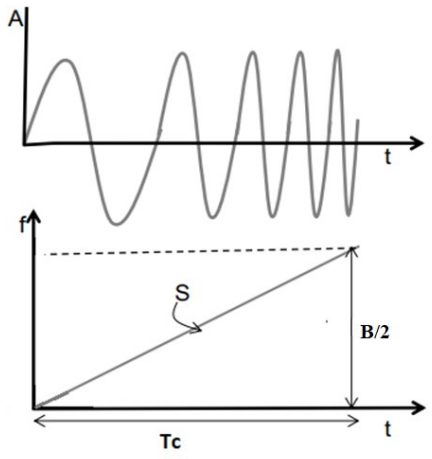

Fig.4 Transmitted signal chirps [87]

We present the relationship between the chirp duration, T_c and the frequency of chirp, *f*, as:

$$f = St + f_{start} \tag{2}$$

where the f_{start} is the carrier frequency f_c. Combining Eq. (1) and Eq. (2), we have:

$$f = \frac{B}{2T_c}t + f_c \tag{3}$$

In addition, we can estimate the maximum range, R_{max}, that can be detected by the radar:

$$R_{max} = \frac{Fs* c}{2*S} \tag{4}$$

where Fs is the sample frequency of analog-to-digital converter (ADC), and *c* is the speed of light.

The transmitted signal equation should be a sinusoidal equation, the transmitted signal x_{TX}:

$$x_{TX}(t) = A_{TX}cos\ (\psi(t)) \tag{5}$$

where

$$\varphi(t) = 2\pi ft + \phi(t) \tag{6}$$

Eq. (3) applied to Eq. (6), and the Eq. (6) can be written as:

$$\varphi(t) = 2\pi(\frac{B}{2T_c}t + f_c)t + \phi(t) \tag{7}$$

where $\phi(t)$ is phase noise from the transmitter. Combining Eq.7 and Eq.5, we have

$$x_{TX}(t) = A_{TX}cos\ (2\pi(\frac{B}{2T_c}t + f_c)t + \phi(t)) \tag{8}$$

Received signal is a time delay of transmitted signal, that is:

$$x_{RX}(t) = A_{RX}\, cos\left(2\pi\left(\frac{B}{2T_c}(t-t_d)+f_c\right)(t-t_d)+\ \phi(t-t_d)\right)$$

$$= A_{RX}\, cos\left(2\pi f_c(t-t_d)+\pi\frac{B}{T_c}(t-t_d)^2+\ \phi(t-t_d)\right) \tag{9}$$

After mixer, we can get IF signal:

$$x_{IF}(t) = A_{IF} cos\ (\psi(t)-\psi(t-t_d)) \tag{10}$$

$$x_{IF}(t) = A_{IF}\, cos\left(2\pi f_c t+\pi\frac{B}{T_c}t^2+\varphi(t)-2\pi f_c t+2\pi f_c t_d-\pi\frac{B}{T_c}(t-t_d)^2-\right.$$

$$\left.\varphi(t-t_d)\right) = A_{IF} cos\ (2\pi f_c t_d+2\pi\frac{B}{T_c}tt_d-\pi\frac{B}{T_c}{t_d}^2+\Delta\varphi(t)) \tag{11}$$

where the beat frequency f_b is defined as:

$$f_b = kt_d = \frac{B}{T_c}t_d \tag{12}$$

Combining Eq. (11) and Eq. (12), the IF signal in Eq. (10) can be written as:

$$x_{IF}(t) = A_{IF}\cos\ (2\pi f_c t+2\pi f_b t-\pi\frac{B}{T_c}{t_d}^2+\Delta\varphi(t)) \tag{13}$$

where the phase difference $\Delta\varphi(t)$ is:

$$\Delta\varphi(t)\ =\ 2\pi f_c\Delta t = 2\pi\frac{c\Delta t}{\lambda}\ = 4\pi\frac{\Delta d}{\lambda} \tag{14}$$

If the target velocity is equal to v_{target}, and the distance Δd is equal to:

$$\Delta d = v_{target} * T_c \tag{15}$$

The phase difference $\Delta\varphi(t)$ in the Eq. (14) can be written as:

$$\Delta\varphi(t) = 4\pi \frac{v_{target} * T_c}{\lambda} \tag{16}$$

The IF signal in the Eq. (13) can be written as:

$$x_{IF}(t) = A_{IF}\cos\left(2\pi f_c t + 2\pi f_b t + 4\pi \frac{v_{target} * T_c}{\lambda}\right) \tag{17}$$

If the distance of target is equal to R_{target}, and the IF signal is updated to:

$$x_{IF}(t) = A_{IF}\cos\left(2\pi f_b t + 4\pi f_c \frac{R_{target}}{c} + 4\pi \frac{v_{target} * T_c}{\lambda}\right) \tag{18}$$

4.2 Psych Center System

Most rooms in the Psych Center are single patient rooms, and the furniture is bolted to the floor and cannot be moved to address patient safety concerns (Fig.5). They do have one double room which can take two patients at the same time. Due to safety concerns, patients with acute psychiatric conditions that might be a danger to themselves or a danger to others are assigned the single patient rooms, and patients who are more stable and less likely to be in danger are assigned the double room. Therefore, we were advised to use the double room for our experiment because the patients in the double room are usually in a better mental state than the patients assigned to the single rooms.

We installed a depth camera, a thermal camera and the Vayyar radar (14 TX, and 13 Rx.) system on ceiling for each subject in the Psych Center. The depth camera data and the thermal camera data are used as the ground truth of radar data. Safety checks are conducted by the staff every 15 minutes, and each patient's status is manually recorded in a log which is used as another ground truth of the radar system.

Fig.5 The furniture in the Psych Center patient room

4.2.1 Radar System for Psych Center

The Vayyar radar in the Psych center was constructed using a frequency modulated continuous wave (FMCW) radar and was originally designed for military applications by the Vayyar company. Therefore, the system prototype used in this study was not commercially available. The Vayyar company has other radar products which are commercially available and have been applied to tracking targets, health pattern monitoring, and image processing [89].

By analyzing the output data from the Vayyar radar in the psych center, we observe that there are 27 antennas: 14 antennas for the transmitting signals (TX), and 13 antennas for the receiving signals (RX). Fig. 6 (a) shows there are 182 * 2 TX RX pairs, which means the number of virtual antennas in the Vayyar radar system is 182. The first column represents the TX antenna ID number, and second column represents the RX antenna ID

number. For instance, Fig. 6 (b) shows the RX antenna ID's =4, 0, 5, 3, 12, 6, 13, 15, 1, 14, 17, 16, and 18 will receive the signal when the TX antenna ID =2 is transmitting. Fig.6 (a) shows the radar raw data 'Smat' size is 182 *187, and the data type class is a complex double number. Thus, each frame has 182 chirps, each chirp has 187 samples, and each sample has two quadrature channels (Fig.6 (c)). Fig.6 (d) shows the frequency parameter 'Freq' is from 6.01 GHz to 7.76 GHz. Thus, the bandwidth of the radar is 1.75 GHz, and the range resolution is:

$$r = \frac{c}{2B} \tag{19}$$

where c is the speed of light 3×10^8 m/s, and B is the total swept bandwidth 1.75 GHz. Based on Eq. (19), the RF sensor range resolution is 8.6cm.

The carrier frequency f_c of the Vayyar radar is 6.014 GHz, hence the wavelength of radar is:

$$\lambda = \frac{c}{f_c} \tag{20}$$

Based on Eq. (20), the wavelength of the Vayyar radar is 5cm.

There are 187 samples in each chirp, 182 chirps in each frame, and the velocity resolution $v_{res}$is:

$$v_{res} = \frac{\lambda}{2T_f} \tag{21}$$

Based on Eq. (21), we obtain that the velocity resolution of the Vayyar radar is equal to 0.31m/s.

There are 14 transmit antennas, 13 receive antennas, and the angle resolution θ_{res}:

$$\theta_{res} = \frac{2}{N_{ant}} \tag{22}$$

where N_{ant} is the total number of antennas. Based on Eq. (22), we obtain that the angle resolution of the Vayyar radar is equal to 0.63^0.

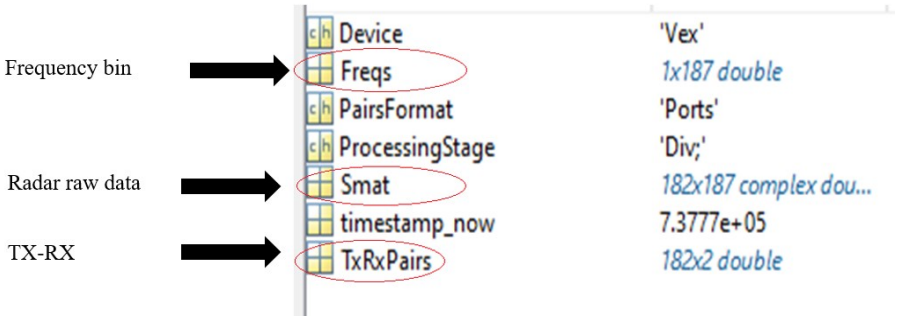

(a)

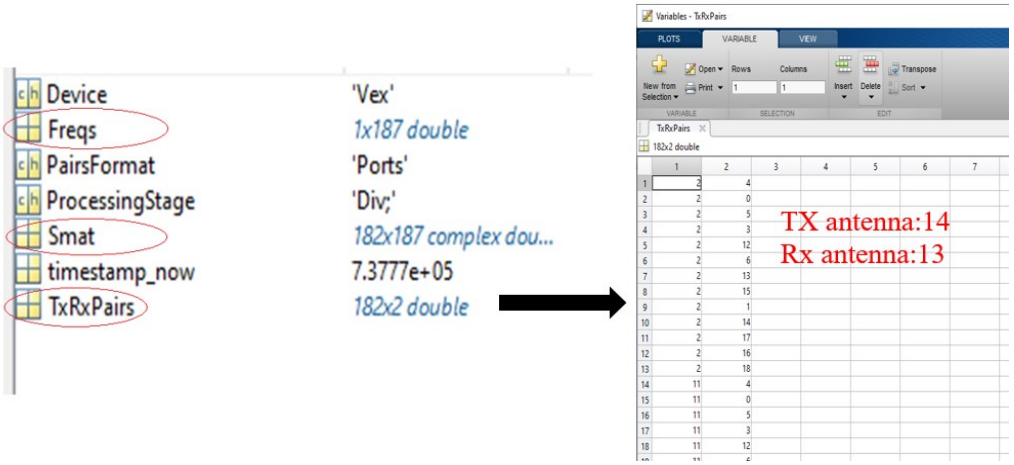

(b)

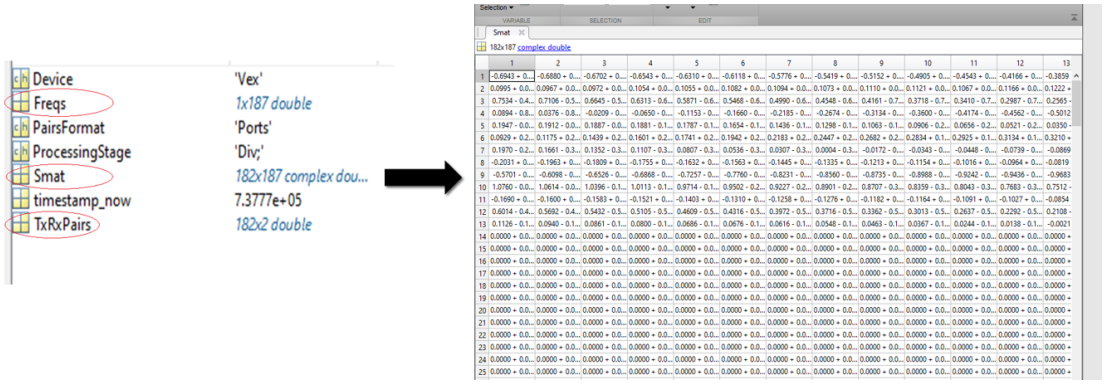

(c)

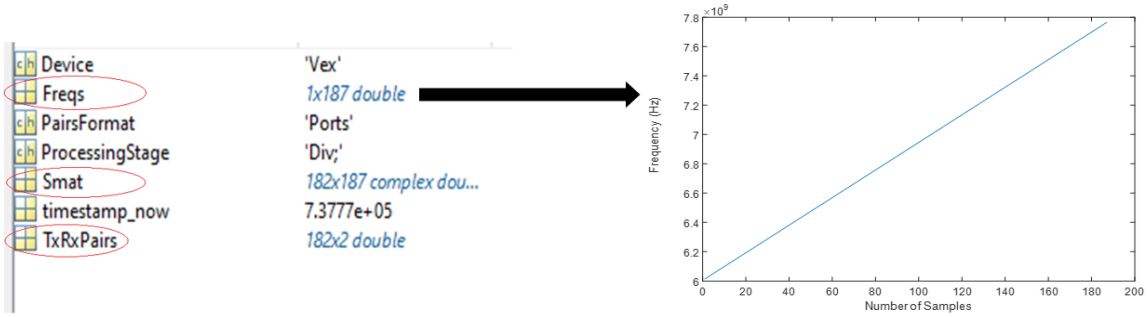

(d)

Fig.6 The Vayyar Radar data. (a) Data structure, (b) TX-RX pairs, (c) IQ quadrature channels' data, (d) Bandwidth

4.2.2 Psych Center Radar System Simulation

In order to better understand the performance of the Vayyar Radar system, we designed a simple Radar Performance App (Fig.7). In the simulation process, we set different numbers of chirps, and two targets. We set the first target location is 2m, the velocity is 0.7m/s, the azimuth angle is 10^0, and second target location is 1.5m, the velocity is 1.5 m/s, and the azimuth angle is 40^0.

We set TX antennas are 14, the RX antennas are 13, the samples of per chirp are 187, the number of chirps 256, the sample frequency is 4.18MHz, the chirp bandwidth is 1.75GHz, the center frequency is 6.014GHz, and all radar's parameters are same with Vayyar radar system. The results from App in the Fig.7 show the maximum range which can be detected by the Vayyar radar is 8.014m, the range resolution is 8.57cm, the maximum velocity which can be measured by the Vayyar radar is 27.88 m/s, the speed resolution is 0.22 m/s, the angle resolution is 0.63 degree.

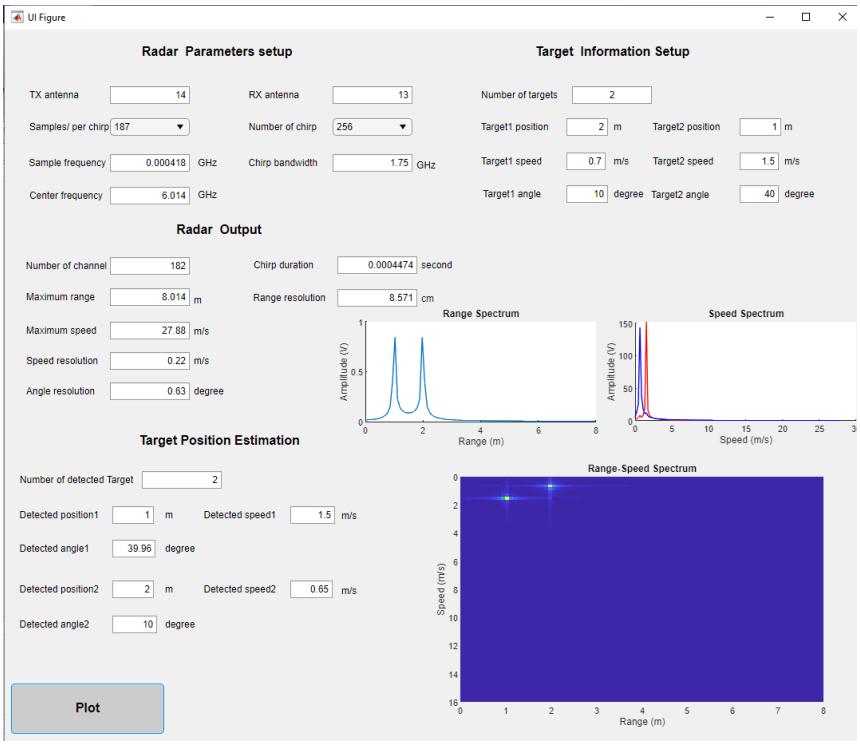
UI Figure
Radar Parameters setup
TX antenna 14
RX antenna 13
Samples/ per chirp 187
Number of chirp 256
Sample frequency 0.000418 GHz
Chirp bandwidth 1.75 GHz
Center frequency 6.014 GHz
Target Information Setup
Number of targets 2
Target1 position 2 m
Target2 position 1 m
Target1 speed 0.7 m/s
Target2 speed 1.5 m/s
Target1 angle 10 degree
Target2 angle 40 degree
Radar Output
Number of channel 182
Chirp duration 0.0004474 second
Maximum range 8.014 m
Range resolution 8.571 cm
Maximum speed 27.88 m/s
Speed resolution 0.22 m/s
Angle resolution 0.63 degree
Range Spectrum
Amplitude (V)
Range (m)
Speed Spectrum
Amplitude (V)
Speed (m/s)
Target Position Estimation
Number of detected Target 2
Detected position1 1 m
Detected speed1 1.5 m/s
Detected angle1 39.96 degree
Detected position2 2 m
Detected speed2 0.65 m/s
Detected angle2 10 degree
Range-Speed Spectrum
Speed (m/s)
Range (m)
Plot

(a)

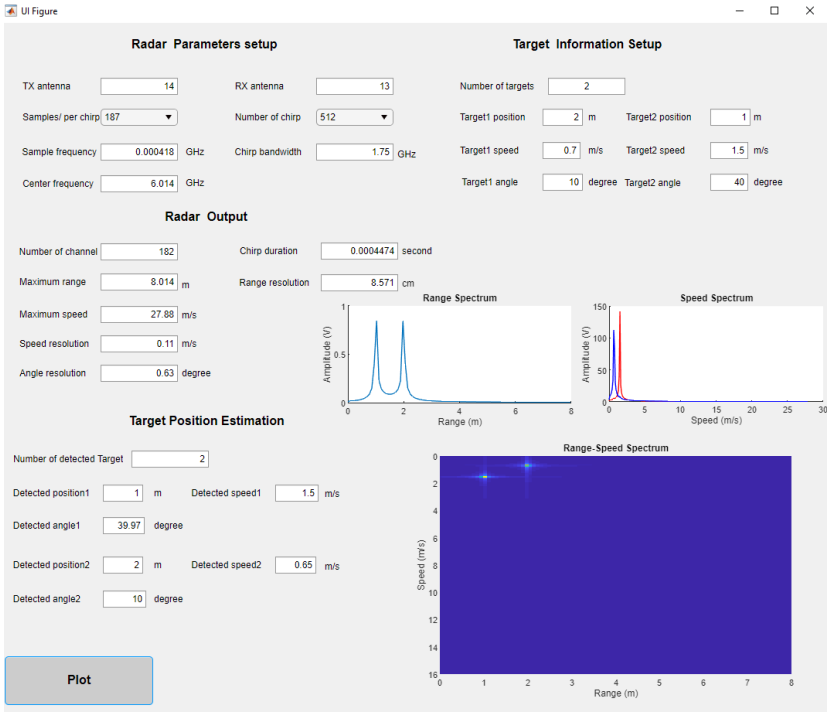
UI Figure
Radar Parameters setup
TX antenna 14
RX antenna 13
Samples/ per chirp 187
Number of chirp 512
Sample frequency 0.000418 GHz
Chirp bandwidth 1.75 GHz
Center frequency 6.014 GHz
Target Information Setup
Number of targets 2
Target1 position 2 m
Target2 position 1 m
Target1 speed 0.7 m/s
Target2 speed 1.5 m/s
Target1 angle 10 degree
Target2 angle 40 degree
Radar Output
Number of channel 182
Chirp duration 0.0004474 second
Maximum range 8.014 m
Range resolution 8.571 cm
Maximum speed 27.88 m/s
Speed resolution 0.11 m/s
Angle resolution 0.63 degree
Range Spectrum
Amplitude (V)
Range (m)
Speed Spectrum
Amplitude (V)
Speed (m/s)
Target Position Estimation
Number of detected Target 2
Detected position1 1 m
Detected speed1 1.5 m/s
Detected angle1 39.97 degree
Detected position2 2 m
Detected speed2 0.65 m/s
Detected angle2 10 degree
Range-Speed Spectrum
Speed (m/s)
Range (m)
Plot

(b)

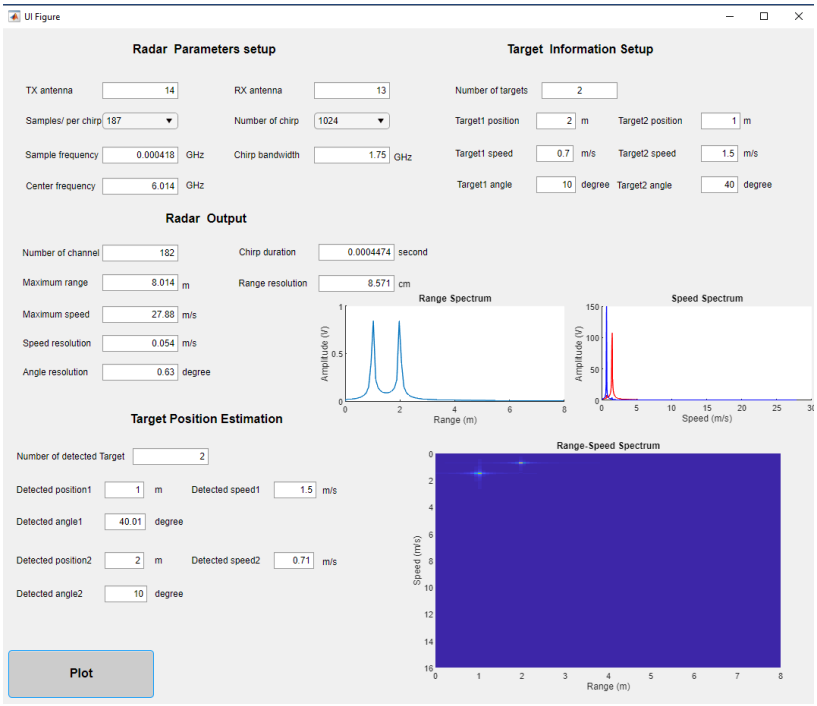

(c)

Fig.7 Radar performance simulation. (a) Number of chirp=252, the velocity resolution=0.22m/s, (b) Number of chirp=512, the velocity resolution=0.11m/s, (c) Number of chirp=1024, the velocity resolution=0.054m/s

We changed the number of chirps to 512, 1024, and it will affect the speed resolution. The speed resolution is changed to 0.11m/s, and 0.054m/s. Therefore, we concluded that:

- The range resolution depends on IF bandwidth.
- The speed resolution depends on the number of chirps in each frame. If the number of chirps is increased, the speed resolution is getting higher.
- Angle resolution depends on the number of antennas.

4.3 The System for Learning Room Structure and Activity Patterns

The RF sensor was deployed in a set of campus rooms containing two offices (A, B) and a meeting room (C) (Fig.8). All the rooms have standard furniture: tables, chairs, and

bookshelves. The meeting room is 5.51m × 7.1m; office A is 3.2 m × 3.71m; office B is 3.2 m × 3.29m.

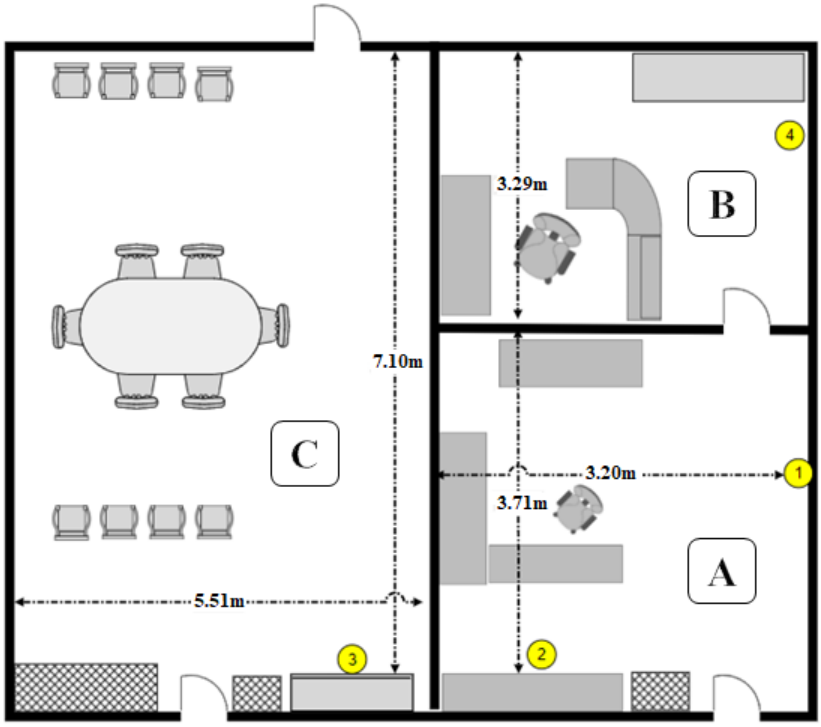

Fig.8 The top view of office and meeting space

In this experiment, the RF sensor is deployed in four different positions (①,②,③,④) in the offices (A, B) and the meeting room (C) (Fig. 8), and motion data are collected over time.

4.3.1 Radar System for Learning Room Structure and Activity Patterns

An RF sensor was constructed using an FMCW radar with two LP0965 direction antennas, one for the transmitting signal, and one for the receiving signal (Fig.9). The linear chirp is generated by two components:

- The VCO (voltage-controlled oscillator) operates in the range of 2.315GHz to 2.536GHz and transmits at 10mW.

- The ramp generator, XR-2206, produces a linear ramp and a synchronization pulse where the rising edge coincides with the start of the up-ramp.

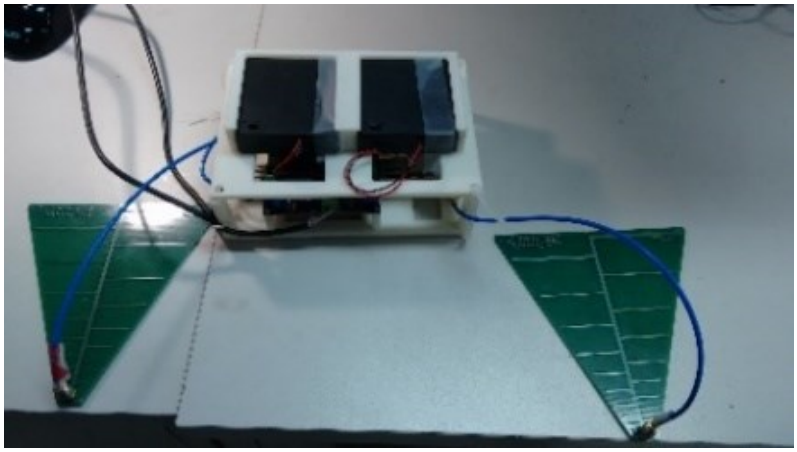

(a)

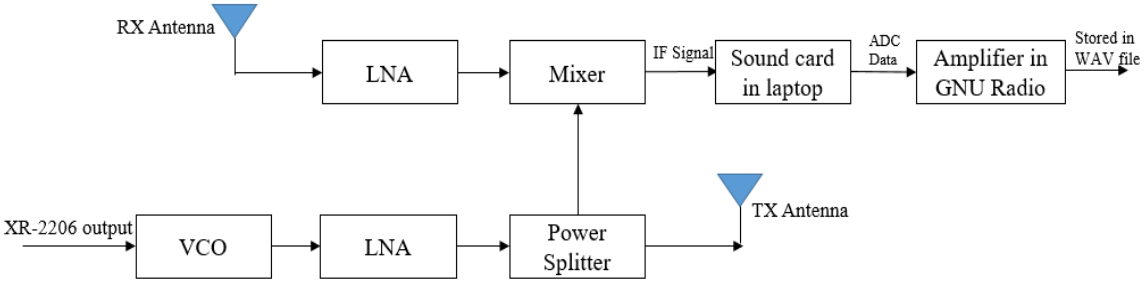

(b)

Fig.9 The RF system (a) FMCW radar system, (b) block diagram of RF sensor. Where LNA is the low noise amplifier

The carrier frequency of the FMCW radar is 2.315GHz, the bandwidth is 221MHz. Based on Eq. (19) and Eq. (20), the RF sensor range resolution is 67.8cm, and the wavelength λ is 0.13 m. There are 960 samples in each chirp, 512 chirps in each frame, the frame time duration T_f is 10.24s. Based on Eq. (21), the RF sensor velocity resolution is 0.63 cm/s.

The transmitted signal and the target echo signal are heterodyned in the mixer stage of the receiver. The intermediate frequency (IF) signal data goes through the ADC (Analog to Digital converter) process. A computer sound card with a 48 kHz sample frequency plays a role of the ADC. The ADC data is amplified in GNU radio, and store as a .wav file, which is processed by Matlab.

4.3.2 Radar System for Learning Room Structure and Activity Patterns Simulation

In order to better understand the performance of the RF system, we used the Radar Performance App in the Fig.10. In the simulation process, we set different numbers of chirps, and two targets. We set the first target location is 2m, the velocity is 0.7m/s, the azimuth angle is 10^0, and second target location is 1.5m, the velocity is 1.5 m/s, and the azimuth angle is 40^0.

We set TX antennas are 1, the RX antennas are 1, the samples of per chirp are 960, the number of chirps 256, the sample frequency is 48kHz, the chirp bandwidth is 221MHz, the center frequency is 2.4GHz, and all radar's parameters are same with RF system. The results from App in the Fig.7 show the maximum range which can be detected by the RF sensor is 325.8m, the range resolution is 67.87cm, the maximum velocity which can be measured by the Vayyar radar is 1.56m/s, the speed resolution is 0.012 m/s, the angle resolution is 110 degree.

We increased the number of chirps to 512, 1024, and it will affect the speed resolution. The speed resolution is changed to 0.006m/s, and 0.003m/s. The speed resolution of the RF system is getting higher.

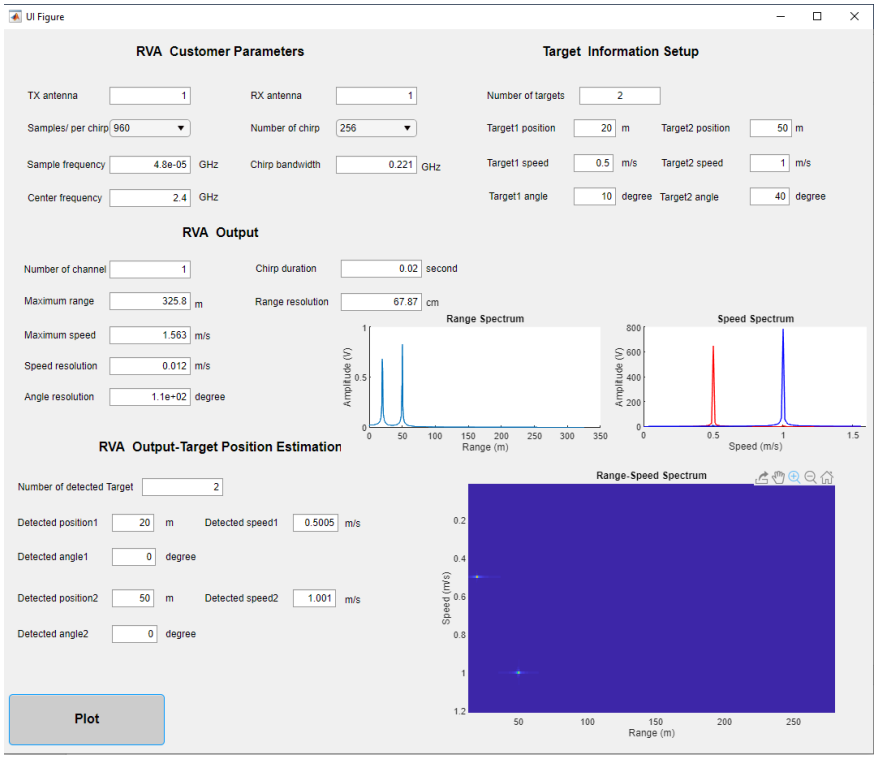
UI Figure
RVA Customer Parameters
Target Information Setup
TX antenna 1
RX antenna 1
Number of targets 2
Samples/ per chirp 960
Number of chirp 256
Target1 position 20 m
Target2 position 50 m
Sample frequency 4.8e-05 GHz
Chirp bandwidth 0.221 GHz
Target1 speed 0.5 m/s
Target2 speed 1 m/s
Center frequency 2.4 GHz
Target1 angle 10 degree
Target2 angle 40 degree
RVA Output
Number of channel 1
Chirp duration 0.02 second
Maximum range 325.8 m
Range resolution 67.87 cm
Maximum speed 1.563 m/s
Speed resolution 0.012 m/s
Angle resolution 1.1e+02 degree
Range Spectrum
Amplitude (V)
Range (m)
Speed Spectrum
Amplitude (V)
Speed (m/s)
RVA Output-Target Position Estimation
Number of detected Target 2
Detected position1 20 m
Detected speed1 0.5005 m/s
Detected angle1 0 degree
Detected position2 50 m
Detected speed2 1.001 m/s
Detected angle2 0 degree
Range-Speed Spectrum
Speed (m/s)
Range (m)
Plot

(a)

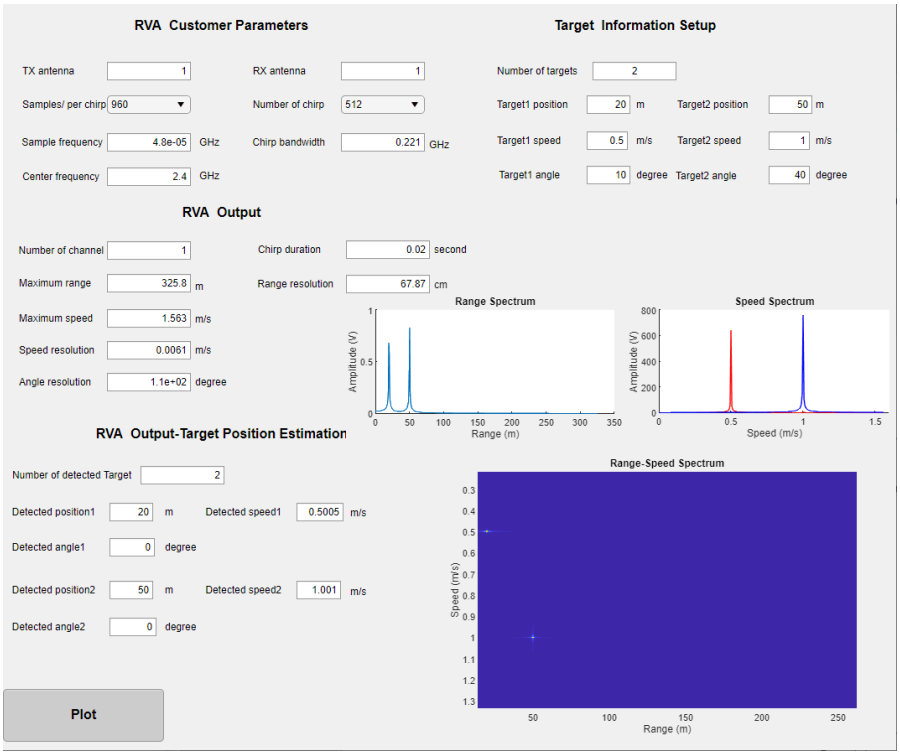
RVA Customer Parameters
Target Information Setup
TX antenna 1
RX antenna 1
Number of targets 2
Samples/ per chirp 960
Number of chirp 512
Target1 position 20 m
Target2 position 50 m
Sample frequency 4.8e-05 GHz
Chirp bandwidth 0.221 GHz
Target1 speed 0.5 m/s
Target2 speed 1 m/s
Center frequency 2.4 GHz
Target1 angle 10 degree
Target2 angle 40 degree
RVA Output
Number of channel 1
Chirp duration 0.02 second
Maximum range 325.8 m
Range resolution 67.87 cm
Maximum speed 1.563 m/s
Speed resolution 0.0061 m/s
Angle resolution 1.1e+02 degree
Range Spectrum
Amplitude (V)
Range (m)
Speed Spectrum
Amplitude (V)
Speed (m/s)
RVA Output-Target Position Estimation
Number of detected Target 2
Detected position1 20 m
Detected speed1 0.5005 m/s
Detected angle1 0 degree
Detected position2 50 m
Detected speed2 1.001 m/s
Detected angle2 0 degree
Range-Speed Spectrum
Speed (m/s)
Range (m)
Plot

(b)

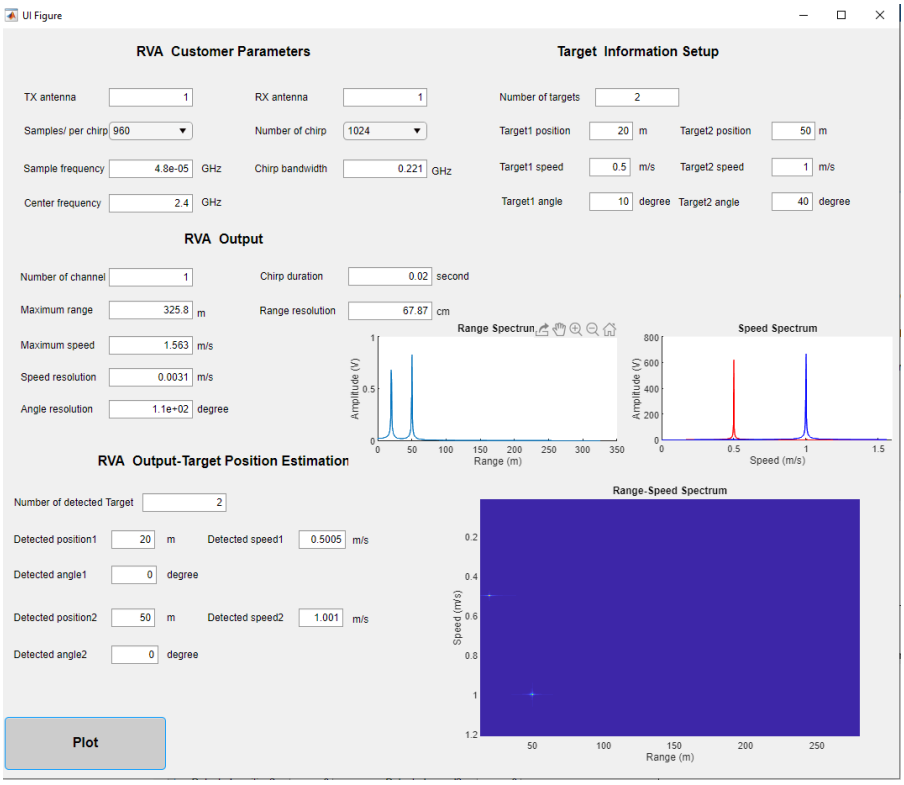

(c)

Fig.10 Radar performance simulation. (a) Number of chirp=252, the velocity resolution=0.012m/s, (b) Number of chirp=512, the velocity resolution=0.006m/s, (c) Number of chirp=1024, the velocity resolution=0.003m/s

The Radar Performance App was designed based on the FMCW radar equations (Eq.(1) -Eq.(22)), which could be used to simulate any FMCW radar system. In the simulation App, students can set the number of TX/RX antennas, bandwidth, number of samples in each chirp, number of chirps in each frame, and center frequency. All those parameters come from the company that provides the radar. Then, the RVA output in the Radar Performance App shows range resolution, speed resolution, angle resolution, maximum range, and maximum speed which can be detected by the radar. In addition, Students could try different parameters in the parameters setup part, and look at the influence of each parameter. This App could help students better understand the radar system's performance.

V. Methodology

5.1 Radar Data Processing

The radar system transmits N equal spaced chirps in over the time T_f, and this unit is called 'frame', the time T_f is called frame time (Fig.11 (a)). The received channel data from the same chirp is stored in the same raw (Fig.11 (b)). In the radar data matrix, each row is corresponding to chirp index, and each column is corresponding to the range bin.

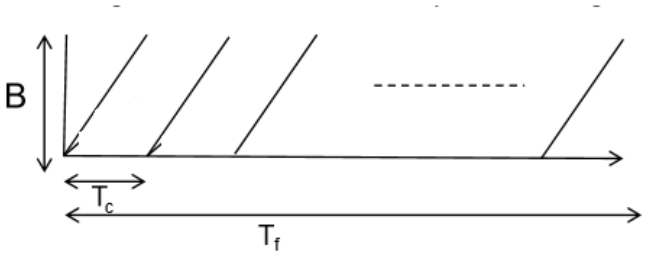

(a)

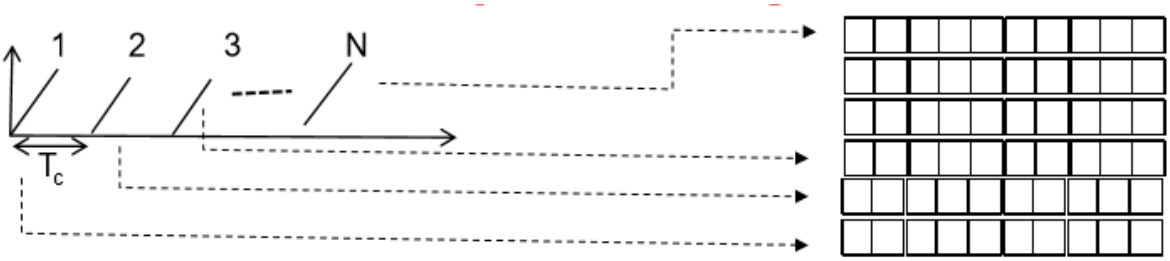

(b)

Fig.11 Radar data structure[87] (a) frame (b) radar data matrix

In our research projects, the company that provided the Vayyar radar was not able/willing to provide more detailed information, such as ADC sample frequency, frame time, and chirp duration. Therefore, we estimate the frame time by Eq. (23):

$$T_f = \frac{total\ \#of\ frame}{9\ hours} \tag{23}$$

After get the frame time, we can calculate the number of frames in per window by:

$$\#frame\ in\ per\ window = window\ size * frmae\ time$$

Then we can read the radar raw data from the hard drive based on the window's size as shown Fig.12 (a). The data in per frame comes from the different antennas. In order to combine the signal from different antennas, first, we used the beamforming algorithm for estimating the angle of arrival (AOA) corresponding to the strongest signal, then coherently combining the signal (Fig. 12(b)). The beamforming algorithm and AOA will be discussed in Section 4.2.

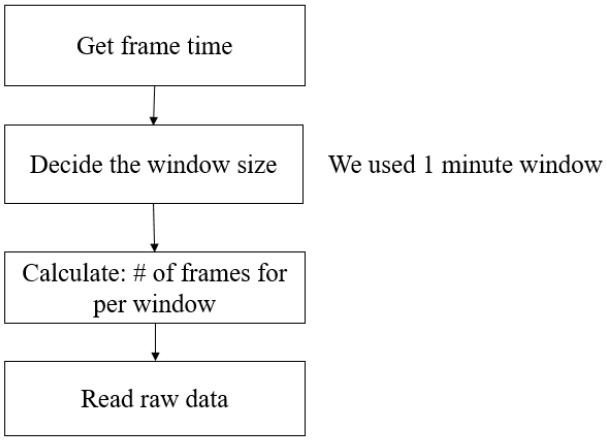

(a)

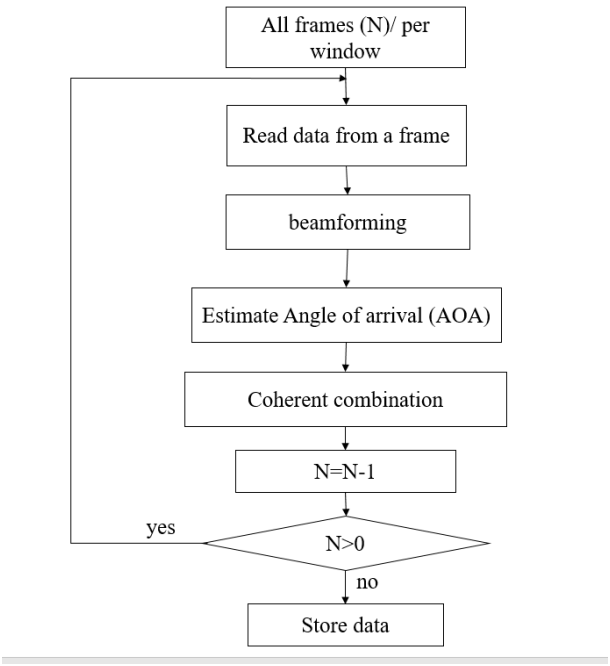

(b)

Fig.12 Flow diagram for data processing (a) read raw data from hard drive (b) frame data processing

5.2 Frame Data Processing

For frame data processing, we have two strategies: constant data frame processing, and the variable data frame processing. Why did we do two different frame data processing strategies? The reason is due to the lack of more detailed information, such as ADC sample frequency, frame time, and chirp duration. Therefore, we are missing the following information:

- The number of frames per second
- The number of chirps per frame
- The distance between the two antennas

Therefore, we run different experiments to identify which one is the best way to do radar signal processing. We used the constant data frame and the variable data frame to process

the radar data, estimated the time when the patient came to the bed, and those times are compared with depth camera information.

5.2.1 Constant Data Frame

In Psych Center data, each night data is collected from 21:00 pm to 6:00 am over 9 hours, and the total frame numbers are N_{frame}. In the first strategy, we used same numbers of chirps in each frame, the frame time are same in over time, and the number of chirps in each frame:

$$N_{chirp} = \frac{N_{frame}}{9*60} \tag{24}$$

5.2.2 Variable Data Frame

In Psych Center data, each night data is collected from 21:00 pm to 6:00 am over 9 hours, and the total frame numbers is N_{frame}. In the second strategy, we used variable numbers of chirps in each frame, and the number of chirps in each frame is based on the time when the frame is created.

5.2.3 Results and Discussion

For psych center 09/10/2019 one night data, we used the constant data frame and the variable data frame to process the radar data, estimated the time when the patient came to the bed, and those times are compared with depth camera information. The depth data shows the patient came to bed at 21:24 (Fig.13), the radar data based on constant data frame processing shows the patient came to bed at 21:26 (Fig.13), however, the radar data based on variable data frame processing shows the patient came to bed at 21:15 (Fig.14). We did the same data processing for different night data for other two patients, the results are shown in Table IV.

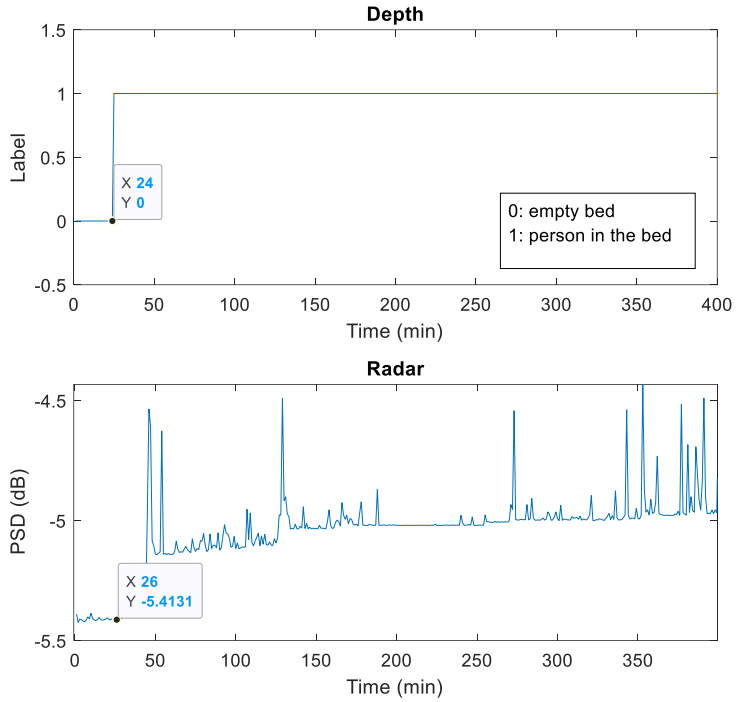

Fig.13 Depth data and Radar data based on the constant data frame

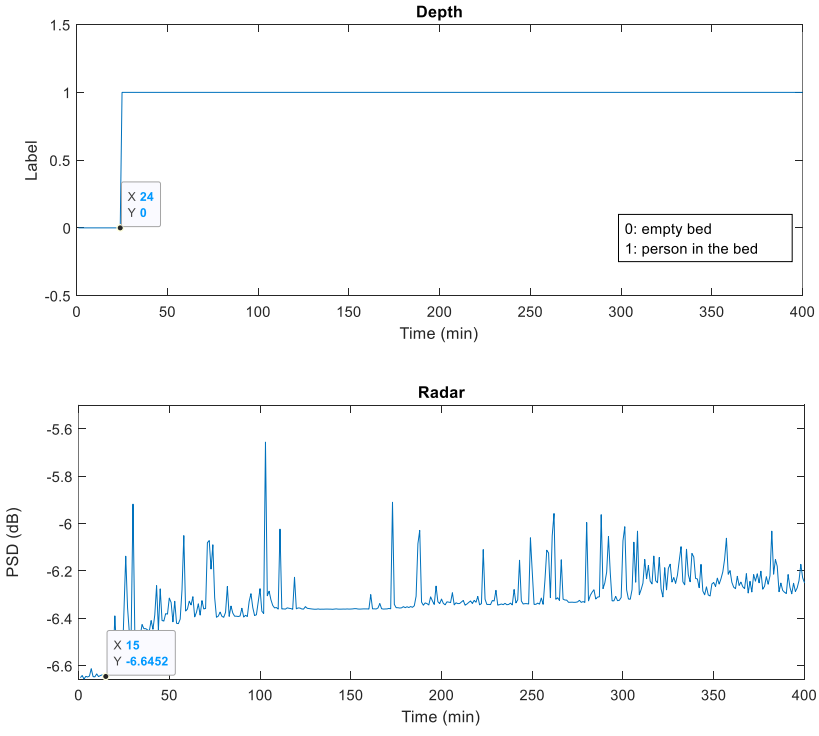

Fig.14 Depth data and Radar data based on the variable data frame

The results in Table IV show that the time from the constant data frame processing is more closed to the time from the depth camera, and the maximum difference between those two times are 3 minutes. However, the time from the variable data frame processing is less accurate; the maximum difference between the time from variable data processing and the time from depth camera is 20 minutes. Therefore, we used constant data frame processing for the psych center project.

Table.IV Constant data frame vs. Variable data frame

Date for Psych Center	The time by using Constant data frame processing	The time by using variable data frame processing	The time from the depth
09/10/2019	26 min	15 min	24 min
09/11/2019	126 min	102 min	123 min
09/12/2019	26 min	21 min	23 min

5.3 Arrival of Angle and Beamforming

A radar measures the spatial distribution of reflectivity in the three-dimension spherical coordinate system of range, azimuth angle and elevation angle.

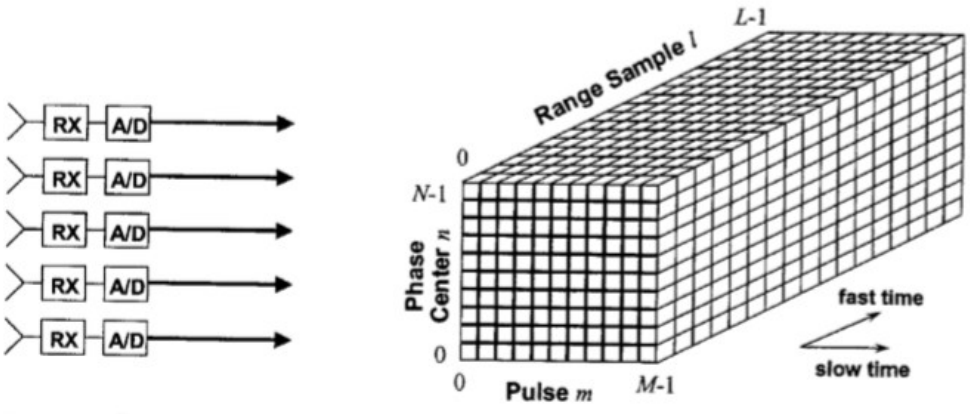

Fig.15 Data structure of a multichannel radar[4]

A phase array is a radar system with multiple receive antennas, and the multiple receive channels are corresponding to the phase center axis in Fig.15. The chirps in a radar system are corresponding to the slow time axis (pulse axis), and the samples in the chirps are corresponding to the fast time axis in Fig.15. Many radar signal processing implement the Fourier transform of slow time and fast time axis to get the range and angle information of the target. These spectral domains correspond to Doppler shift and angle of arrival.

The angle of arrival indicates the direction of incoming signal. In Fig.16 (a), θ_1, and θ_2 are the arrival angle of the signal 1 and the signal 2, respectively. The phase information will be change over antennas, the time delay are between the two antennas be defined [90 -91]:

$$\tau = \frac{distance}{velocity} = \frac{dcos\theta}{c} \tag{25}$$

Where θ is arrival angle, c is speed of light, and d is the distance between the antennas.

An array is commonly referred to as a uniform linear array, therefore, we find that:

$$\tau_k = (k-1)\frac{dcos\theta}{c} \quad \text{for } \theta\epsilon[-90^0\ ,\ 90^0] \tag{26}$$

Where k is the number of antennas in an array.

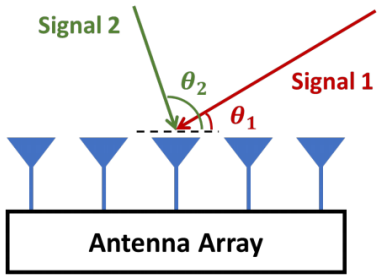

(a)

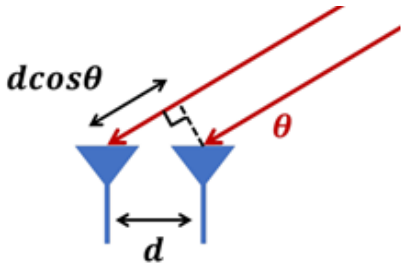

(b)

Fig.16 Arrival angle of an antenna array[91]

The reflection power of different incoming angles varies. We evaluate the spatial spectrum for every possible direction and try to find the arrival angle with a higher reflection power for the receive power. There are different ways to estimate the arrival angle:

- Beamforming
- MUSIC

We choose the case that the patient is lying in the bed and use the beamforming that is a coherent combination of data from multiple RX antennas. In Psych Center, we have 14 TX and 13 RX, and the number of the virtual antennas are:

$$number\ of\ virtual\ antennas = 14 * 13 = 187 \tag{27}$$

Assembling the 187 antennas samples into vector form given the array at a fixed time:

$$\boldsymbol{y} = [y[0]\ \ y[1]\ \cdots\ y[N]] \tag{28}$$

where N is number of antennas, and the one antenna samples y[n] is represented by:

$$y[n] = Ae^{-j2\pi ndsin\theta/\lambda} \tag{29}$$

Hence the vector $\boldsymbol{y}$ is represented by:

$$\boldsymbol{y} = A\left[1 \;\; e^{-\frac{j2\pi d sin\theta}{\lambda}} \;\; \cdots \;\; e^{-\frac{j2\pi(N-1)dsin\theta}{\lambda}}\right] = A\boldsymbol{a_s}(\theta) \tag{30}$$

Conventional nonadaptive beamforming is implemented as weight sum of the element signals:

$$z(\theta) = \boldsymbol{h}'\boldsymbol{y} \tag{31}$$

Where **h** is a vector of complex weights

$$\boldsymbol{h} = [h_0 \;\; h_1 \;\; \cdots \;\; h_{N-1}]' = \boldsymbol{w}' \odot \boldsymbol{a_s}(\theta) \tag{32}$$

Where we choose the same weight for all vectors in order to estimate the angle with the higher power. The weights are matched to an angle of θ_0. The response of a beamforming steered to θ_0 to an incoming wavefront at angle θ is

$$z(\theta) = \boldsymbol{h}'\boldsymbol{y} = \hat{A}\sum_{n=0}^{N-1} a_n e^{-j2\pi nd(sin\theta - sin\theta_0)/\lambda} \tag{33}$$

We just have one subject; therefore, the steered beamforming angle is zero degree. Fig.12 shows the arrival angle estimating from two methods. Fig.12 (a) shows the results of conventional beamforming method, and Fig.12 (b) shows the results of MUSIC method. We can estimate the arrival angle -9^0 and -3^0.

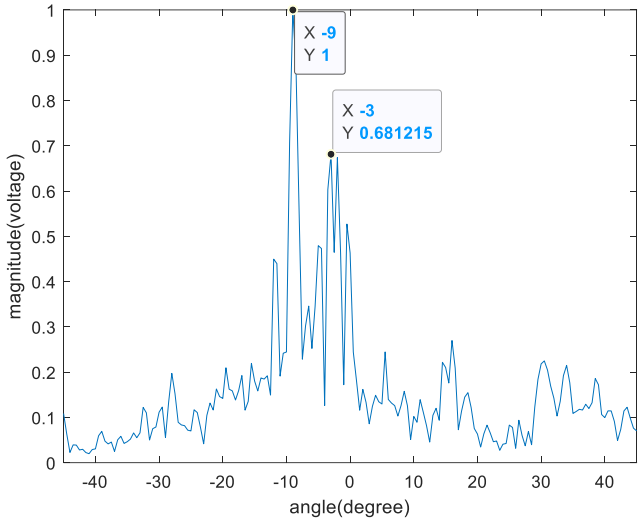
X -9
Y 1
X -3
Y 0.681215
magnitude(voltage)
angle(degree)
1
0.9
0.8
0.7
0.6
0.5
0.4
0.3
0.2
0.1
0
-40
-30
-20
-10
0
10
20
30
40

(a)

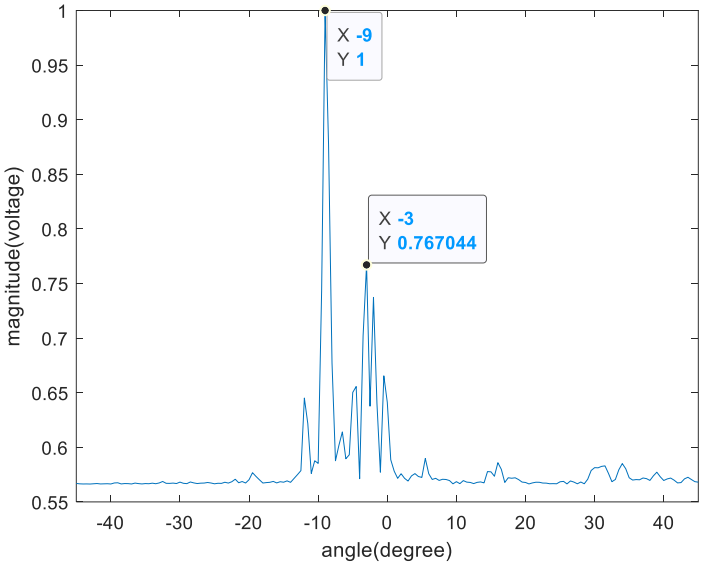
X -9
Y 1
X -3
Y 0.767044
magnitude(voltage)
angle(degree)
1
0.95
0.9
0.85
0.8
0.75
0.7
0.65
0.6
0.55
-40
-30
-20
-10
0
10
20
30
40

(b)

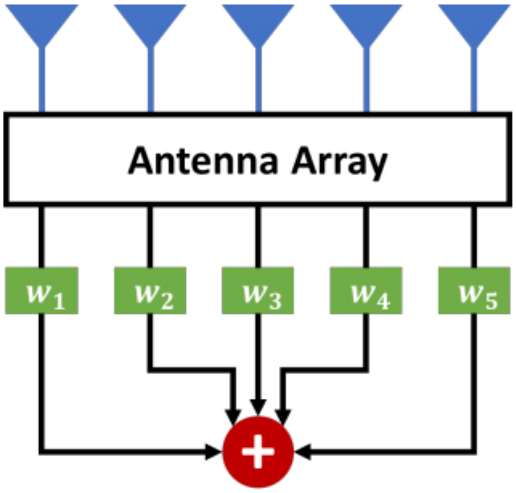

(c)

Fig.17 Arrival angle of an antenna array. (a) conventional beamforming, (b) MUSIC, (c) coherent combination signals from multiple antennas[91]

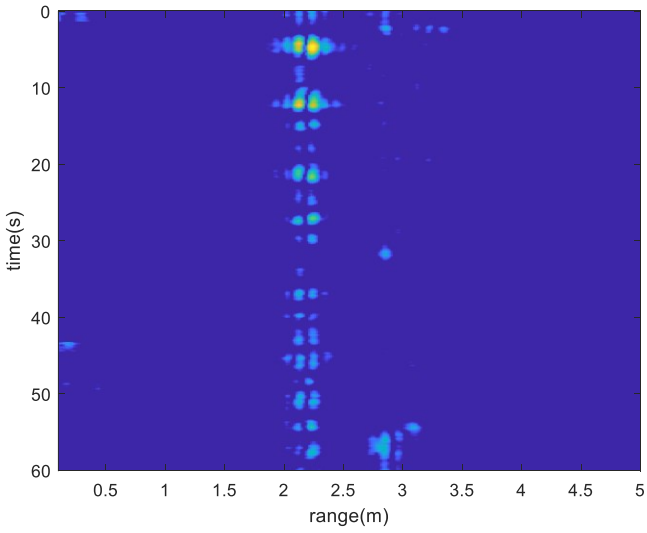

(a)

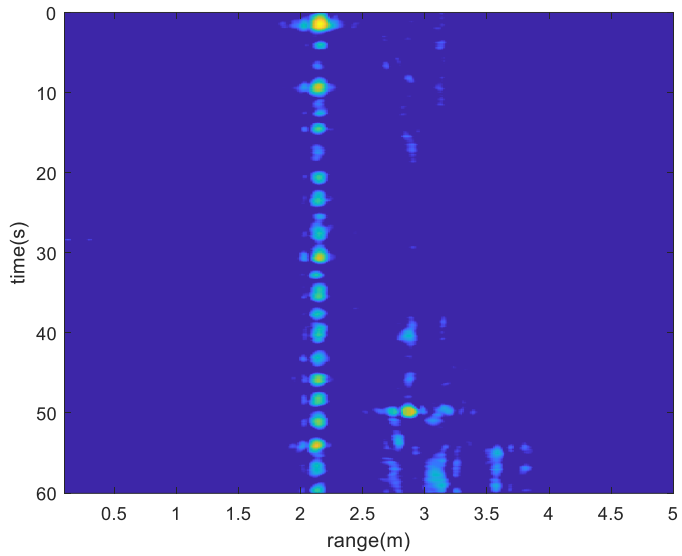

(b)

Fig.18 Different Arrival angle results. (a) Arrival angle $\theta = -9^0$, (b) Arrival angle $\theta = -3^0$,

5.3 Matched Filter

In wireless communication systems, the primary emphasis is on signal-to-noise ratio (SNR). How do we remove the noise power, and increase the signal power? The higher SNR improves the detection performance of the radar system.

Assume the receiver output, $y(t)$, the received power $x(t)$, and the relationship between the output and the input in frequency domain:

$$Y(\Omega) = H(\Omega)X(\Omega) \tag{34}$$

where $H(\Omega)$ is the frequency response of the filter. The power of signal at the instant time t_m:

$$|y(t_m)|^2 = \left|\frac{1}{2\pi}\left(\int_{-\infty}^{\infty} X(\Omega)H(\Omega)e^{-j\Omega t_m}d\Omega\right)\right|^2 \tag{35}$$

Consider the noise power of the radar system is white noise with power density $\frac{N_0}{2}$ watts per hertz. The total noise power is then:

$$n_p = \frac{N_0}{4\pi}\int_{-\infty}^{\infty}|H(\Omega)|^2 d\Omega \tag{36}$$

The SNR measured at time t_m:

$$SNR = \frac{|y(t_m)|^2}{n_p} = \frac{\left|\frac{1}{2\pi}(\int_{-\infty}^{\infty} X(\Omega)H(\Omega)e^{-j\Omega t_m}d\Omega)\right|^2}{\frac{N_0}{4\pi}\int_{-\infty}^{\infty}|H(\Omega)|^2 d\Omega} \tag{37}$$

Clearly, the choice of $H(\Omega)$ that will maximize the SNR. According to the Schwarz inequality is

$$\int A(\Omega)B(\Omega)\,d\Omega \leq \{\int A(\Omega)d\Omega\}\{\int B(\Omega)d\Omega\} \tag{38}$$

Applying the Schwarz inequality to SNR equation, we can get:

$$SNR = \frac{|y(t_m)|^2}{n_p} = \frac{\left|\frac{1}{2\pi}(\int_{-\infty}^{\infty} X(\Omega)H(\Omega)e^{-j\Omega t_m}d\Omega)\right|^2}{\frac{N_0}{4\pi}\int_{-\infty}^{\infty}|H(\Omega)|^2 d\Omega} \leq \frac{\left(\frac{1}{2\pi}\right)^2\left|\int_{-\infty}^{\infty} X(\Omega)e^{-j\Omega t_m}d\Omega\right|^2\left|\int_{-\infty}^{\infty} H(\Omega)d\Omega\right|^2}{\frac{N_0}{4\pi}\int_{-\infty}^{\infty}|H(\Omega)|^2 d\Omega} \tag{39}$$

Therefore, the SNR is maximized when

$$H(\Omega) = \alpha X^*(\Omega)e^{-j\Omega t_m} \tag{40}$$

In time domain, it will be:

$$h(t) = \alpha x^*(t_m - t) \tag{41}$$

This receiver filter, $H(\Omega)$ is called a matched filter, because the response is "matched" to the signal waveform and can maximize the SNR of the radar system.

5.4 Target Detection

Doppler processing is the term applied to filtering or spectral analysis (FFT) the signal received from a fixed range over a period of time corresponding to several chirps. In general, the slow time signal of a range bin consists of noise, clutter, and the echo from target. If the reflection power from the target below the clutter power or noise, the target cannot be detected. Therefore, the noise and clutter can be removed in the first step of the target detection, as shown in the Fig.19.

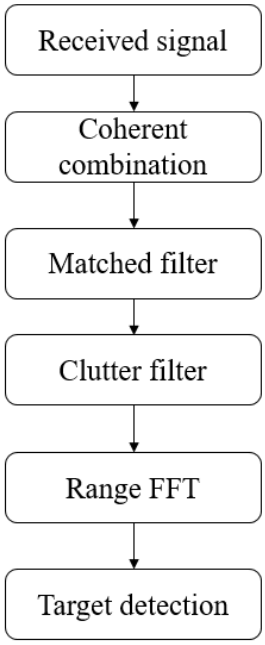

Fig.19 the flow diagram for the wall position estimation

After passing through the matched filter, the noise and clutter in the chirp data can be removed by:

$$y(t,N) = y(t,N) - mean\,(y(t,N)) \tag{42}$$

We perform the FFT algorithm for each chirp in order to get the target range information, and it is called range FFT processing, as Fig.15.

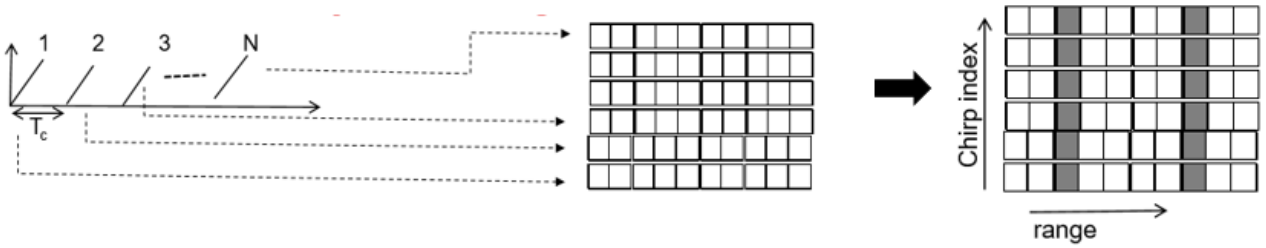

Fig.20 the range FFT[87]

In Psych center data, we used two different methods for detecting target:

- Constant false alarm rate (CFAR) detection method
- Cross correlation detection method

A. Constant false alarm rate (CFAR) detection method

Constant false alarm rate (CFAR) detection, also frequently referred to as "adaptive threshold detection" or "automatic detection", is a set of techniques designed to provide predictable detection and false alarm behavior in realistic interference scenarios.

In psych center data processing, we used the cell-averaging CFAR, which used adaptive calculation of the threshold for the CFAR detection.

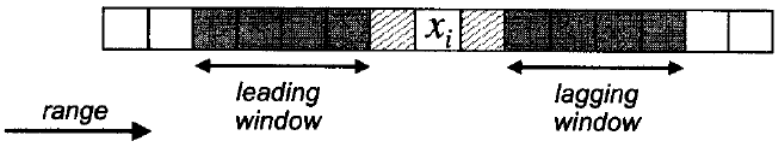

(a)

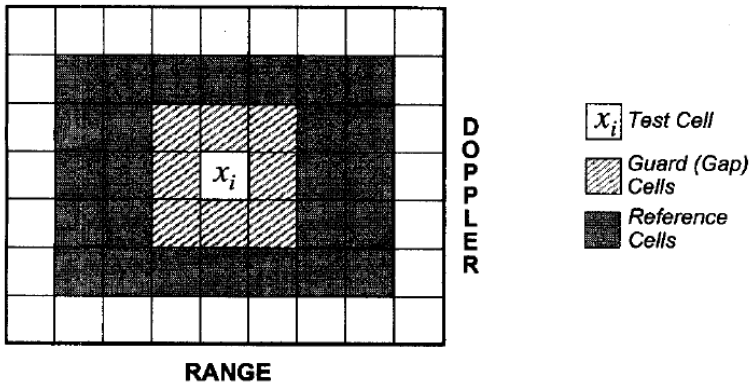

(b)

Fig.21 CFAR windows[4]. (a) one-dimensional window for range-only processor. (b) two-dimensional window for range-Doppler processor

Fig. 20 (a) shows a one-dimensional data vector of range cells with the cell under test, x_i, in the middle. The data in grey cells to either side, representing data from ranges nearer and farther from the radar than the cell under test, are averaged to estimate the noise parameter. These cells are called the reference cells. The cross-hatched cells immediately adjacent to the cell under test, called guard cells, are excluded from the average. Generally, more than one guard cell would be skipped on each side of the cell under test. The combined reference cells, guard cells and cell under test are referred to as the CFAR window. Fig. 16(b) shows two dimensional CFAR windows, which is used for psych center target detection. The estimated threshold is defined as:

$$\hat{T} = \frac{\alpha}{N}\sum_{i=1}^{N} x_i \tag{43}$$

For a given false alarm power $\overline{P_{FA}}$, the required threshold multiplier, α is

$$\alpha = N(\overline{P_{FA}}^{-\frac{1}{N}} - 1) \tag{44}$$

B. Cross correlation detection method

p_i and p_j denote the two received signal power from two chirps, $i\ and\ j$, and can be represented as [92-94]:

$$p_i = s_i + n_i \tag{45}$$

$$p_j = s_j + n_j \tag{46}$$

s_i and s_j are signal power, and n_i and n_j are the noise power. We assume the noises are the zero mean additive white Gaussian noises. Calculating the cross correlation between the two chirps:

$$R_{p_i p_j} = E[p_i p_j] = E[(s_i + n_i)(s_j + n_j)] = E[s_i s_j] + E[s_i n_j] + E[n_i s_j] + E[n_i n_j] \tag{47}$$

The signals are from two chirps are correlated, but the noise are not correlated because they are random, therefore,

$$E[s_i n_j] = E[n_i s_j] = E[n_i n_j] = 0 \qquad i \neq j \tag{48}$$

Finally, we can increase the signal-to-noise ratio of the signal, and it will be a more accurate way to detect the target.

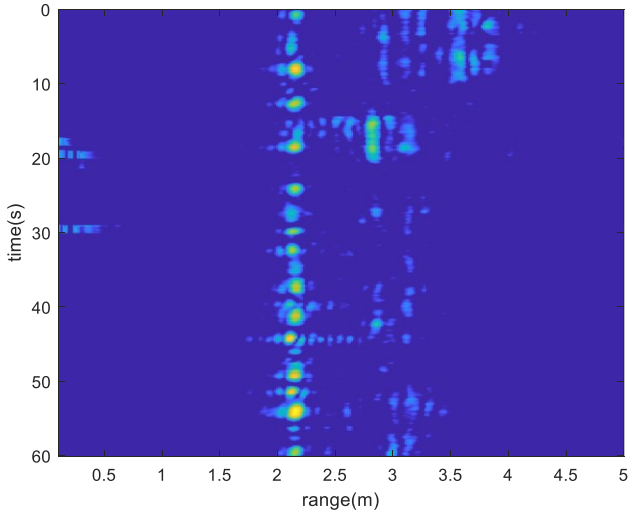

(a)

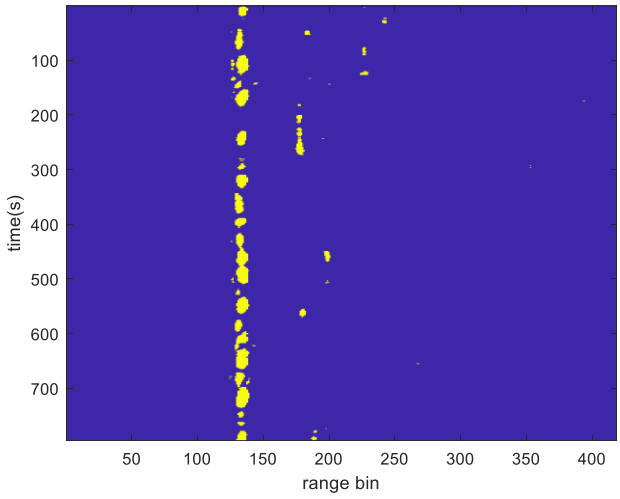

(b)

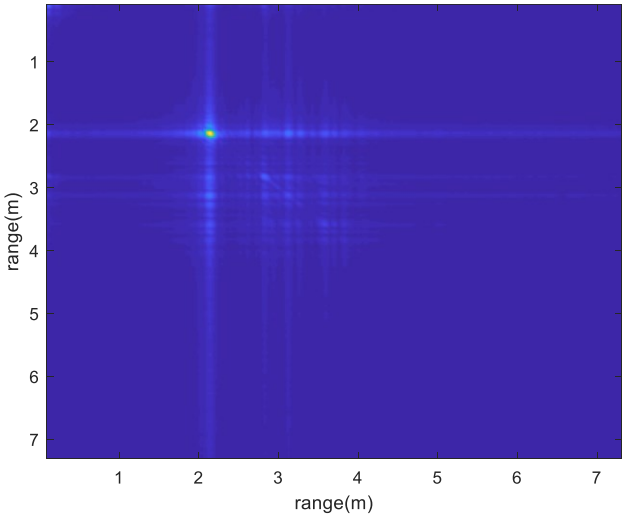

(c)

Fig.22 Target detection (a) range FFT results, (2) CFAR detection results, (c) cross correlation results

The target position shows in the area 2.3m from the range FFT results in the Fig.21 (a). The target's range bin shows 148 around from the CFAR detection in the Fig.21 (b). The cross-correlation results in the Fig.21 (c) indicates the target's position in the area 2.1m--2.3m. Compared those three results, we can get a more accurate target position and the

range bin. The range bins from range FFT, CFAR, and the Cross-correlation algorithm were used the features to classify the in bed vs. out of bed.

VI. Out of Bed vs. in Bed Classification

6.1 Preprocessing

6.1.1 Outlier Removal

An outlier is defined as the point that lies very far from the mean of the corresponding random variable [95 -98].

The radar data has many multipath signals, and the noise from the environment. This will cause the outlier problem. The noise data and the multipath signal are very far from the mean of the data set and will produce large errors during the training data set and may have disastrous effects. In order to get higher accuracy for the classification, first, we need to remove those outliers. This distance is measured with respect to a given threshold, usually a number of times the standard deviation. For a normally distributed random variable, a distance of two times the standard deviation covers 95% of the points, and a distance of three times the standard deviation covers 99% of the points. We defined the threshold that is two times standard deviation, and removed the outlier points.

6.1.2 Data Normalization

We used the different features in the classification process. The features ranges have big differences, some features have large values, such as PSD, and some features have small values, such as the phase variation. The features with large value may have larger influence in the cost function than features with small values, although this does not necessarily reflect their respective significance in the design of the classifier. Therefore, we need to

normalize all features after outlier removal processing. For N available data of features, we have the mean, μ, and the variance, σ, of the data set:

$$\mu = \frac{1}{N}\sum_{i=1}^{N} x_i \tag{49}$$

$$\sigma^2 = \frac{1}{N-1}\sum_{i=1}^{N}(x-\mu) \tag{50}$$

Then the normalized features x_N:

$$x_N = \frac{x-\mu}{\sigma^2} \tag{51}$$

6.1.3 Missing Data

Missing data is a common problem in the engineering application. For example, the wireless communication system. The radar is the wireless commutation system, which consists of the transmitter and the receiver. The transmitter transmitted the radio frequency signal, and the receiver collected the signal by reflecting objects. But the receiver signal will be included in the target signal, the multipath signal, and the noisy signal. If the signal-to-noise ratio is low, the data of the receiver will be missed during the outlier removal processing. The most common techniques in dealing with missing data include schemes that:

- All missing data is equal to zero.
- All missing data is equal to the mean of observed data.
- All missing data is equal to the $[\mu - \beta\sigma, \mu + \beta\sigma]$, where μ is the mean of observed data, σ is the variance of observed data.

All missing data of the radar in the Psych center project is imputed by the mean of observed data.

6.1.4 Classifier and Confusion Matrix

The classifier's role is to divide the feature space into the regions that corresponding to either class A or class B. If a feature vector **x**, corresponding to an unknown pattern, falls in the class A region, it classified as class A, otherwise as class B. This does not necessarily mean that the decision is correct. If it is not correct, a misclassification has occurred. Therefore, we used the confusion matrix to evaluate the classifier performance. In the confusion matrix in the Fig. 23, the accuracy and the recall will be calculated by:

$$acurracy = \frac{TP+TN}{TP+TN+FP+FN} \tag{52}$$

$$recall = \frac{TP}{TP+FN} \tag{53}$$

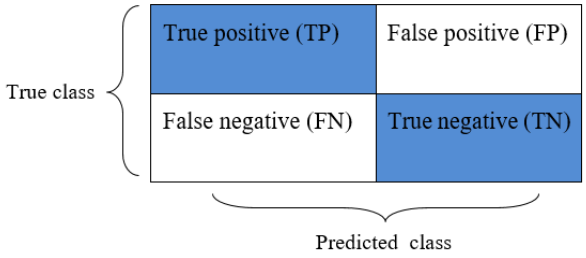

Fig.23 Confusion matrix

6.2 Classification Results for Out of Bed vs. In Bed

6.2.1 Single Patient's Balanced Data Classification

During the nighttime period, the patients in the Psych center spent most of their time in bed; therefore, the dataset collected was imbalanced for classifying two classes that are patient in bed vs. patient out of bed. At the beginning, we started from the balanced data of one patient. We used five features:

- PSD: power spectrum density
- Phase: phase information of target's range bin

- Phase variation: phase variation of target's range bin

We normalized those three features, and created two new features:

- feature x_3 is generated by:

$$x_3 = PSD * phase * phase\ variation \tag{54}$$

- feature x_8 is created by:

$$x_8 = e^{(phase-PSD)^2} \tag{55}$$

a) The depth camera and nurse's notes

The depth camera data and the nursing notes in the log are used as the ground truth of the radar data. The depth camera data is labeled manually. For instance, the data are from the patient whose ID is 4; patient information is given in Table III.

Table.V Patient ID=4 information

Patient ID	Sex	Age	Height	Weight	BMI	Start time	End time
4	M	19	113	182.8	34	21:00 pm	6:00 am

The nurse's notes in the log show the patient came to the bed between the 21:20 pm to 21:43 pm in the Fig. 24 (a). Then, we checked the camera data; the depth camera results show the patients came to bed at 21:38 pm, as illustrated in the Fig. 24 (b). In addition, the patient went to the bathroom at 04:46 am, according to the depth data.

CLINICAL PATIENT INFO		
09/18/2019 06:50 CDT	Patient Room	Sleeping
09/18/2019 06:15 CDT	Patient Room	Sleeping
09/18/2019 06:00 CDT	Patient Room	Sleeping
09/18/2019 05:45 CDT	Patient Room	Sleeping
09/18/2019 05:39 CDT	Patient Room	Sleeping
09/18/2019 05:15 CDT	Patient Room	Sleeping
09/18/2019 05:03 CDT	Patient Room	Sleeping
09/18/2019 04:51 CDT	Patient Room	Sleeping
09/18/2019 04:35 CDT	Patient Room	Sleeping
09/18/2019 04:20 CDT	Patient Room	Sleeping
09/18/2019 04:05 CDT	Patient Room	Sleeping
09/18/2019 03:51 CDT	Patient Room	Sleeping
09/18/2019 03:36 CDT	Patient Room	Sleeping
09/18/2019 03:17 CDT	Patient Room	Sleeping
09/18/2019 03:00 CDT	Patient Room	Sleeping
09/18/2019 02:45 CDT	Patient Room	Sleeping
09/18/2019 02:32 CDT	Patient Room	Sleeping
09/18/2019 02:19 CDT	Patient Room	Sleeping
09/18/2019 02:05 CDT	Patient Room	Sleeping
09/18/2019 01:50 CDT	Patient Room	Sleeping
09/18/2019 01:37 CDT	Patient Room	Sleeping
09/18/2019 01:15 CDT	Patient Room	Lying in Bed
09/18/2019 01:02 CDT	Patient Room	Sleeping
09/18/2019 00:45 CDT	Patient Room	Sleeping
09/18/2019 00:34 CDT	Patient Room	Sleeping
09/18/2019 00:23 CDT	Patient Room	Sleeping
09/18/2019 00:03 CDT	Patient Room	Sleeping
09/17/2019 23:48 CDT	Patient Room	Sleeping
09/17/2019 23:23 CDT	Patient Room	Sleeping
09/17/2019 23:05 CDT	Patient Room	Sleeping
09/17/2019 22:54 CDT	Patient Room	Sleeping
09/17/2019 22:34 CDT	Patient Room	Sleeping
09/17/2019 22:18 CDT	Patient Room	Sleeping
09/17/2019 22:03 CDT	Patient Room	Sleeping
09/17/2019 21:50 CDT	Patient Room	Sleeping
09/17/2019 21:43 CDT	Patient Room	Sleeping
09/17/2019 21:19 CDT	Day/Dining Room	Sitting/Standing
09/17/2019 21:03 CDT	Day/Dining Room	Sitting/Standing
09/17/2019 20:54 CDT	Day/Dining Room	Sitting/Standing
09/17/2019 20:44 CDT	Day/Dining Room; Re	Interacting with othe
09/17/2019 20:22 CDT	Day/Dining Room	Sitting/Standing
09/17/2019 20:12 CDT	Day/Dining Room	Sitting/Standing
09/17/2019 19:59 CDT	Day/Dining Room; Da	Sitting/Standing; Inte
09/17/2019 19:42 CDT	Day/Dining Room	Sitting/Standing
09/17/2019 19:05 CDT	Off Unit	group

(a)

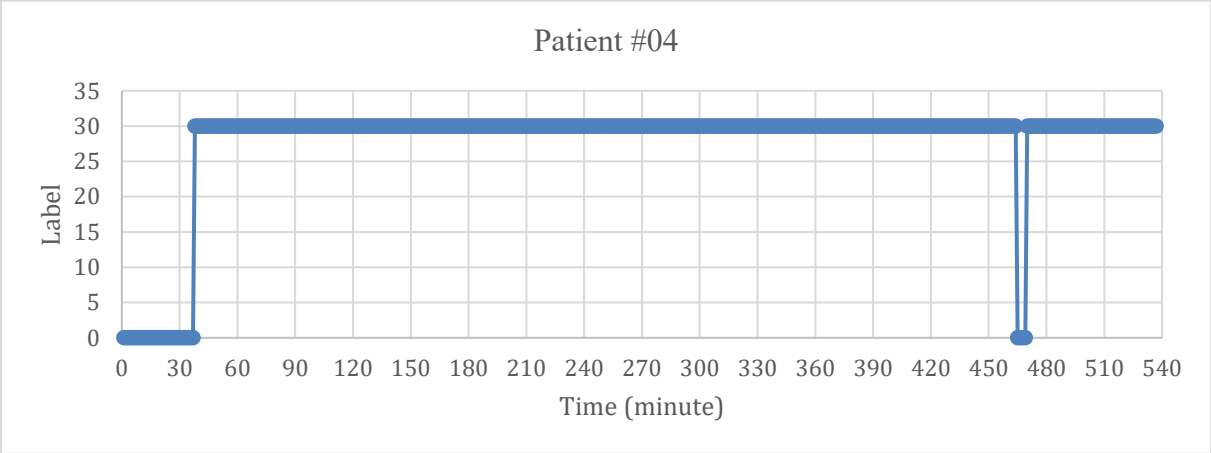

(b)

Fig.24 The Nurse's Notes and depth data. (a) Nurse's note in the log (b) depth camera information. Class 1 is empty bed, label is 1, and Class 2 is the patient in the bed, and label is 30

b) Classifying Empty bed vs. Bed with a person using two features

We used two features, phase and PSD, to classify two classes: Empty bed (class1) vs. Bed with a person (class2). One hour of data was used, with 30 minutes data from the empty bed class, and 30 minutes from the patient in bed class.

Table.VI Classifier with two features

Labels	Empty bed (class1) vs. Patient in bed (class2)
Features	PSD, phase
Data	Total one hour of data, with 30 minutes data from the empty bed class, and 30 minutes from the patient in bed class. 90% samples for training data, 10% samples for testing data; the process is repeated 10 times (10 fold cross validation)
Statistics	RBF
Classifier	SVM

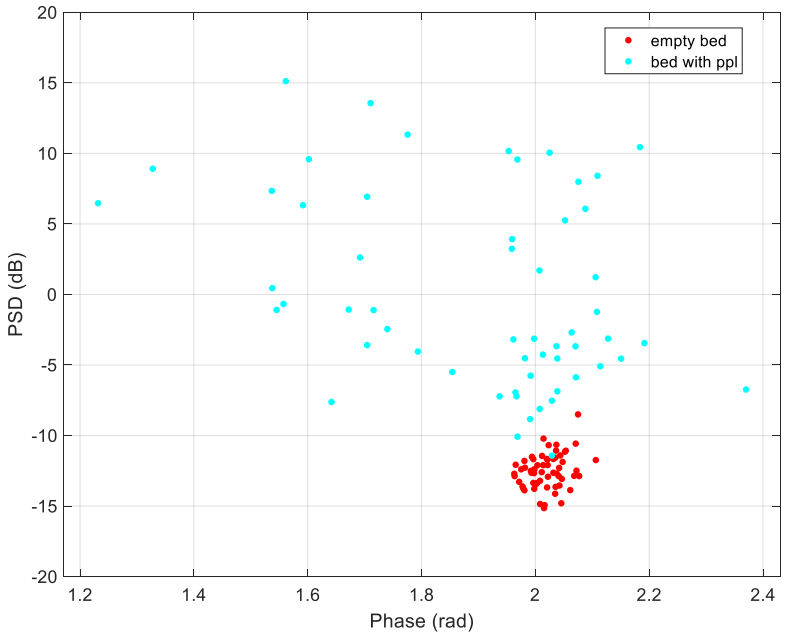

(a)

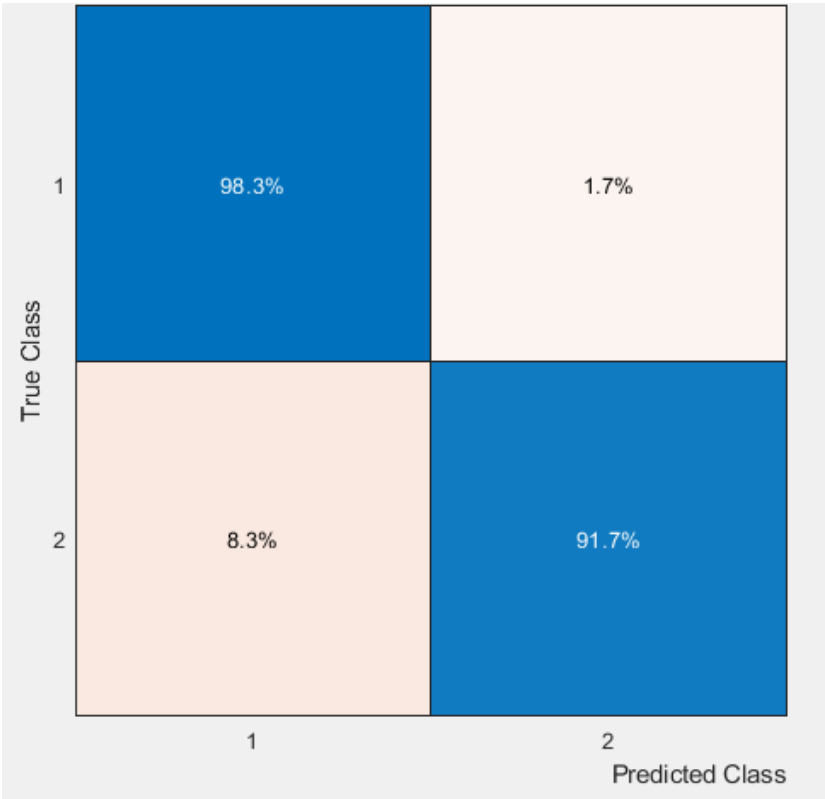
98.3%
1.7%
8.3%
91.7%
1
2
True Class
1
2
Predicted Class

(b)

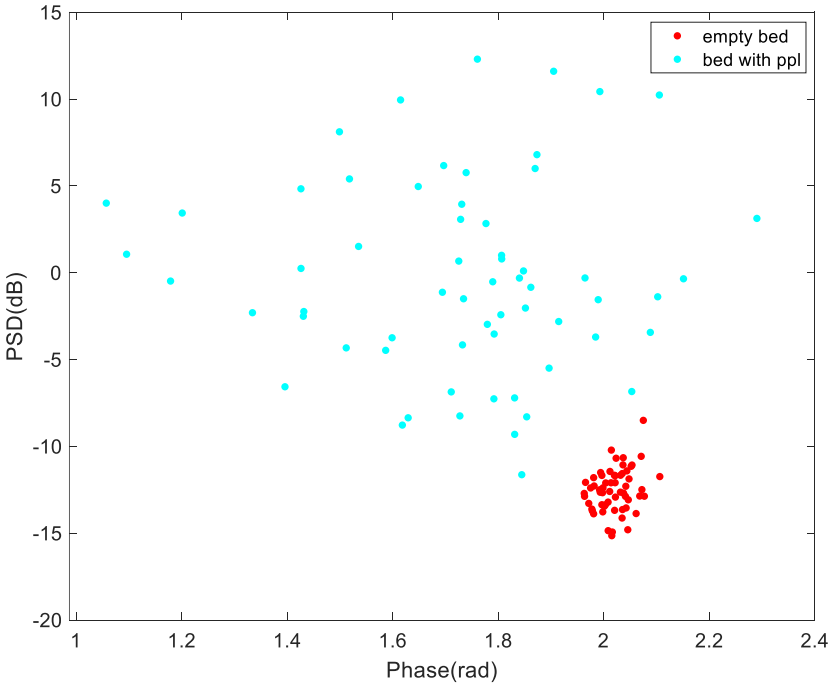
empty bed
bed with ppl
PSD(dB)
Phase(rad)
15
10
5
0
-5
-10
-15
-20
1
1.2
1.4
1.6
1.8
2
2.2
2.4

(c)

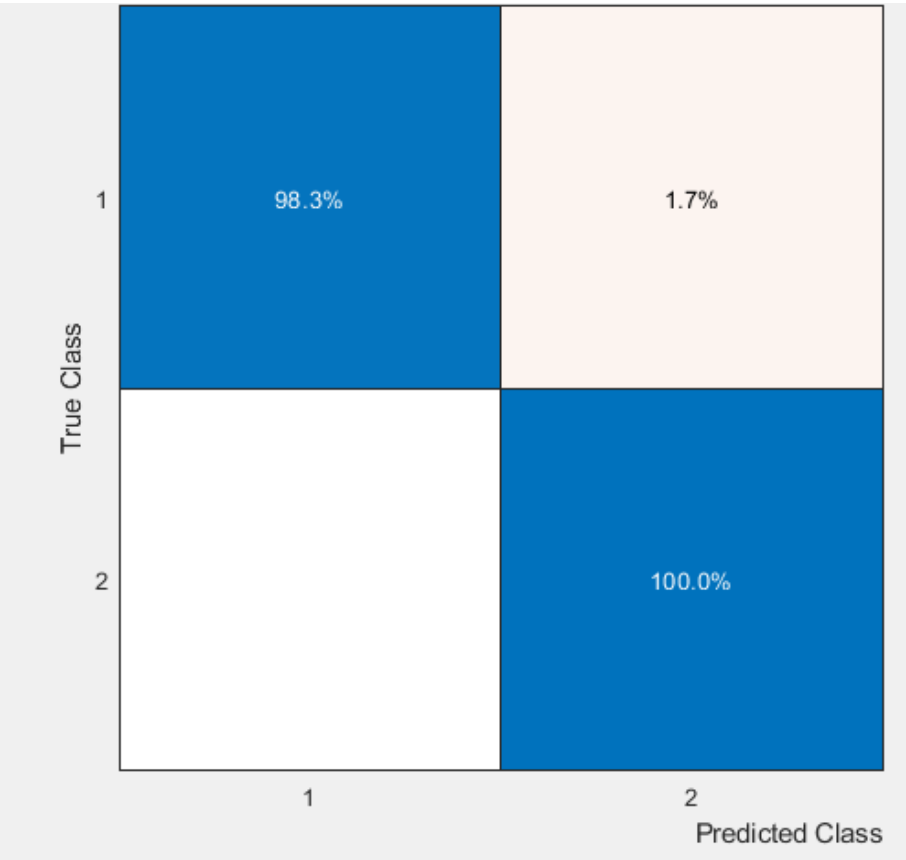

(d)

Fig.25 Classification by using two features (a) Class1: empty bed (red) class, and data collection time period: 21:00 – 21:30. Class 2: patient was lying in the bed (green) class, and data collection time period: 21:44 --- 22:14. (b) Confusion matrix for (a), (c) Class1: empty bed (red) class, and data collection time period: 21:00 – 21:30. Class 2: person was lying in the bed (green) class, and data collection time period: 12:00 am --- 12:30am, (d) Confusion matrix for (c)

c) Classifying Empty bed vs. Bed with a person using three features

We used three features, phase variation, feature x_3 and feature x_8 , to classify two classes: Empty bed (class1) vs. Bed with a person (class2). First, the outliers in all features are removed, then, the features are normalized by the method in the Section 6.1.2, using the mean of the observed data set. One hour of data was used, with 30 minutes data from the empty bed class, and 30 minutes from the patient in bed class.

Table.VII Classifier with three features

Labels	Empty bed (class1) vs. Patient in bed (class2)
Features	phase variation (x_5), x_3, x_8
Data	Total one hour samples data, with 30 minutes data from the empty bed class, and 30minutes from patient in bed class. 90% samples for training data, 10% samples for testing data; the process is repeated 10 times (10 fold cross validation)
Kernel Function	RBF
Classifier	SVM

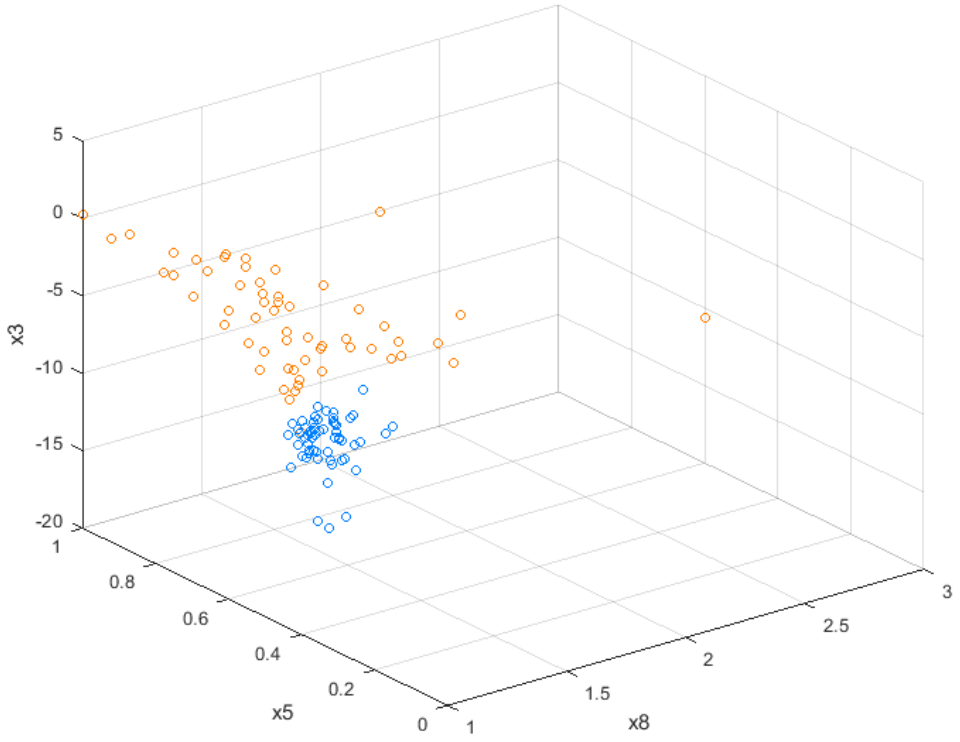

(a)

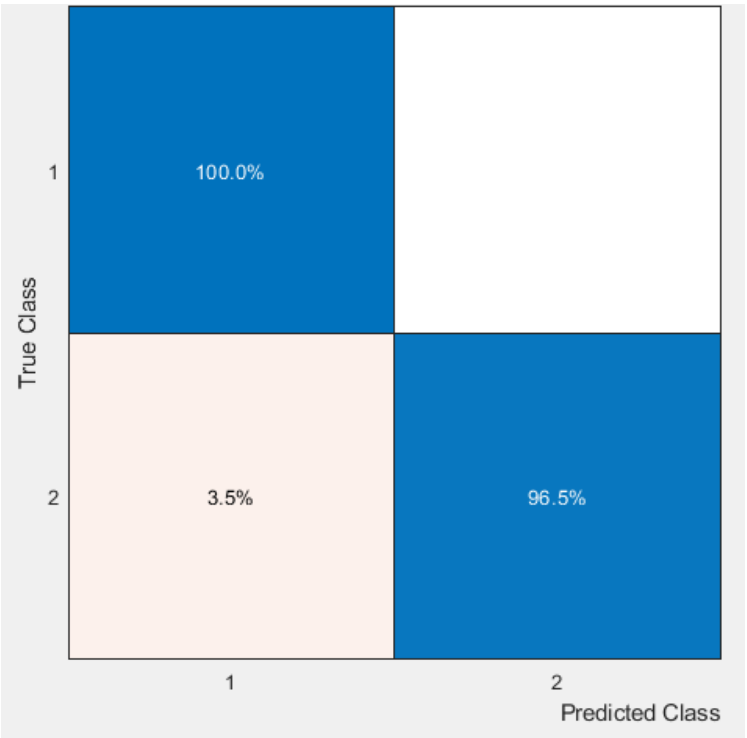
100.0%
3.5%
96.5%
True Class
Predicted Class
1
2
1
2

(b)

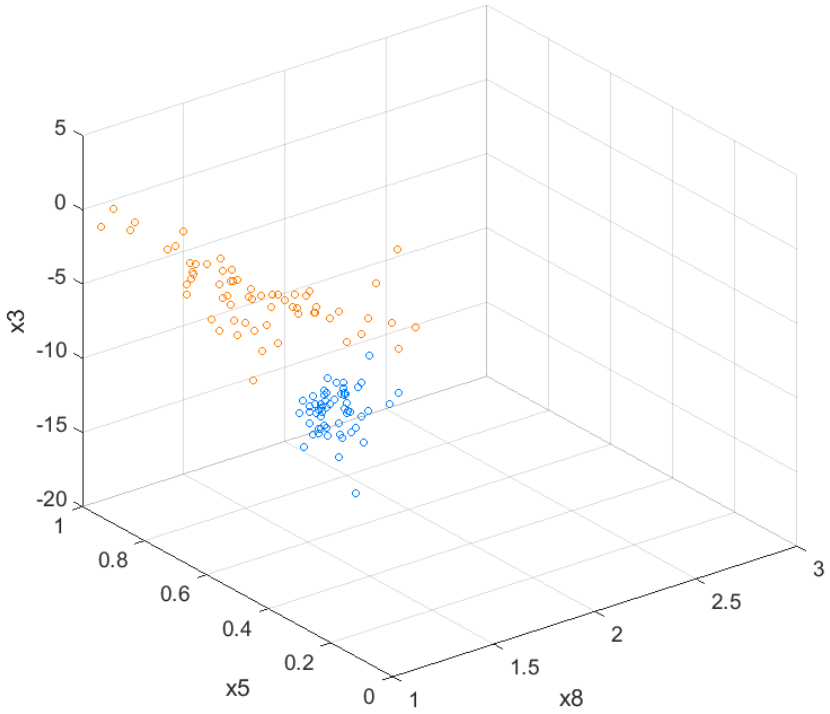
x3
x5
x8
5
0
-5
-10
-15
-20
1
0.8
0.6
0.4
0.2
0
1
1.5
2
2.5
3

(c)

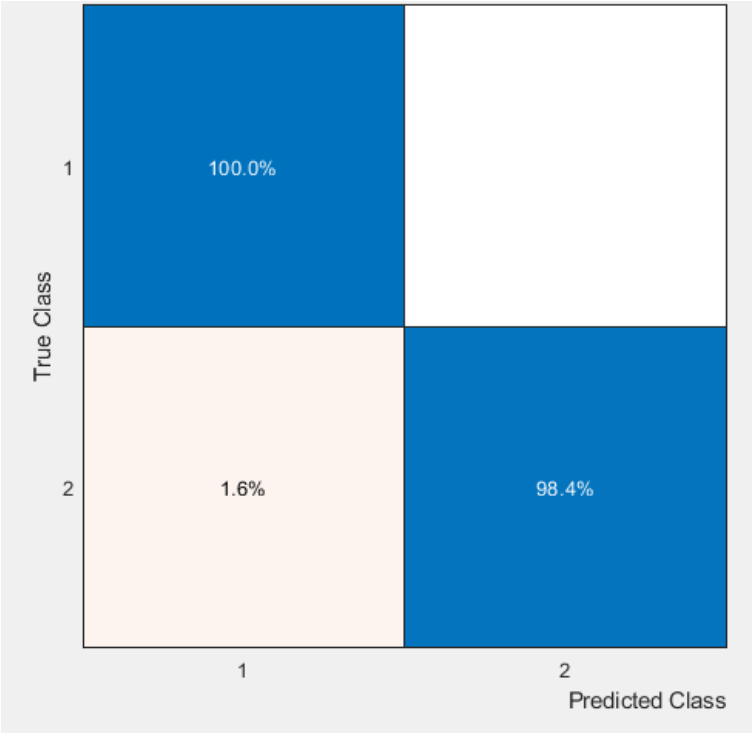

(d)

Fig.26 Classification by using three features (a) Scatter plot. Class1: empty bed (blue) class, and data collection time period: 21:00 – 21:30. Class 2: patient was lying in the bed (orange) class, and data collection time period: 21:44 --- 22:14. (b) Confusion matrix for (a), (c) Scatter plot. Class1: empty bed (blue) class, and data collection time period: 21:00 – 21:30. Class 2: person was lying in the bed (orange) class, and data collection time period: 12:00 am --- 12:30am, (d) Confusion matrix for (c)

6.2.2 Single Patient's One Night Data Classification

We used the same features in Section 6.1.1 for classifying one full night of data for the same patient. First, the outlier in all features are removed, then, the features are normalized by the method in Section 6.1.2, using the mean of the observed data set. The classifier information as follows:

Table.VIII Classifier for one night data

Labels	Empty bed (class1) vs. Patient in bed (class2)
Features	PSD, phase, phase variation (x_5), x_3, x_8
Data	Total 9 hours data for one patient
Kernel Function	RBF
Classifier	SVM

a) We used the same features, same classifier and the same patient's one night data as in Section 6.1.1; the results are shown in Fig. 27(a). There were 39 data samples from class 1, and 481 data samples from class 2. If we use the same classifier as in Section 6.1.1 to the imbalanced data set, the results are shown below:

Accuracy = 92%

Recall = 0%

b) We used the same features, same classifier as in Section 6.1.1, but used a second full night of data which was from the patient whose ID is 1; results are shown in Fig.. 27(b). There were 124 data samples from class 1, and 386 data samples from class 2. If we use same classifier as in Section 6.1.1 to that imbalanced data set, and we got the accuracy and the recall as follows:

Accuracy = 99%

Recall = 97%

c) We used the same features, same classifier as in Section 6.1.1, but used a third one night data which was from the patient whose ID is 7, the results are shown in the Fig .27(c). In this case, there was not any data sample from class 1, and 505 data samples from class 2. If we used same classifier in the Section 6.1.1 to those imbalanced data set, and we got the accuracy and the recall as follows:

Accuracy = 99%

Recall = 100%

Empty bed	0	39	0%	100%
Person in bed	5	476	1%	99%

(a)

Empty bed	123	1	99%	1%
Person in bed	4	382	1%	99%

(b)

Empty bed	0	0	100%	0%
Person in bed	1	504	1%	99%

(c)

Fig.27 Confusion matrix. (a) Confusion matrix of one night data classification for Patient ID=4. (b) Confusion matrix of one night data classification for Patient ID=1. (c) Confusion matrix of one night data classification for Patient ID=7.

6.2.3 Discussion

In this section, we used five features, PSD, phase, phase variation, feature x_3, and feature x_8, to classify the out of bed vs. in the bed classes. We offer the following conclusions.

1) When the data is a balanced data set from one patient at every 30 minutes, the classifier SVM with kernel function RBF has higher accuracy and higher recall to classify two classes.
2) When the data is an imbalanced data set from one patient at one night, the accuracy and the recall of the classifier SVM with kernel function RBF depends on the level of data imbalance.
3) If the data is totally imbalanced, such as, less than 10% samples data from class 1, and more than 90% samples from class 2, the recall and the accuracy of the SVM would be low.

4) If the data is imbalanced, for instance, more than 20% samples data from class 1, and less than 80 % data from class2, the recall and the accuracy of SVM would be higher.
5) If the data is imbalanced, there was no sample data from class 1, and all samples were from class2, the recall and the accuracy of SVM would be higher.

6.3 Imbalanced Data Set Classification for The Out of Bed vs. In The Bed

In the psych center, we have seven different patients, and the patient's information is shown in Table I. We have 6 male patients and one female patient, and their ages are from 19 to 49. We used six patient data to train the classifier, and out of one patient data for testing the classifier. In order to improve classifier accuracy for an imbalanced data set, we increased the feature number to 12. Those features are important, simple to extract, and useful for discriminating patterns in different classes [90,95].

1) PSD

We can calculate the periodogram:

$$P_{xx}^{i}(f) = \frac{1}{M}\left|\sum_{n=1}^{M} x_i(n)\, e^{-j2\pi f n}\right|^2 \qquad i = 0,1,\ldots K-1$$

We obtain PSD:

$$P_{xx}^{B}(f) = \frac{1}{K}\sum_{i=0}^{K} P_{xx}^{i}(f)$$

2) Accumulation of PSD
3) PSD variation

$$var[P_{xx}^{B}(f)] = \frac{1}{K^2}\sum_{i=0}^{K} var(P_{xx}^{i}(f))$$

4) Mean of PSD

$$E[P_{xx}^{B}(f)] = \frac{1}{K}\sum_{i=0}^{K} E(P_{xx}^{i}(f))$$

5) Phase of target's range bin

6) Phase variation of target's range bin

7) Phase standard deviation of target's range bin

8) Mean of phase variation

9) Mean phase standard deviation

10) Target's range bin from cross correlation algorithm

11) Target's range bin from range FFT

12) Created new Feature 12 was by:

$$\text{Feature12} = \text{Feature1} * \text{Feature 11}$$

Table.IX Classifier for imbalanced data set

Labels	Empty bed (class1) vs. Patient in bed (class2)
Features	12 features
Data	Total number of patients are seven, we used the data from six patients for training, and of the remaining patient's data for testing , (10-fold cross validation for all patients' data)
Kernel Function	polynomial function
Classifier	SVM

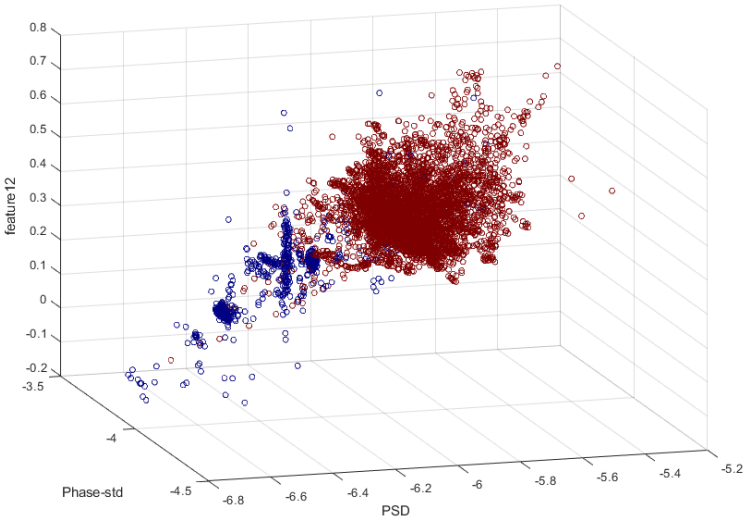

(a)

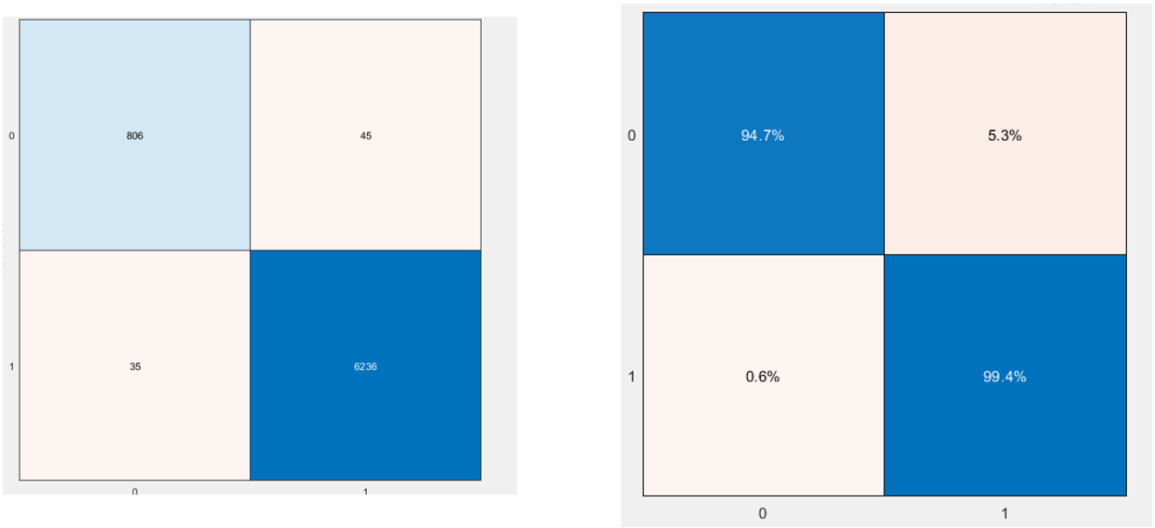

(b)

Fig.28 Psych Center data classification. (a) Scatter plot. (b) Confusion matrix, class 1 is empty bed and labeled 0, class2 is person in bed and labeled 1

We used seven patients, and 12 nights of data to train the classifier. The classifier used the SVM algorithm with polynomial kernel function. 12 features were used to the classifier. From the results in Fig.26 (b), we can see that the classifier has 97% accuracy and 96% recall to the imbalanced data set from Psych Center.

VII. Respiration Rate Estimation

7.1 Respiration Estimation in Different Sleeping Postures

Our target application of monitoring patients in a psychiatric hospital offers additional challenges over previous related work. Due to safety concerns, sensors must be non-contact and without any components accessible, including wires, cables, or even units mounted in view on the wall. In our current IRB-approved study in a Psychiatric Center, sensors were embedded into the area above the ceiling and mounted over the bed at a height of 2.3 m. We have simulated this set-up in the lab, where a respiration belt is used for ground truth and tested the system with body postures of patients observed in the psychiatric hospital. We present work on respiration rate estimation with different sleep postures, with the aim of investigating a contactless monitoring system for psychiatric patients in the hospital that can estimate the breathing rate of patients during typical sleeping postures, and find the torso area when the patients use other postures, such as reading books in bed or reversing the body on the bed.

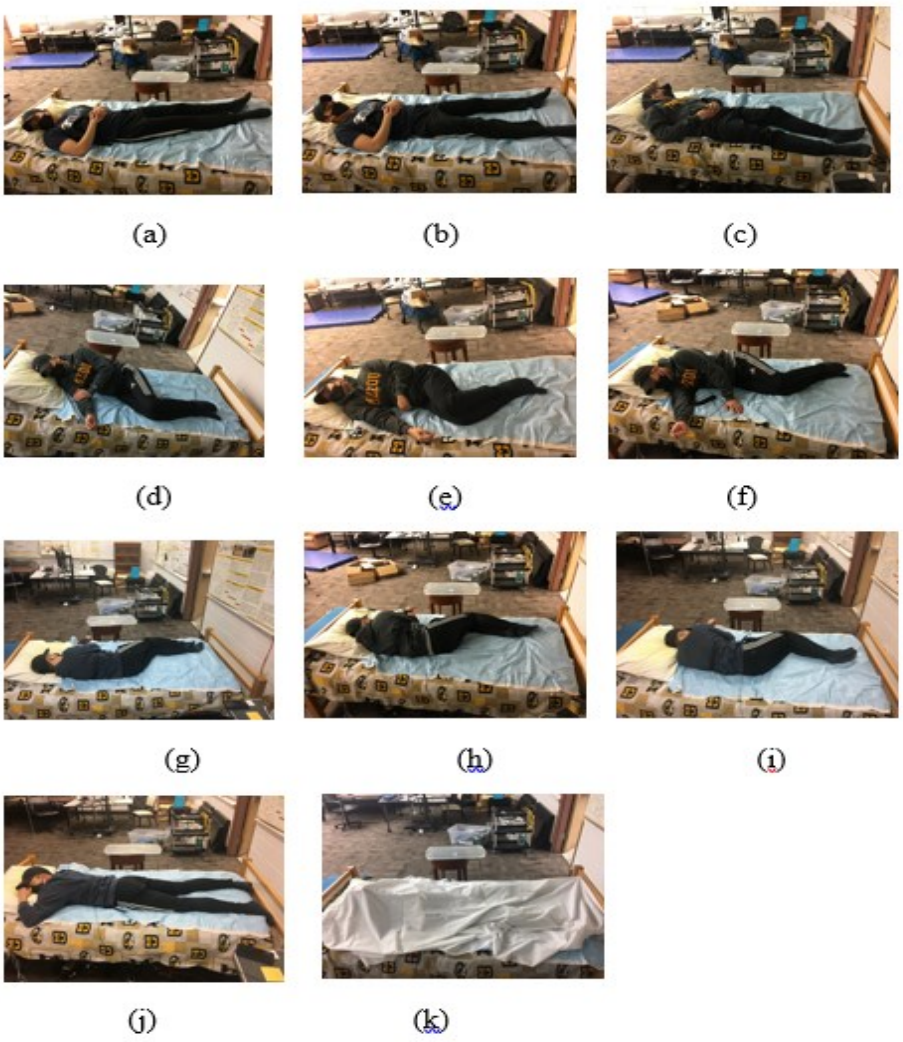

Fig.29 Eleven test sleeping postures. (a)-(c) Back. (d)-(f) Right side. (g)-(i) Left side. (j) Stomach. (k) Covered with a blanket

7.2 Signal Processing

A. RF Sensor

The RF sensor was constructed using the Vayyar Radar system with a carrier frequency of 6.014 GHz to capture all reflections by the FMCW (frequency modulation continuous waveform) signal. The RF sensor has 27 antennas, 14 transmitting antennas and 13 receiving antennas. Each frame has 182 chirps, each chirp has 187 samples, and each

sample has two quadrature channels. The radar bandwidth is 1.75 GHz, and the range resolution is 8.6cm.

The carrier frequency f_c of the RF sensor is 6.014 GHz, the radar wavelength is 5cm, and the angle resolution equal to 0.63 degrees.

The data were collected by the Vayyar radar system. The detectable distance was from 0 m to 5 m, the azimuth angle was from -45 degrees to 45 degrees, the elevation angle was from -45 degrees to 45 degrees. These radar parameters were fixed in the data acquisition system. All the data from the radar were stored in .mat files on the computer.

At the same time, the breathing rate was collected by a respiration belt for ground truth data. The respiration belt data was collected by a data acquisition system with a frequency of 1 kHz.

B. Finding the Person on the Bed

The .mat files included the following information: the TX-RX pairs, bandwidth, and the reflection signal from different distances. In order to combine the signal from different antennas, first, we used the multiple signal classification (MUSIC) algorithm for estimating the angle of arrival θ corresponding to the strongest signal. The received signal y for antenna n is represented by:

$$y[n] = Ae^{-j2\pi ndsin\theta/\lambda} \tag{56}$$

where d is distance between two antennas, 3cm, and A is the received power of the RF signal. Coherently combining the signal, $z(\theta)$ from different antennas over one minute, we use:

$$z(\theta) = A\sum_{n=0}^{N-1} e^{-j2\pi nd(sinsin\,(\theta) - sin\,(\theta_0))/\lambda} \tag{57}$$

where the beamforming steered angle θ_0 is equal to 0 degrees.

Second, the combined signals implemented the range FFT and the constant false alarm detection (CFAR) processing for detecting the subject position. For instance, if one subject slept on his back in the middle of bed (Fig.29 (b)), the received strong reflection from the subject shows in the area 2.3m from the RF sensor (as in Fig.31).

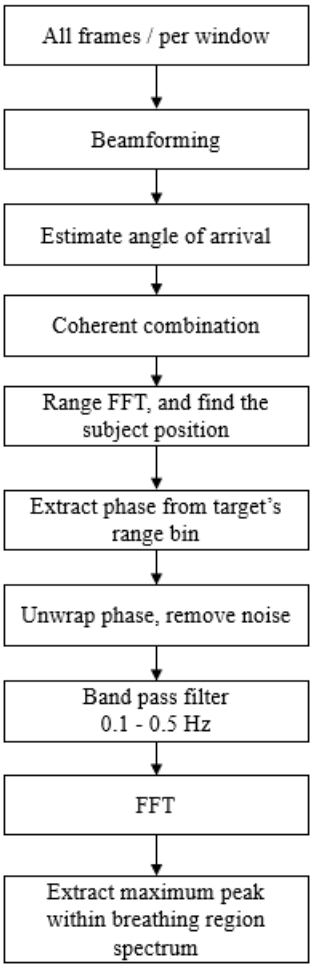

Fig.30 Flow diagram for respiration rate estimation

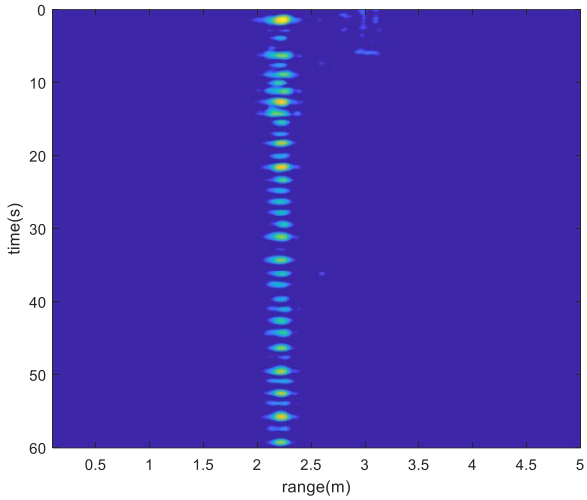

(a)

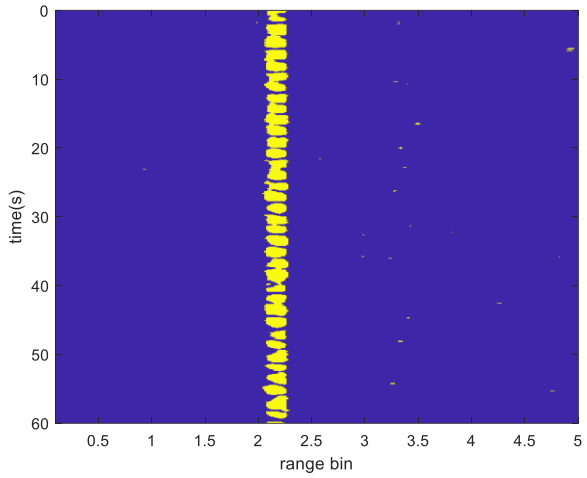

(b)

Fig.31 The subject position detection when sleeping on the back in the middle of bed. (a) range FFT (b) CFAR detection

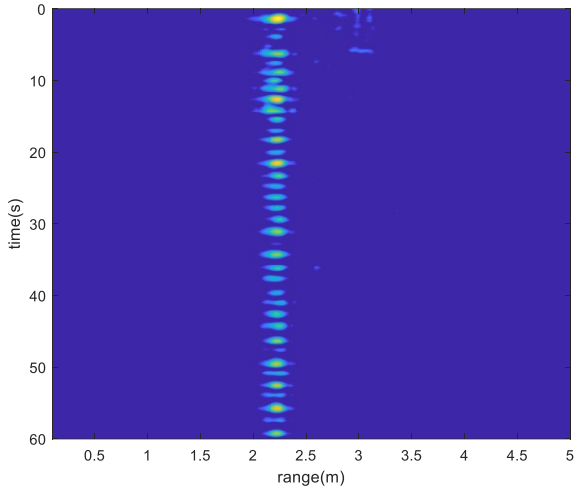
time(s)
range(m)
0
10
20
30
40
50
60
0.5
1
1.5
2
2.5
3
3.5
4
4.5
5

(a)

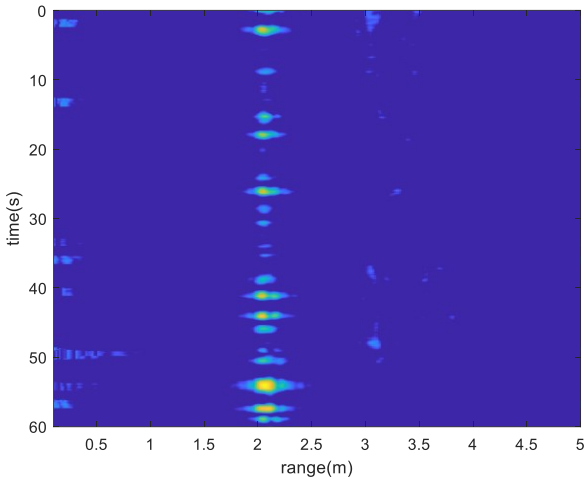
time(s)
range(m)
0
10
20
30
40
50
60
0.5
1
1.5
2
2.5
3
3.5
4
4.5
5

(b)

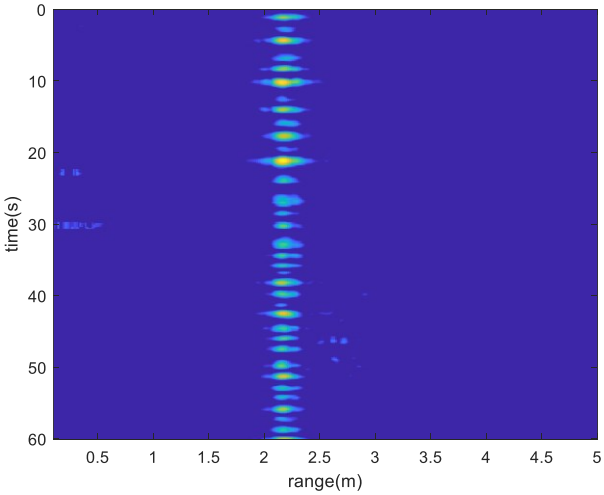
time(s)
range(m)
0
10
20
30
40
50
60
0.5
1
1.5
2
2.5
3
3.5
4
4.5
5

(c)

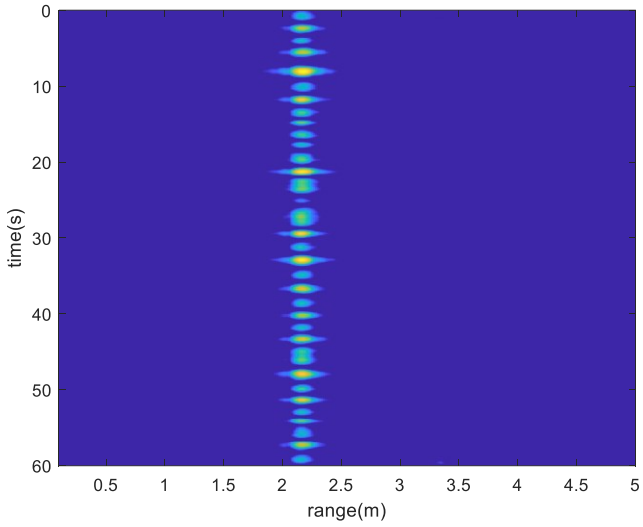

(d)

Fig.32 The Subject position detection, (a) back sleep, (b) side sleep (right), (c) stomach sleep, (d) Sleeping while covered by a blanket

C. Estimating Respiration Rate

After accurately locating the range bin, we extracted phase information corresponding to the range FFT peaks. We used the unwrapping of the phase information, removed the noise in the phase, filtered the phase, and implemented the FFT to the phase. The respiration rate then corresponds to the frequency of the dominant phase FFT peak within the breathing-region spectrum [17]. The respiration belt sensor is used as the ground truth of the RF sensor.

$$phase = unwrap(tan^{-1}(\frac{Q\ channel\ data}{I\ channel\ data})) \tag{58}$$

For instance, the respiration rate from belt sensor in Fig 33(a) is 18bpm. In same time period, the respiration rate from RF sensor in Fig.33 (b) is:

$$\text{Respiration rate} = 0.32*60 = 19\text{bpm} \tag{59}$$

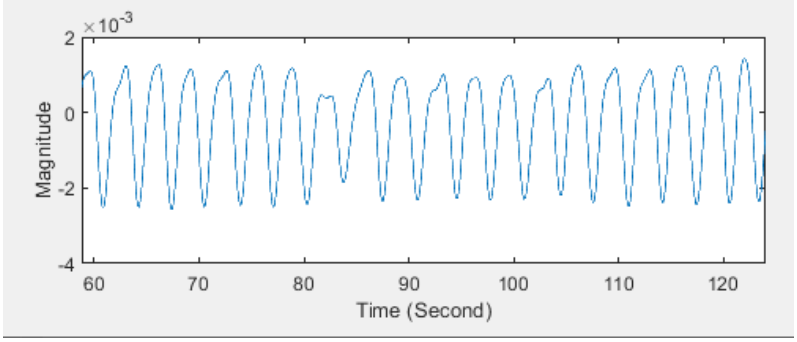

(a)

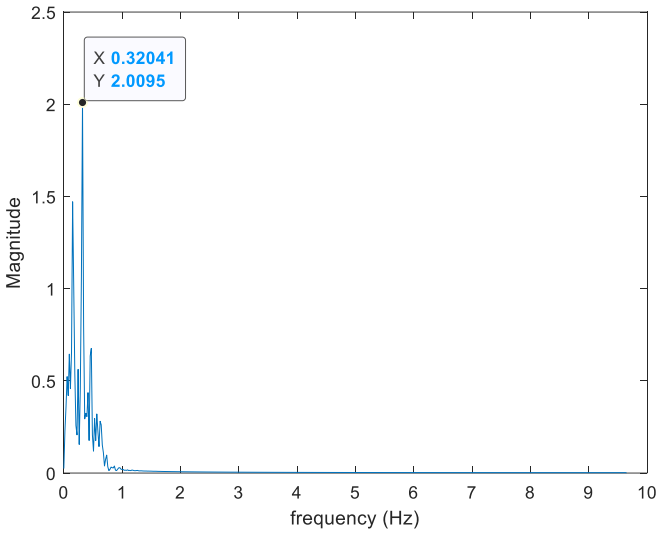

(b)

Fig.33 The respiration estimation. (a) Respiration signal from respiration belt sensor is used as the ground truth of RF sensor. (b) RF sensor respiration rate estimation

7.3 Finding Torso Area

In the psychiatric hospital setting, the patient has different postures on the bed. Some patients will read books or flip their head to the other side of the bed when they cannot sleep. This will cause a new challenge in finding the torso area for estimating the respiration rate (as in Fig.34).

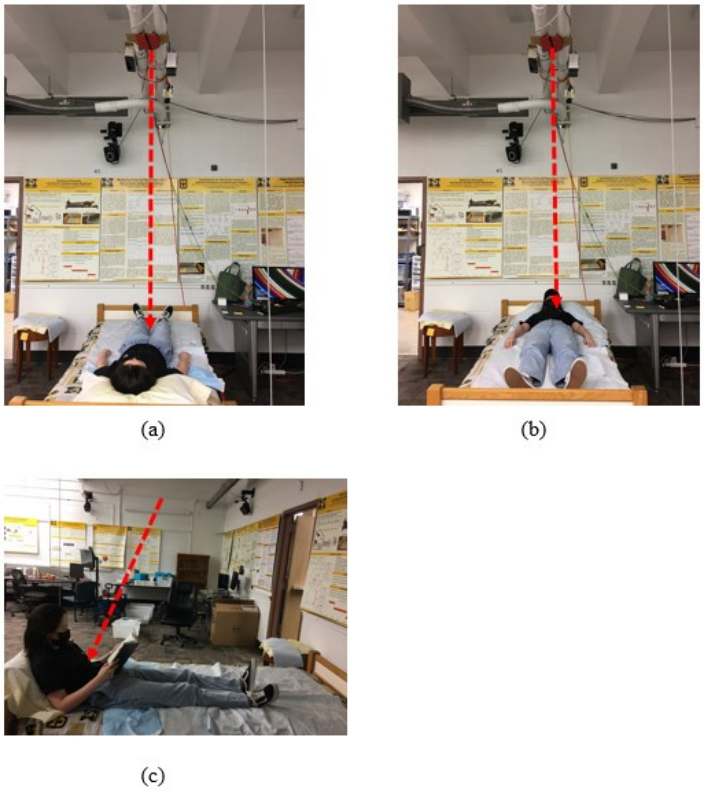

Fig.34 Sleeping postures (a) on the back. (b) reversing the body in bed. (c) sitting up in bed, reading

First, we need to distinguish the torso area from the leg area. The torso area of a human being is larger than the leg area; hence, the reflection signal from the torso will be stronger. For instance, the CFAR detection from legs is shown as Fig. 35(b), which is different from the reflection signal from the torso area in Fig. 35(a). Even if we extract the phase information from the range FFT peaks in the legs' reflection signal to estimate the respiration rate, the result will be much lower than a normal respiration rate of human beings because there is no phase vibration signal. Therefore, we can distinguish the legs from the torso area. To automate the process, we use steer beamforming from -45 degree to 45 degree by using a 5-degree step size to search for the torso area (see also Fig. 36).

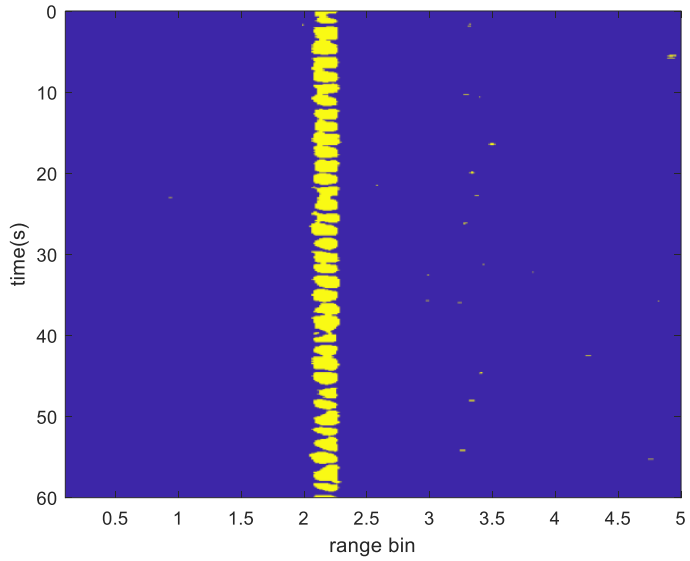

(a)

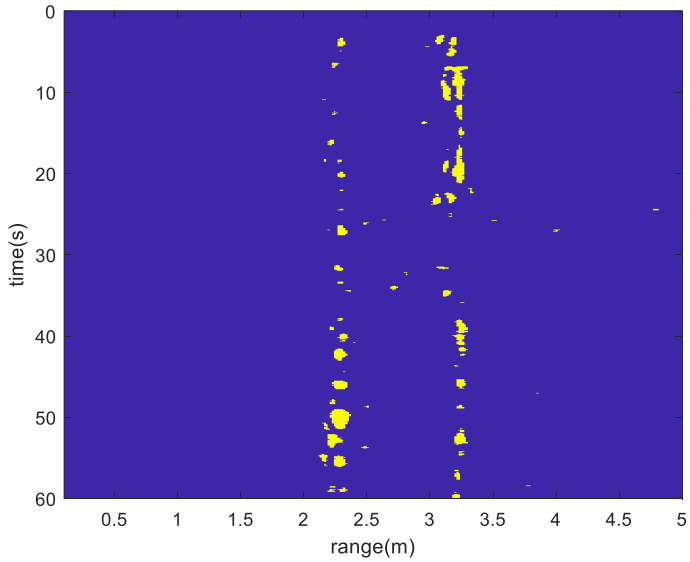

(b)

Fig.35 CFAR detection (a) back sleeping. (b) reflection signal from legs

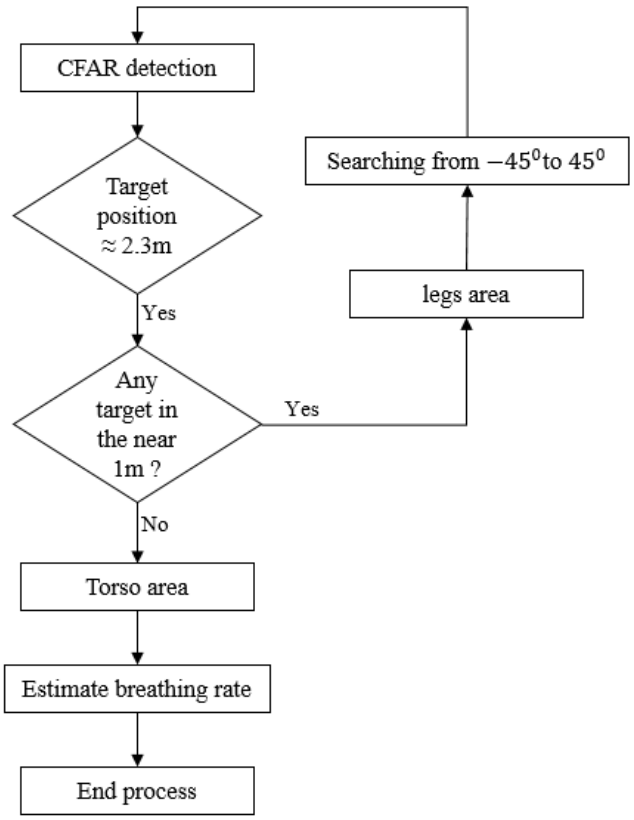

Fig.36 The flow diagram for finding torso area

7.4 Experimental Set Up and 2021 Lab Data Set Results

We present the respiration rate estimation via the RF sensor on different sleep postures. Data were collected from three healthy younger adults and two elder adults in a controlled lab setting; see Table II for subject details. Subject 1 and subject 2 were asked to lie on the bed in eleven different sleeping postures, as shown in Fig. 29. Five subjects were asked to flip their head to the opposite side of bed (see Fig. 34 (a) (b)). Subjects 3-5 were asked to sit up in bed while reading. The RF sensor was installed over the bed in the same position and distance to bed as the patient room setting in the University of Missouri Psychiatric Center.

A. Estimation of respiration on different sleeping postures

The RF sensor with the Vayyar radar was deployed on the ceiling of the Eldercare and Rehabilitation Technology lab, and the TX/RX antennas in the RF sensor are directed toward the torso area of the subjects. The data were collected by the RF sensor and the respiration belt sensor at same time. The respiration belt sensor's data were used as the ground truth for the respiration rate. The distance between the bed and the RF sensor was 2.3m, which was the same set-up as the patient hospital room in the Psychiatric Center.

In addition, we installed a depth sensor in the Psychiatric Center patients' room as a coarse ground truth of the RF system. That is, a patient's general location and body posture appear as shadowy silhouettes. According to the depth data, we found that there were eleven common sleeping postures of these patients. Hence, we asked each subject in this current lab study to emulate the most common sleeping postures, holding each posture for at least 6 minutes. The sleep postures are described below:

a) Back

The Psychiatric Center patients slept on their back much of the time, varying the angle of the body with respect to the bed (Fig.29 (a)-(c)).

b) Side

The side sleeping postures were also popular positions with the Psychiatric Center patients. These include both right side sleeping postures (Fig.29 (d)-(f)) and left side sleeping postures (Fig.29 (g)-(i)), again with varying angles of the body with respect to the bed.

c) Stomach

Some patients slept on their stomach (Fig.29 (j)).

d) Covered by a Blanket

A few patients preferred to sleep with a blanket covering the body and face. This is a test for capturing torso motion under the blanket.

We examined the respiration estimation algorithm accuracy on all eleven different sleeping postures (Fig.29). The results in Table X show the average respiration estimation accuracy on the three back postures is 92%. The average respiration estimation accuracy on the six side postures is 84%, the respiration estimation accuracy on the stomach position is 76%, and the respiration estimation accuracy on the case of a blanket covering is 90%.

Table.X Sleeping Postures and respiration rate Estimation Accuracy

Position	***Subject 1 Accuracy***	***Subject 2 Accuracy***
Back (a)	***90%***	***94%***
Back (b)	***93%***	***95%***
Back (c)	***91%***	***94%***
Right side (d)	***86%***	***95%***
Right side (e)	***88%***	***85%***
Right side (f)	***85%***	***80%***
Left side (g)	***82%***	***82%***
Left side (h)	***84%***	***86%***
Left side (i)	***80%***	***80%***
Stomach (j)	***75%***	***77%***
Covered by a blanket (k)	***90%***	***90%***

7.5 Estimation Results of Respiration Rate When the Torso Area's Position Was Changed

Additional body postures were tested, based on observations of the Psychiatric Center patients. According to the depth data, we found that some patients sit up in bed, while reading or flip their head to the opposite side of the bed when they cannot sleep. Hence, we asked each subject in this current lab study to emulate three sleeping postures, holding each posture for at least 5 minutes. The sleep postures are described below:

a) Back

The Subjects slept on their back much of the time (Fig.32 (a)).

b) Reverse Back

The Subjects slept on their back but flipped their head on the other side of the bed (Fig.32 (b)).

c) Sitting in bed

The Subjects read a book on the bed (Fig.32 (c)).

We examined the torso area searching algorithm for respiration estimation accuracy on three different sleeping postures. The results in Table XI show the average respiration estimation accuracy on the back sleeping postures is 90%. The average respiration estimation accuracy when the subjects flipped their head on the other side of bed is 87%, the respiration estimation accuracy on the reading position is 86%.

Table.XI Position Postures and respiration rate Estimation Accuracy

Position	***Subject 1***	***Subject 2***	***Subject3***	***Subject4***	***Subject 5***
Back (a)	***90%***	***94%***	***89%***	***88%***	***87%***
Reverse back (b)	***88%***	***89%***	***87%***	***86%***	***86%***
Sitting in bed(c)	—	—	***88%***	***85%***	***87%***

7.6 Experimental Set Up and 2018 Lab Data Set Results

The 2018 Contactless Extraction of Heart and Respiratory Rate Sensing project was developed to estimate respiratory rate (RR) based on four sleeping postures using the radar, thermal camera, and depth sensing devices. I used the radar data of this project in my dissertation, and the belt sensor data as ground truth for the radar data. The depth camera data and thermal camera data are used as a reference.

Nine students/employees of University of Missouri-Columbia, aged from 18 to 50 years old participated in this project for a short-term respiratory rate study with different body postures (Table III). Every subject was asked to lie in four different sleeping postures: back sleeping, right sleeping, left sleeping and stomach sleeping; each body posture was kept for three minutes. We examined the respiration estimation algorithm accuracy on the four different sleeping postures. The results in Table XII show the average respiration estimation accuracy on the back postures is 92%. The average respiration estimation accuracy on the side postures is 84%, and the respiration estimation accuracy on the stomach position is 82%.

Table.XII Sleeping Postures and Respiration Rate Estimation Accuracy

Sleeping poster	Subject 2	Subject 6	Subject 8	Subject 9	Subject 10	Subject 11	Subject 12	Subject 13	Subject 15	Average accuracy
back	90%	85%	87%	100%	100%	86%	83%	87%	97%	91%
left	82%	92%	64%	88%	91%	86%	90%	86%	81%	84%
right	85%	81%	77%	88%	77%	82%	91%	91%	87%	84%
stomach	89%	95%	88%	79%	69%	85%	73%	80%	80%	82%

7.7 Experimental Results Discussion

From the results in Section 7.4-7.6, we found that the accuracy of the respiration rate depends on the sleep posture and the sleeping position. We offer the following conclusions.

(1) When the patients are sleeping on their back, the torso area is directed toward the RF sensor. When sleeping in the middle of the bed, the movement of the torso area is easily detected by the RF sensor; hence, we can get an accurate respiration rate. If the patient's position moved toward the side of the bed in a back sleeping posture, it does not significantly affect the respiration rate estimation.

(2) When the patients are sleeping on their side and in the middle of the bed, the movement of their side can be detected by the RF sensor. The movement of the patient's side during the breathing is much smaller than the movement of the

abdomen; therefore, the accuracy of respiration rate estimation on the side sleeping posture is lower than the accuracy on the back sleeping posture because of the motion amplitude. If the patient's position moved toward the side of the bed on a side sleeping posture, it does not significantly affect the respiration rate estimation.

(3) When the patients are sleeping on their stomach, the patient's back is directed toward the RF sensor, and the movement of the torso area is between the bed and patient's back which is a small, obstructed signal. Therefore, the accuracy of the respiration estimation on the stomach sleeping posture is lower.

(4) When the patients are sleeping on their back while covered by a blanket, we still can get higher accuracy, because the RF sensor can sense through the blanket, and capture the movement of the torso area.

7.8 Respiration Estimation and Restless Time Estimation Results for Psych Center Patients

We used the patient's night data to track their motion in bed, estimate the breathing rate during their peaceful sleeping periods, and estimate restless time and sleep quality for each night. Safety checks are conducted by the staff every 15 minutes, and we set the staff's motion that is detected by radar as an unknown case. The flow diagram is shown in Fig. 37.

A. Unknown case

Safety checks are conducted by the staff every 15 minutes, and each patient's status is manually recorded in a log, which includes the location of the patient as well as breathing

and sleeping status. At night, staff will often enter the patient's room with a flashlight to perform these checks. The motions from the staff or the nurse are detected by the radar, and we set those data as unknown cases. For instance, there were big changes in the range bin at 374 minutes of the radar data in the Fig.38 (a); at same time, depth camera data showed the patient was in the bed with motion, and the nurse's notes indicate the nurse came to the patient's room for the safety check as shown in Fig.38 (b). Therefore, we set those data as unknown cases, and remove from the data.

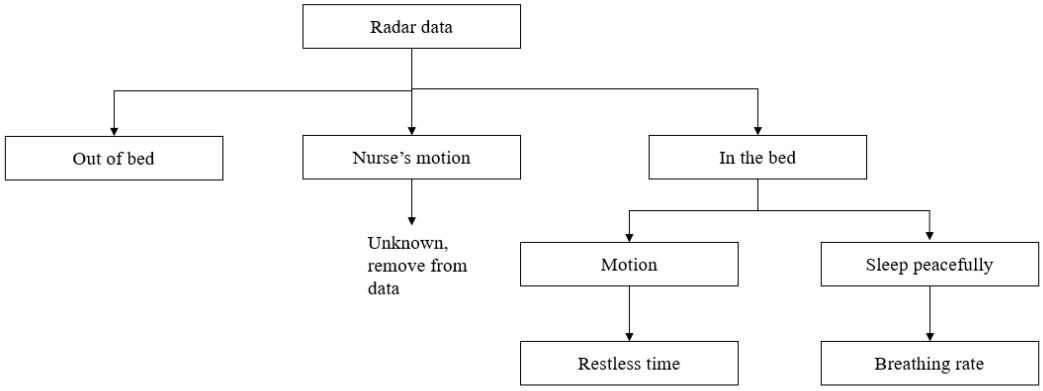

Fig.37 Flow diagram of data processing for psych center patient

1) Out of bed vs. In bed

As a first step, we need to identify whether the patient is out of the bed or in the bed. In correlating the depth camera data with the range bin of the radar data, the range bin has large changes when the patient is out of bed., as described in Section 5.1. We used 12 features including the range bin and SVM classifier to classify the data into two classes; class 1 is out of bed, and class 2 is in the bed.

2) The motion in the bed

If the data is from class 2 which is patient in the bed, we check the range bin changes. We set the threshold:

$$\text{Threshold} = \text{mean (range bin)} + 30\% * \text{mean (range bin)} \quad (59)$$

If the range bin changes are greater than the threshold, we identify the data from the patient's motion data and estimate the restless:

$$\text{Restless estimation} = \#\text{of motion event /total event} \quad (60)$$

The restless time from depth camera was estimated by the Eq. (60). For instance, the restless estimation of the patient in Fig.38 (a) is:

Restless estimation based on depth = 9.1%

Restless estimation based on radar = 9.6%

Table.XIII Restless Estimation for Psych Center Patients

Patient ID	Date	depth	radar
2	9/10/2019	48%	33%
2	9/11/2019	13%	12%
2	9/12/2021	38%	43%
1	9/10/2019	5%	4%
1	9/11/2019	13%	12%
1	9/12/2019	6%	7%
3 (covered by a blanket)	9/17/2019	30%	40%
7	9/24/2019	15%	18%
4	9/17/2019	44%	54%
5	9/18/2019	9%	13%
10(has lots of leg motion)	10/2/2019	17%	7%
10	10/3/2019	10%	14%

3) Breathing rate

If the range bin changes are less than the threshold, we identify the patient is sleeping peacefully in the bed and estimate the breathing rate by using our respiration algorithm in Section 7.1 – 7.3 . The flow diagram of the breathing rate is shown at the Fig.30. The breathing rate estimation in one-minute periods for the patient in Fig.39 (a) is shown in the Fig. 39(b). The respiration rate corresponds to the frequency of the dominant phase FFT peak within the breathing-region spectrum, which is shown in equation (61).

$$\text{Respiration rate} = 0.2 * 60 = 12 \text{ bpm} \tag{61}$$

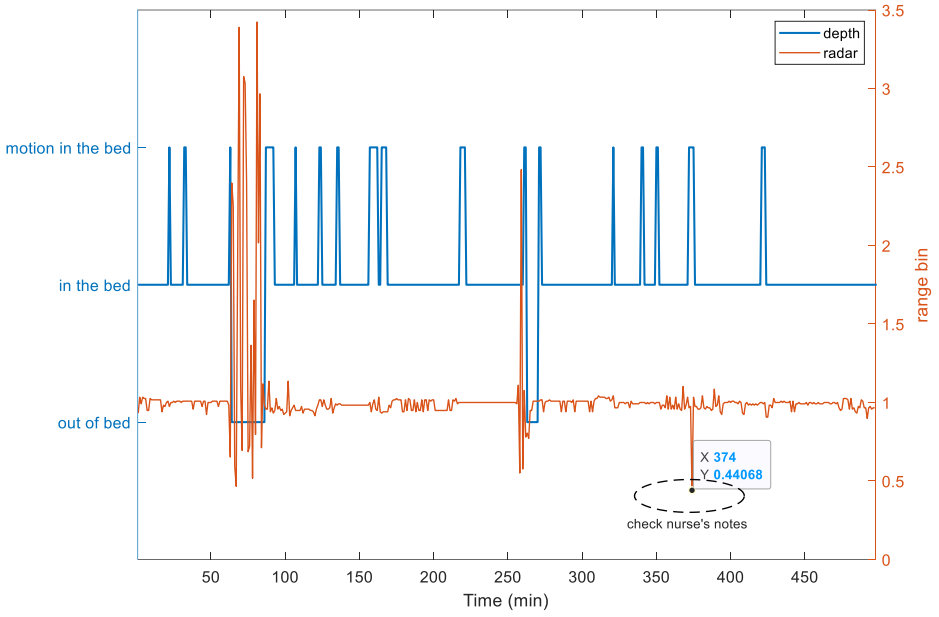

(a)

CLINICAL PATIENT INFO		
09/19/2019 06:09 CDT	Exam	Labs
09/19/2019 05:51 CDT	Patient Room	Sleeping
09/19/2019 05:40 CDT	Patient Room	Sleeping
09/19/2019 05:16 CDT	Patient Room	Sleeping
09/19/2019 05:02 CDT	Patient Room	Sleeping
09/19/2019 04:46 CDT	Patient Room	Sleeping
09/19/2019 04:32 CDT	Patient Room	Sleeping
09/19/2019 04:22 CDT	Patient Room	Sleeping
09/19/2019 04:04 CDT	Patient Room	Sleeping
09/19/2019 03:51 CDT	Patient Room	Sleeping
09/19/2019 03:44 CDT	Patient Room	Sleeping
09/19/2019 03:17 CDT	Patient Room	Sleeping
09/19/2019 03:00 CDT	Patient Room	Sleeping
09/19/2019 02:47 CDT	Patient Room	Sleeping
09/19/2019 02:39 CDT	Patient Room	Sleeping
09/19/2019 02:22 CDT	Patient Room	Sleeping
09/19/2019 02:01 CDT	Patient Room	Sleeping
09/19/2019 01:46 CDT	Patient Room	Sleeping

(b)

Fig.38 Depth data, Radar data and nurses' notes. (a) Depth data and Radar data (c) Nurse's notes in log

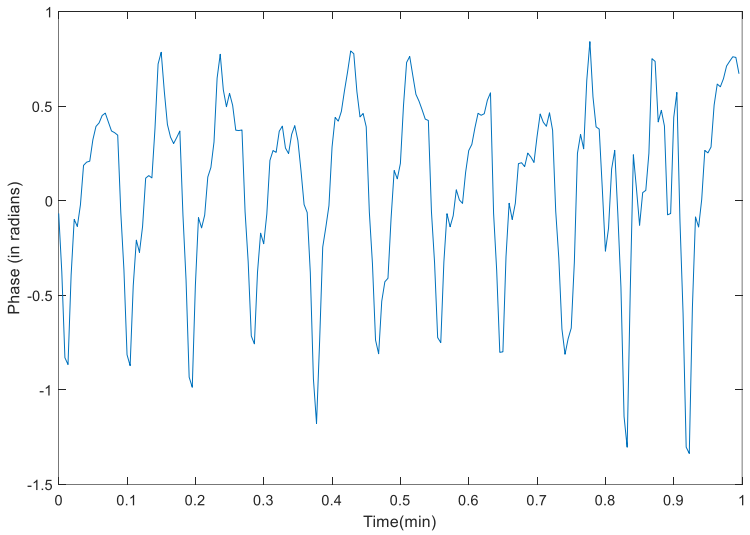

(a)

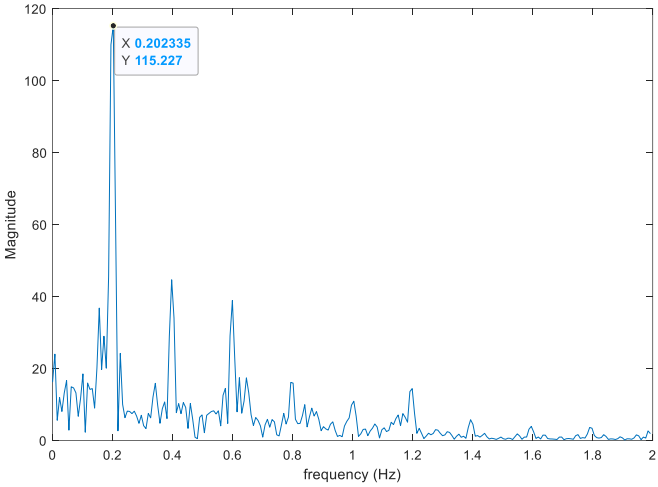

(b)

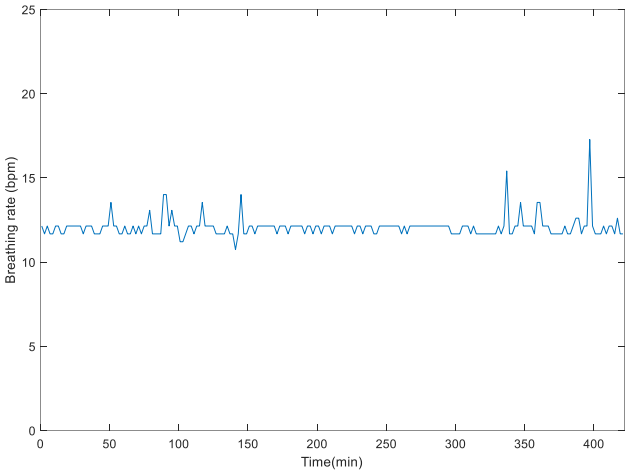

(c)

Fig.39 Breathing rate estimation in one-minute periods. (a) The phase of target's range bin. (b) the breathing rate in the frequency domain (c) The breathing rate during night period

We use this strategy to estimate the Psych center patients' respiration rate of different nights, and the results are shown in Fig. 40-46. From the results, we offer the following conclusions:

- The depth camera data and the nursing notes in the log are used as the ground truth of the radar data. The depth camera data is labeled manually; there are three classes: 0: empty bed, 2: person in bed still, 3: person in bed with motion. We got the nursing

notes from the psych center staff. PSD and the respiration rate were calculated by using radar data in Fig. 40-46.

- The motion of patients is not detected by the radar in some cases. The main reason is that the radar is more sensitive to the motion in the upper body, and to posture changes. The motion in the legs can be detected by the depth camera, but it is difficult for the radar to identify the motion from legs because we set the azimuth angle range as -45 degree to 45 degree. We can detect the patient's whole-body motion during the large azimuth angle range. For instance, the patient (ID=10) data in Fig.42(a), the motion in the patient's legs is detected by the depth camera, the radar data is not able to detect the motion. This will affect the accuracy of restless time estimation.
- The staff will enter the patient's room every 15 minutes with a flashlight to perform these checks. Sometimes, two or three staff members will come to the patient's room to check the patient. This will make the radar data noisy and will affect the restless time estimation because it is difficult to identify where the motion comes from.
- Respiration rate estimation depends on the patient's still time in bed. If the patient is more stable in bed, we can get a more accurate respiration rate; otherwise, the small motion of the torso area will be hidden in the body motion of the patient.
- Our respiration estimation algorithm has higher robustness for the instant of small motion, such as hand movement, or leg movement. The patient's small hand movement or leg movement in Fig.42 does not affect the respiration estimation.

- The accuracy of respiration rate estimation depends on the accuracy of restless time estimation. Restless time estimation indicates the patient's peaceful time, and our algorithm has a higher accuracy for the respiration estimation when the patient is sleeping peacefully.
- For different sleeping postures, our respiration estimation algorithm has a lower accuracy for stomach sleeping.
- A few patients in psych center preferred to sleep with a blanket covering the body and face as shown Fig.44. The radar can detect the motion under the blanket and find the patient's still time to estimate their respiration rate. This cannot be done by the depth camera system.

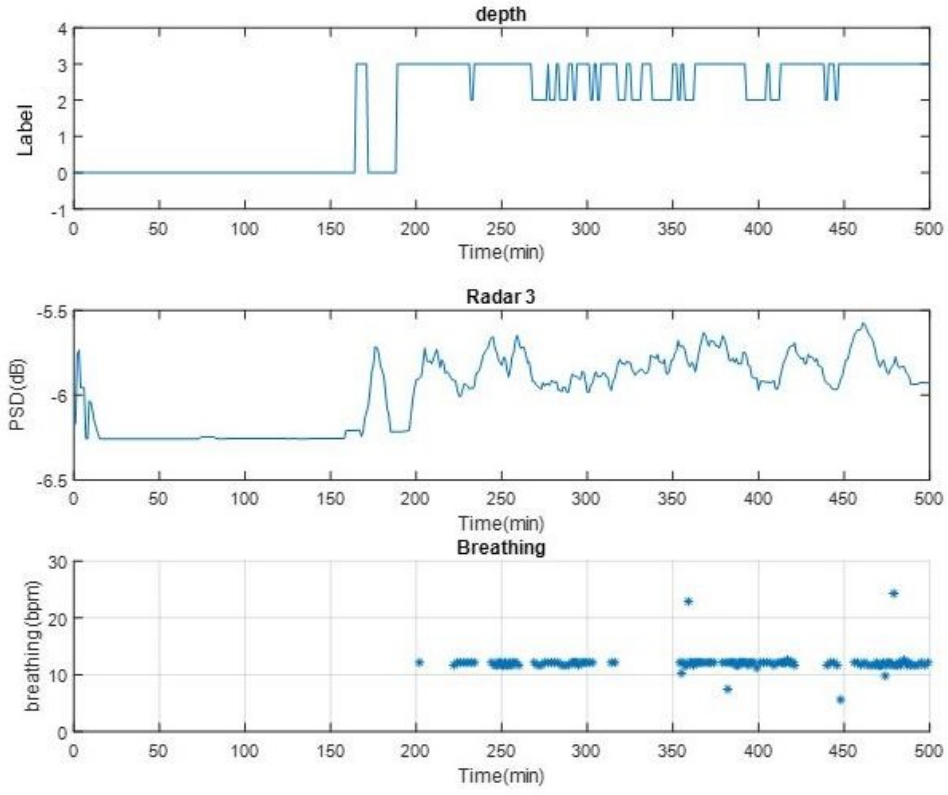

(a)

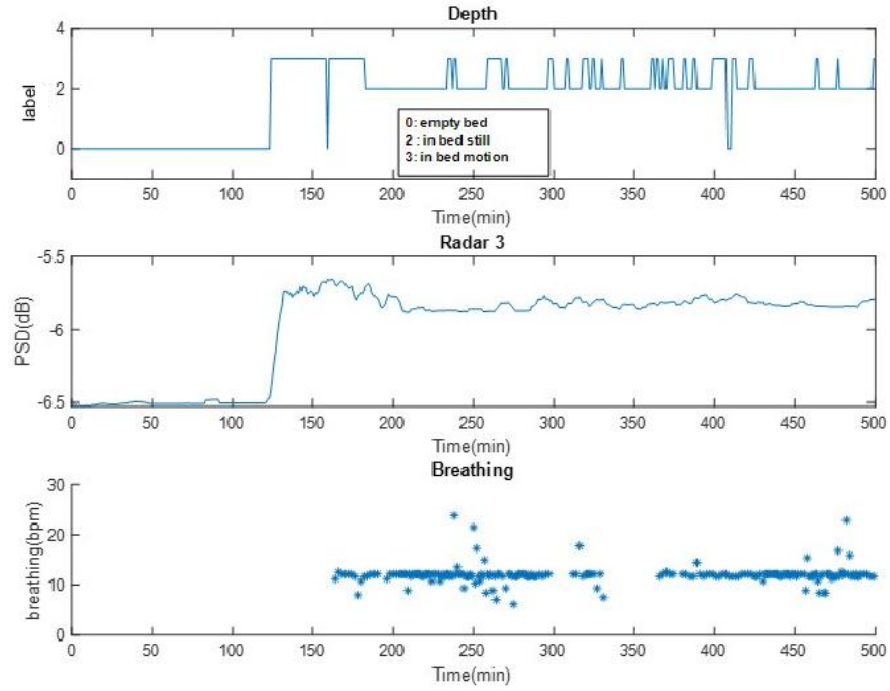

(b)

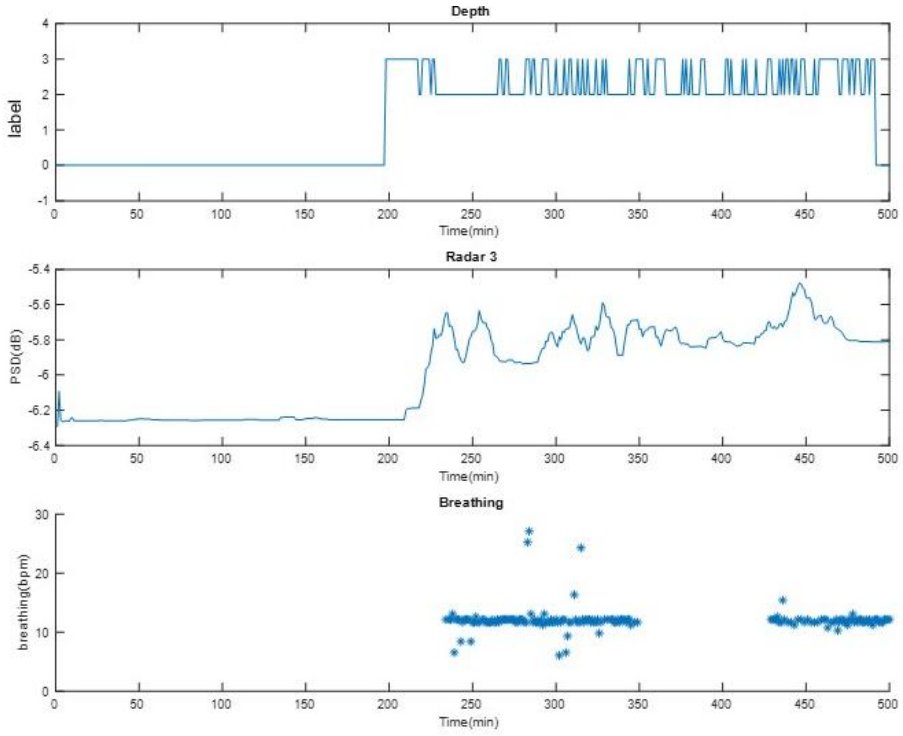

(c)

Fig.40 Depth camera labels, the radar data, and the breathing rate from patient ID=2 (a) Date: 09/10/2019. (b) Date: 09/11/ 2019(c) Date: 09/12/ 2019

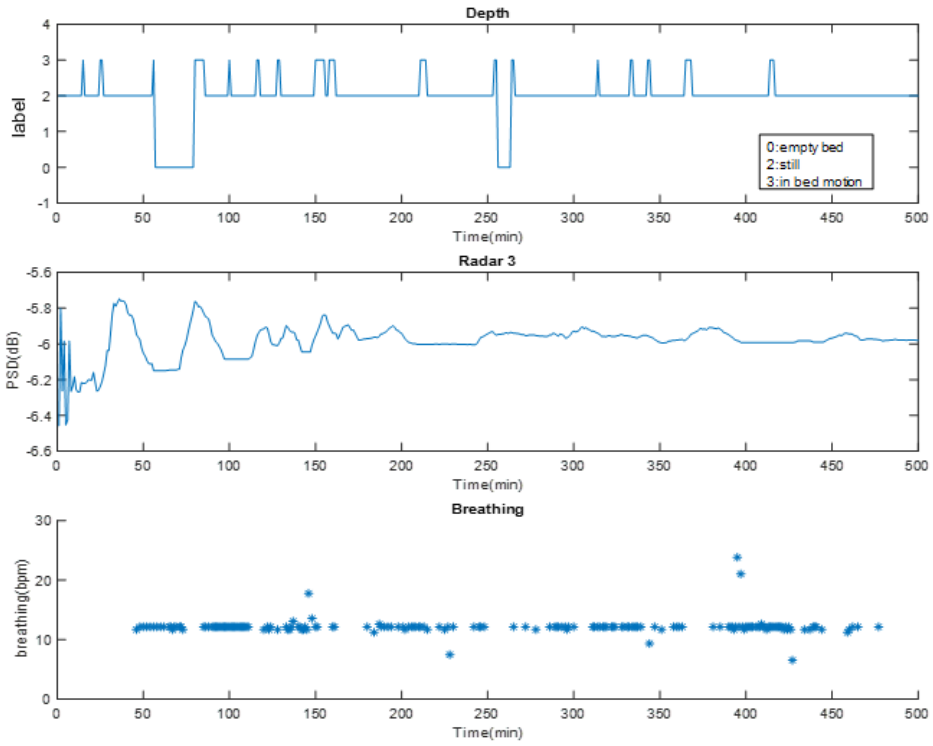

Fig.41 Depth camera labels, the radar data, and the breathing rate from patient ID=5, date: 09/18/2019.

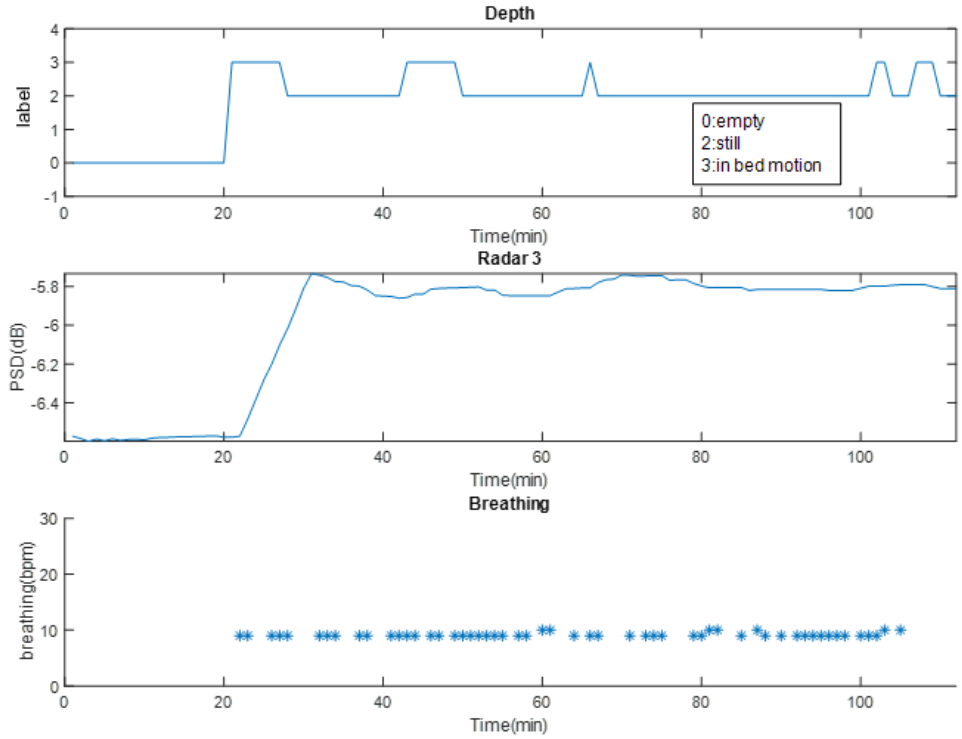

(a)

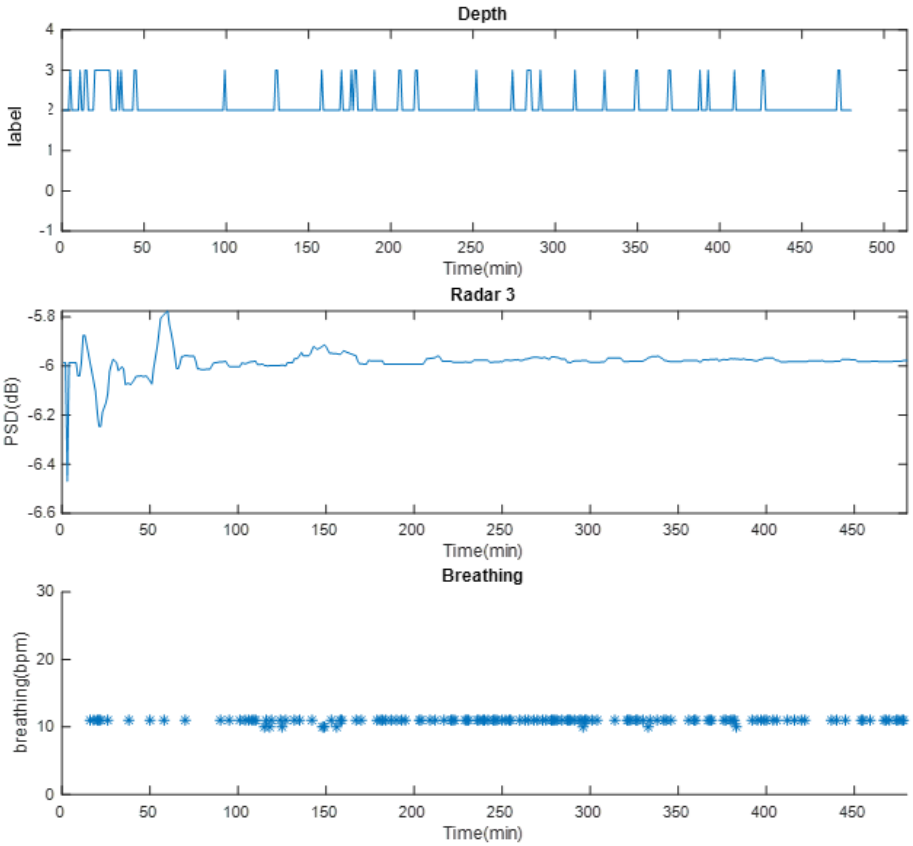

(b)

Fig.42 Depth camera labels, the radar data, and the breathing rate from patient ID=10 (a) Date: 10/02/2019.

(b) Date: 10/03/ 2019

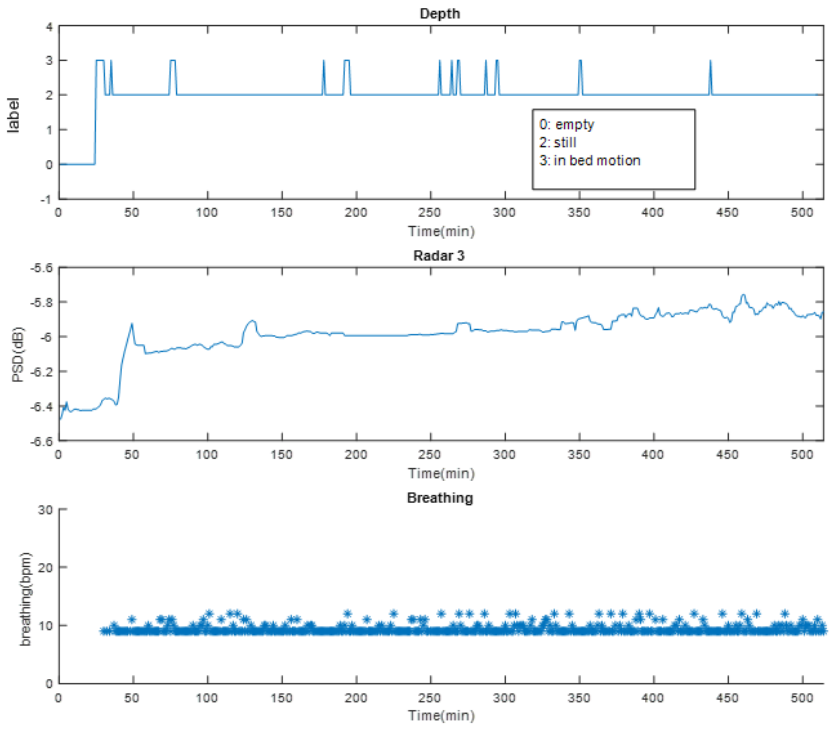
Depth
label
0: empty
2: still
3: in bed motion
Time(min)
Radar 3
PSD(dB)
Time(min)
Breathing
breathing(bpm)
Time(min)

(a)

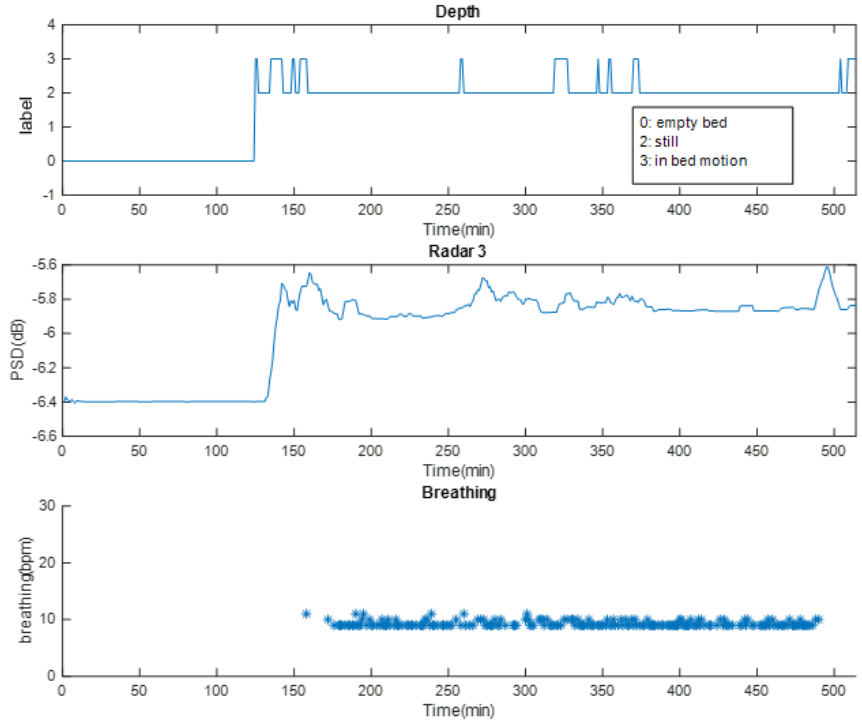
Depth
label
0: empty bed
2: still
3: in bed motion
Time(min)
Radar 3
PSD(dB)
Time(min)
Breathing
breathing(bpm)
Time(min)

(b)

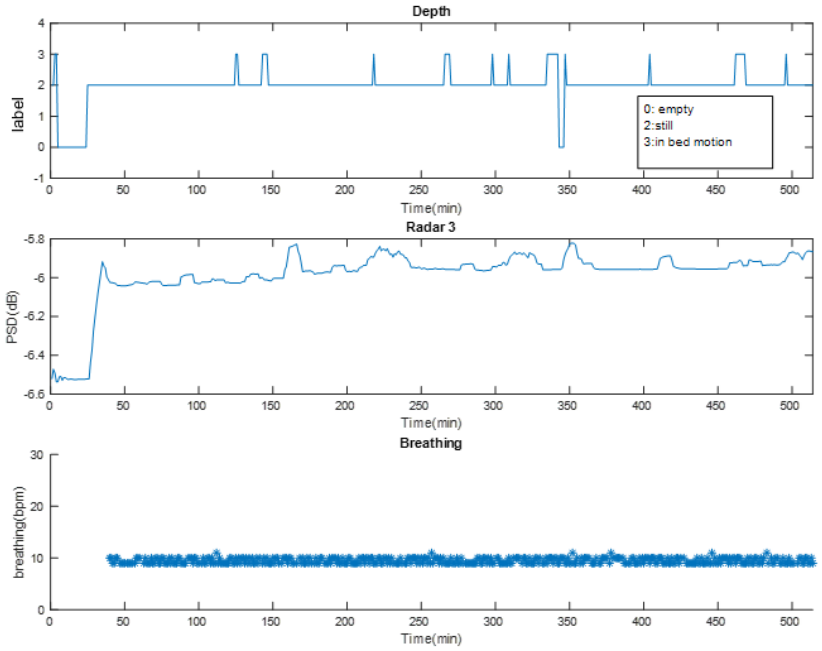

(c)

Fig.43 Depth camera labels, the radar data, and the breathing rate from patient ID=1 (a) Date: 09/10/2019. (b) Date: 09/11/ 2019. (a) Date: 09/12/2019

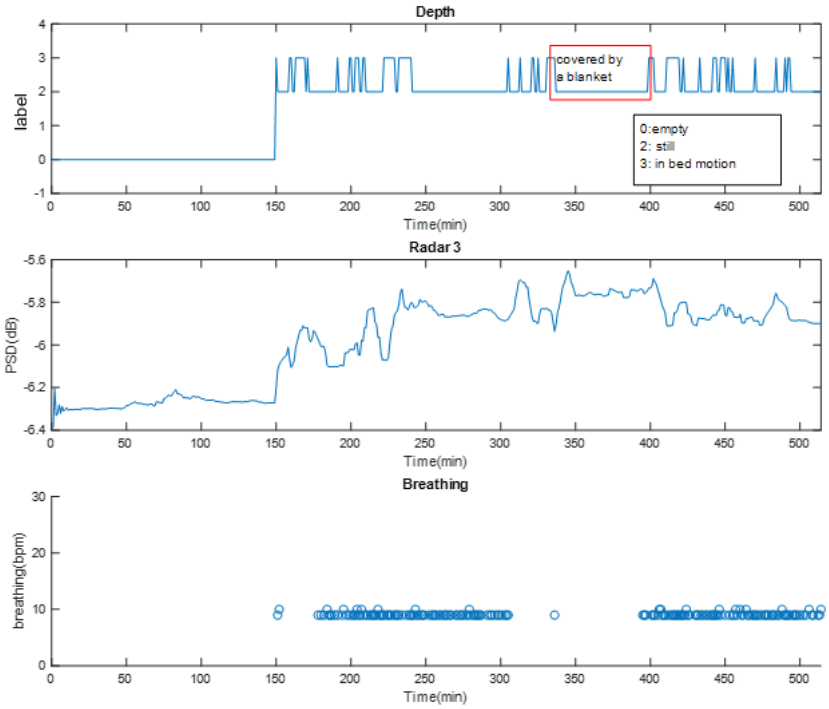

Fig.44 Depth camera labels, the radar data, and the breathing rate from patient ID=3, date: 09/17/2019.

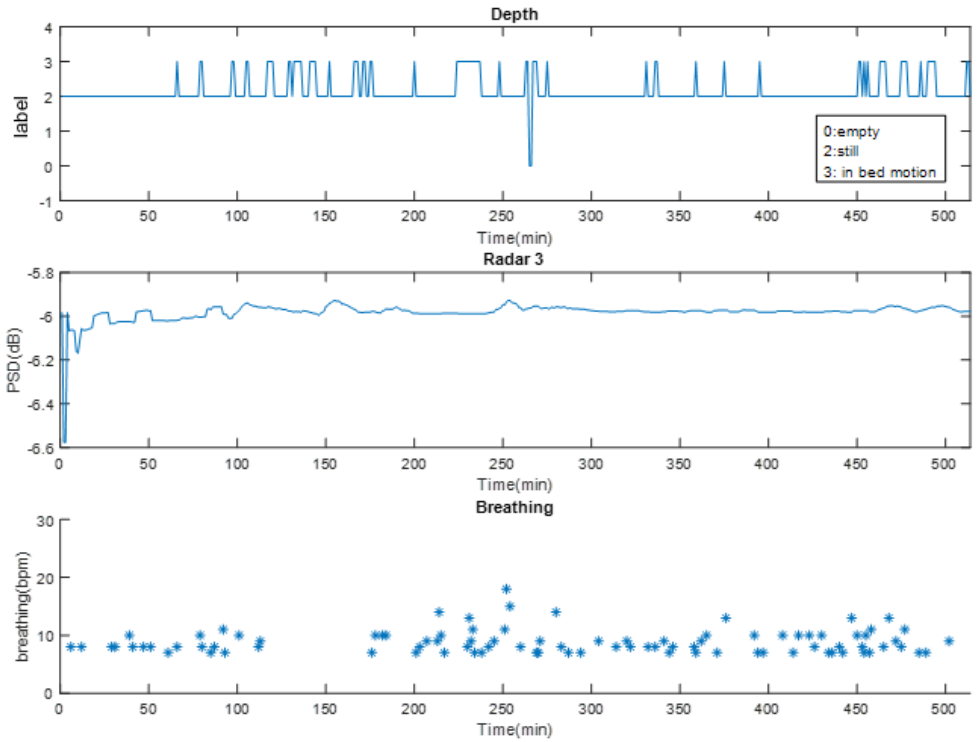

Fig.45 Depth camera labels, the radar data, and the breathing rate from patient ID=7, date: 09/24/2019.

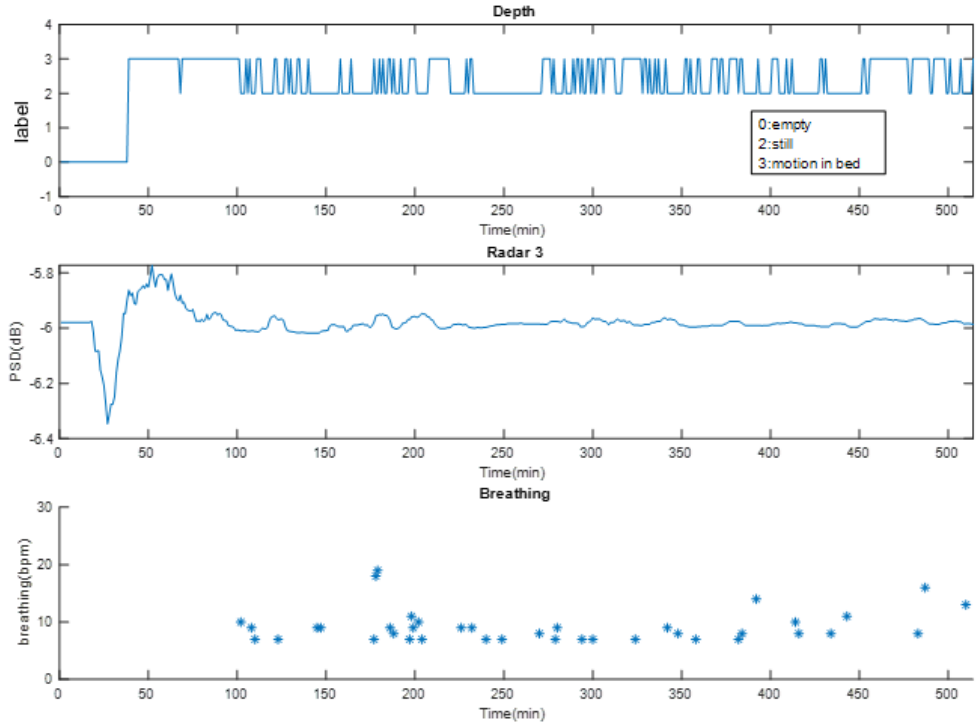

Fig.46 Depth camera labels, the radar data, and the breathing rate from patient ID=4, date: 09/17/2019.

VIII. Learning Room Structure and Activity Patterns

8.1 Learning Room Structure from The RF Clutter Pattern

A series of experiments was carried out to investigate the wall locations between offices. First, The RF sensor was deployed in office (A) position ①, as shown in Fig.8. The transmitting antenna and the receiving antenna were directed towards the meeting room. When the RF sensor transmits electromagnetic radiation, signals penetrate the wall in the office, and reflect from all objects in both office (A) and the meeting room (C). If there is no moving target, the main component of the received signal is the pattern of clutter echoes due to echoes from the surface scatter; the strongest reflection in this clutter comes from the wall. In order to determine the wall position, we used the beat frequency corresponding to the maximum peak in the received signal to calculate the estimated wall location, described below (Fig. 31(a)):

1) The beat frequency of the RF sensor is calculated by the equation below:

$$f_b = Fs * (0: N/2)/N \tag{62}$$

where N is the number of samples in each chirp.

2) Perform the FFT algorithm for each chirp.

3) Find peaks in each chirp due to the strongest reflection from the wall, and find the corresponding beat frequency.

4) Store all estimated beat frequency results from (3), generate a histogram, and find the maximum intensity value.

5) Calculate the distance R according to the beat frequency in (4) by the equation below:

$$R = \frac{c * f_b}{2 * slope} \tag{63}$$

6) The RF sensor is deployed in office (A) position②, as shown in Fig. 8. The transmitting antenna and the receiving antenna are directed towards office (B), and the process from step (1) to step (5) is repeated for finding the wall location between office (A) and office (B). The results are shown in Fig.35 (b).

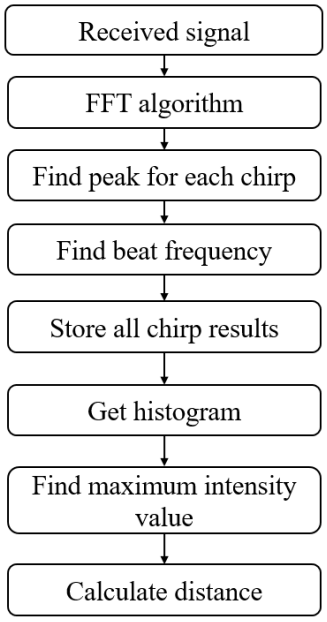

(a)

Wall position	Actual distance	Estimated distance
A-C wall	3.20 m	3.49m
A-B wall	3.71m	3.62m

(b)

Fig.47 Estimating wall position from the RF clutter pattern. (a) the flow diagram for the wall position estimation. (b) the actual and the estimated wall positions

8.2 Learning Room Structure from Movement Patterns

In the naturalistic home setting, the active movement of people occurs in the open spaces in the room, i.e., not where the wall is located. In this method, the room structure is learned

by capturing the active movement of people over time and generating clusters that represent this open space.

In this experiment, the RF sensor is deployed in four different positions (①,②,③,④) in the offices (A, B) and the meeting room (C) (Fig. 8), and motion data are collected over time. Four different experiment scenarios were tested in this naturalistic setting:

- In position ①, the TX/RX antennas in the RF sensor are directed toward office (A) and the meeting room (C). A person walked in office (A) for 30 minutes, and then entered the meeting room (C) and walked for another 30 minutes. The RF sensor collected the motion data both in front of and behind the wall. The same experiment scenario was conducted in position ④ where the antennas of the RF sensor are directed towards office (B) and the meeting room (C), and a person walked in office (B) for 30 minutes, then entered the meeting room (C) and walked for another 30 minutes.
- In position ②, the antennas of the RF sensor are directed toward office (A) and office (B). A person walked in office (A) for 30 minutes, and then entered office (B) and walked for another 30 minutes.
- In position ③, the TX/RX antennas of the RF sensor are directed towards the door in the meeting room; data were collected while a person walked back and forth in the room for 30 minutes.

The range FFT on each chirp and the velocity FFT on each frame are performed for the RF sensor data in order to get the range and the velocity information of the person located in the rooms. A clustering algorithm is run on the RF motion data set, which has three features: velocity, range, and received power.

In order to get the possible number of clusters, the Improved Visual Assessment of Cluster Tendency (iVAT) algorithm is applied to the RF motion data set [99-100]. The iVAT image in Fig.36 (a) shows that the number of preferable tendency clusters is three. Furthermore, the Fuzzy C-Means algorithm is implemented for the RF data set by using the cluster numbers from the iVAT algorithm [101-103].

Fig.36(b) shows that there are three clusters, the first cluster (red) indicates the motion in the meeting room, the second cluster (cyan) indicates the motion in office (A), the third cluster (blue) indicates the motion in office (B). The area between the red cluster and the cyan and blue clusters represents the possible wall position between the offices (A, B) and the meeting room C. The area between the cyan and blue clusters represents the possible wall position between office (A) and office (B).

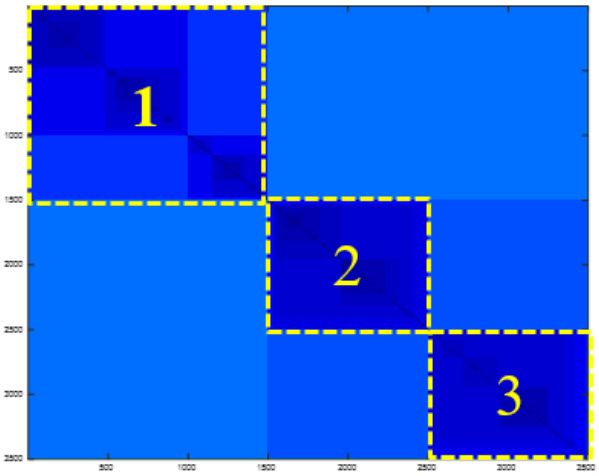

(a)

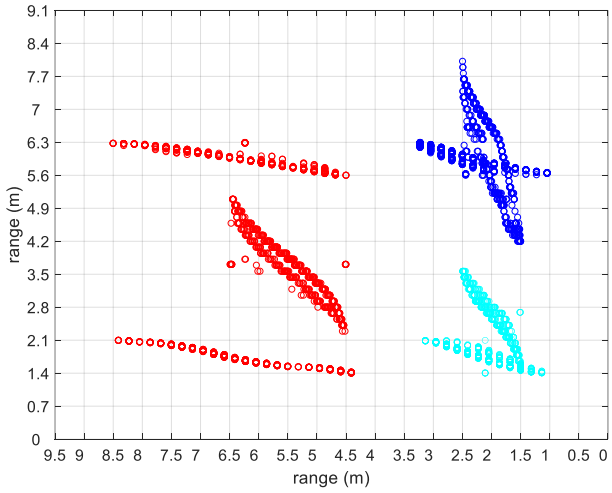

(b)

Wall position	Actual distance	Estimated distance
A-C wall	3.20 m	3.5m ~ 4.4m
A-B wall	3.71m	3.7m ~ 4.1m

(c)

Fig.48 The Learning room structure from active movement patterns (a) partitioned iVAT image (b) clustered motion data by FCM (c) the estimated wall positions

8.3 Discussion

Two different methods are presented for the wall position estimation via RF signals in a naturalistic setting, which include learning room structure from the RF clutter patterns, and learning the open space from the active movement patterns.

The results in Fig.35(b) show the wall position estimation between the offices (A, B) and the meeting room (C) is 3.49m based on the RF clutter patterns; the accuracy of this method is 91% compared to the actual distance as measured manually using a tape measure. Meanwhile, the method using active movement indicates there is no motion between the range of 3.5m to 4.4 m. Therefore, we estimate the final wall position between the offices

and the meeting is 3.49 m. The wall position between office (A) and office (B) is 3.62m based on the RF clutter patterns; the accuracy of this method is 98% compared to the manually measured distance. At the same time, the method using motion patterns shows there is no motion between 3.7m to 4.1m. Hence, we estimate the wall position is 3.62m.

8.4 Background Filter Design

RF sensors have a higher accuracy for tracking motion in the line of sight (LOS) due to the electromagnetic radiation travel in a direct path from the transmitter to the receiver. However, the RF signal will be attenuated in the obstructed environment (OBS), such as a signal penetrating a wall. The motion reflection behind the wall will be weaker (Fig.38 (a)) or sometimes even be hidden (Fig.38 (c)) due to a strong wall reflection; this effect can result in difficulties when calculating the motion density in different rooms. In order to get the activity density, we designed a background filter based on the estimated wall position in section III to remove the wall reflection effects.

First, we deployed the RF sensor in position ① in office (A) to collect the active movement in meeting room (C). Fig.38 (a) shows there is motion in the area 3.9m ~ 7.9m from the sensor. Meanwhile, a constant reflection shows in the area 3.4m ~ 3.7m from the sensor. In section III, we estimated the wall position between office (A) and meeting room (C) is 3.49m; therefore, we assume the constant reflection in Fig.38 (a) is from the wall. A Butterworth band-stop background filter is designed based on the wall beat frequency calculated by equation (3). The magnitude and phase responses of the background filter are shown in Fig. 37. The background filter is applied in the RF signal processing, and the result is show in Fig.38 (b).

Second, we deployed the RF sensor in office (A) to collect motion in office (B). A similar signal processing approach was used, and the results are shown in Fig.38 (d). The hidden motion reflection and the small constant reflection (Fig.38 (c)) due to a strong wall reflection becomes clearer in Fig.38 (d) after the background filter is applied to the RF sensor data.

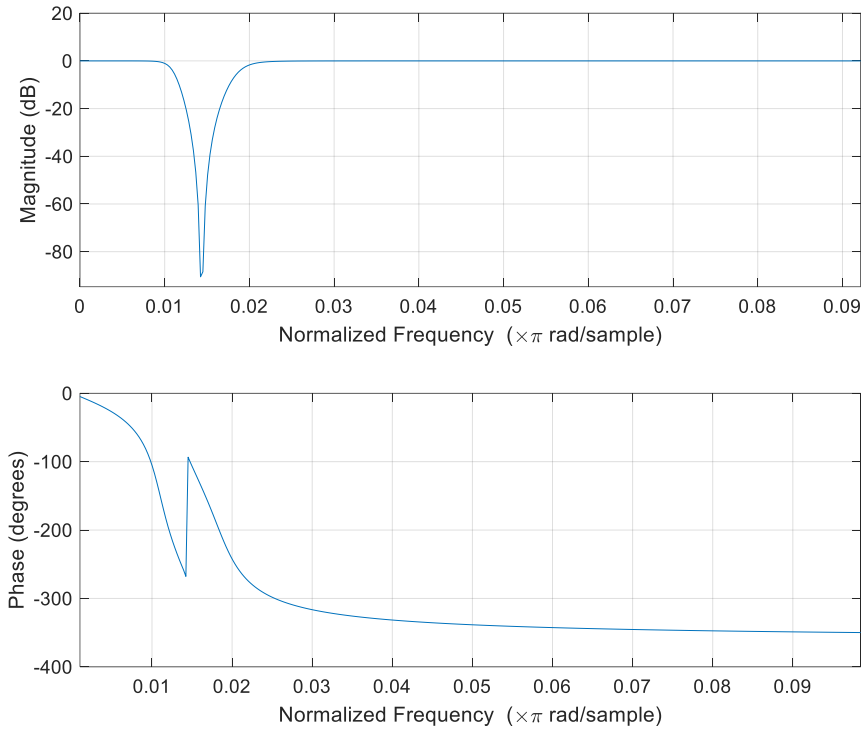

Fig.49 The Magnitude and Phase Response of Background filter.

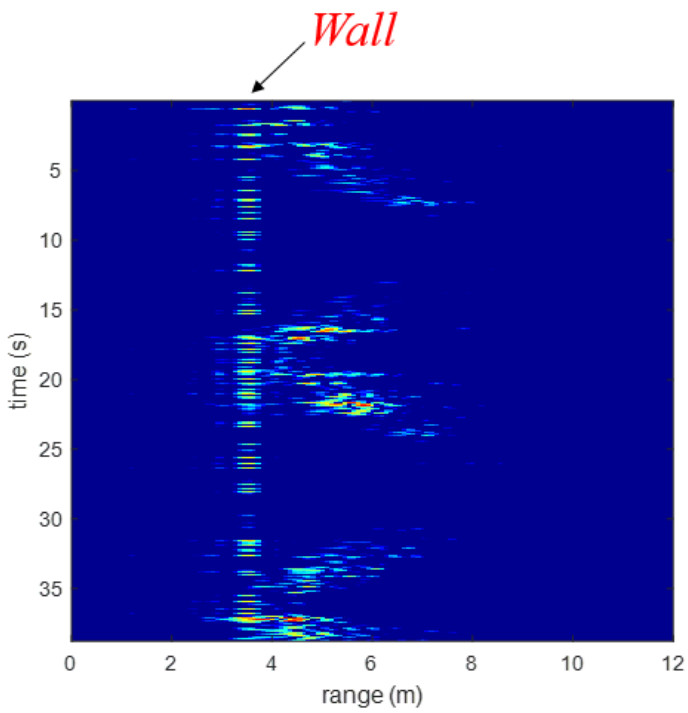
Wall
time (s)
range (m)
5
10
15
20
25
30
35
0
2
4
6
8
10
12

(a)

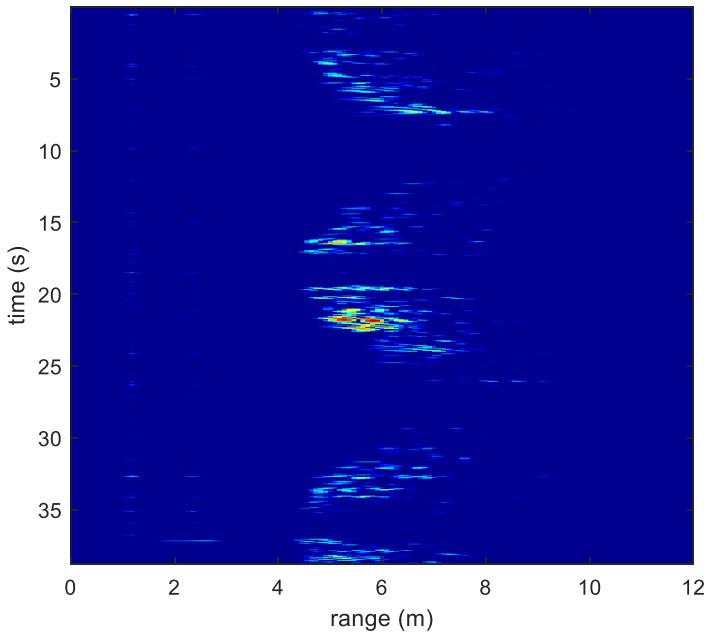
time (s)
range (m)
5
10
15
20
25
30
35
0
2
4
6
8
10
12

(b)

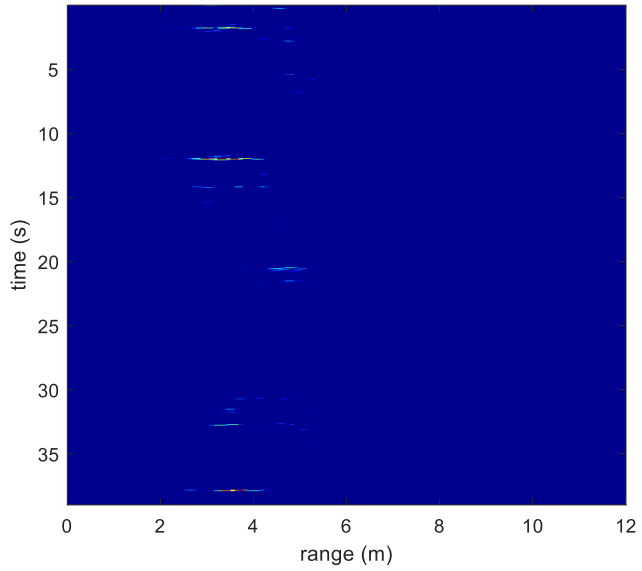

(c)

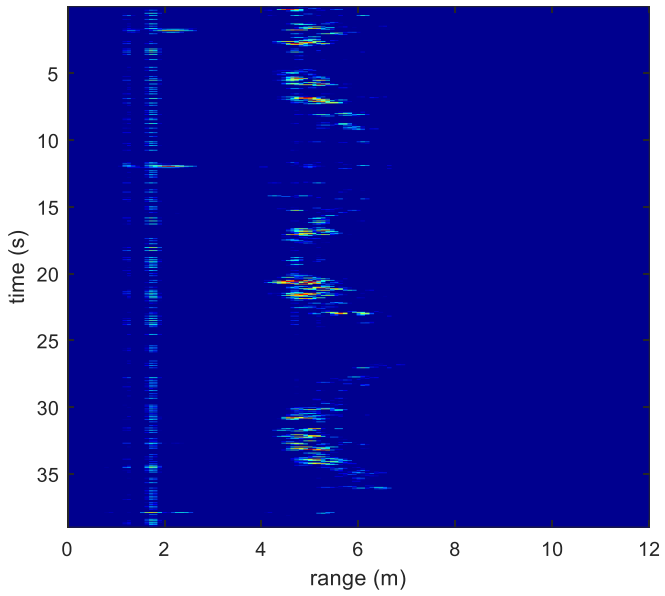

(d)

Fig.50 The Background filter. (a) motion in meeting room C without the background filter (b) motion in meeting room C with the background filter. (c) motion in office B without the background filter. (d) motion in the office B with the background filter

8.5 Activity Density

Data from the RF sensor deployed in four different positions of the office rooms and the meeting room are processed using the background filter for removing the wall reflection, as described in Section V. The filtered data are processed using the range FFT and the velocity FFT to get the range and velocity information of a target. Then fuzzy rules are applied to the resulting motion dat , which has three features: velocity, range and received power, for estimating the activity level, which can be viewed as an activity density, i.e., amount of activity per unit of time (Fig.39 (a)). The processing steps are included in several steps as follow:

1) Define the input and output of fuzzy rules. The motion velocity and the received power are used as input to a system of fuzzy rules; the output of the fuzzy rules is the activity level of motion in the room.

2) Create the membership functions for the fuzzy rule system. Based on the gait information of older adults, the average velocity of older adults in daily routines is 0.5 m/s. Hence, the input variable 'velocity' can be represented by the Gaussian membership function in Fig.39 (b). The expected signal-to-noise ratio in the radar system is ± 10dB. According to the signal-to-noise ratio, the second input variable 'received power' can be represented by the triangle membership function in Fig.39 (c). The triangle membership function is used for the fuzzy output 'activity density' in Fig.39 (d).

3) Create the compositional rules for the fuzzy rule system.

In the radar system, static objects have a constant amplitude and phase in each chirp, whereas the moving target has variable amplitude and phase information. When the target

velocity is higher, the variation of phase and amplitude in the received signal is higher. Therefore, the velocity information and the received power are used as the antecedent of the fuzzy system to create the fuzzy rules as follow:

Rule 1. If the velocity is low, and the received power is low, then motion density is low.

Rule 2. If the velocity is moderate, and the received power is normal or high, then the motion density is moderate.

Rule 3. If the velocity is high, and the received power is high, then the motion density is high

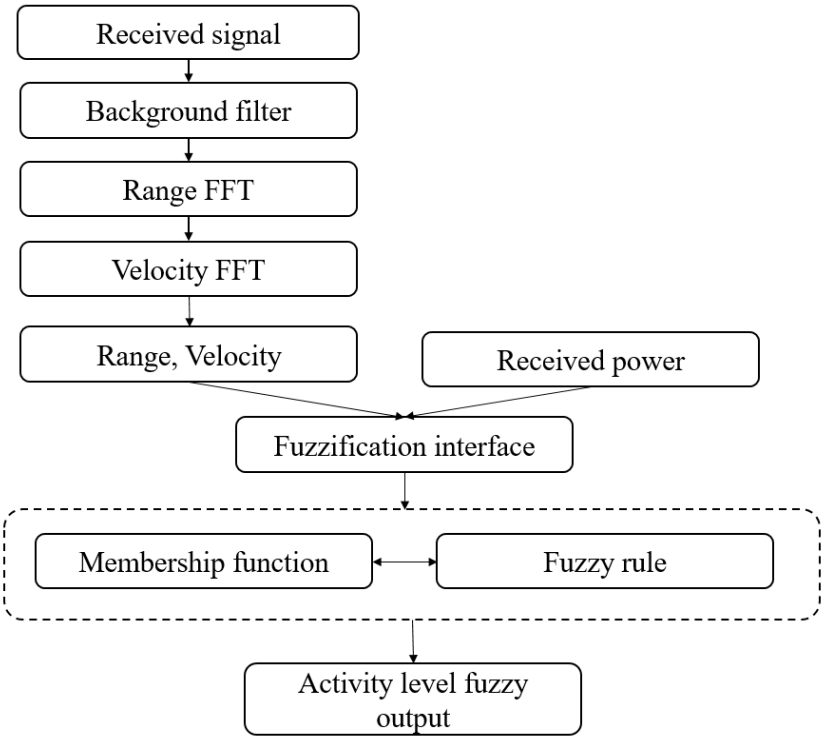

(a)

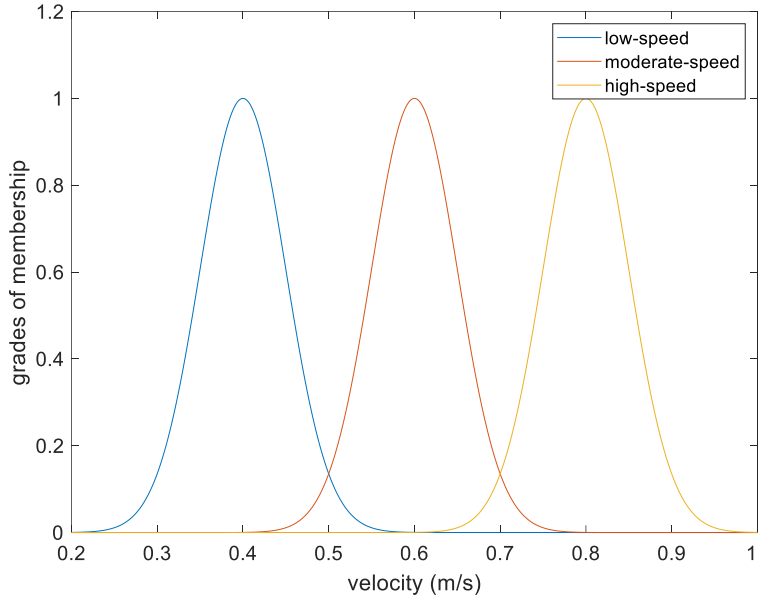
low-speed
moderate-speed
high-speed
grades of membership
velocity (m/s)
0
0.2
0.4
0.6
0.8
1
1.2
0.2
0.3
0.4
0.5
0.6
0.7
0.8
0.9
1

(b)

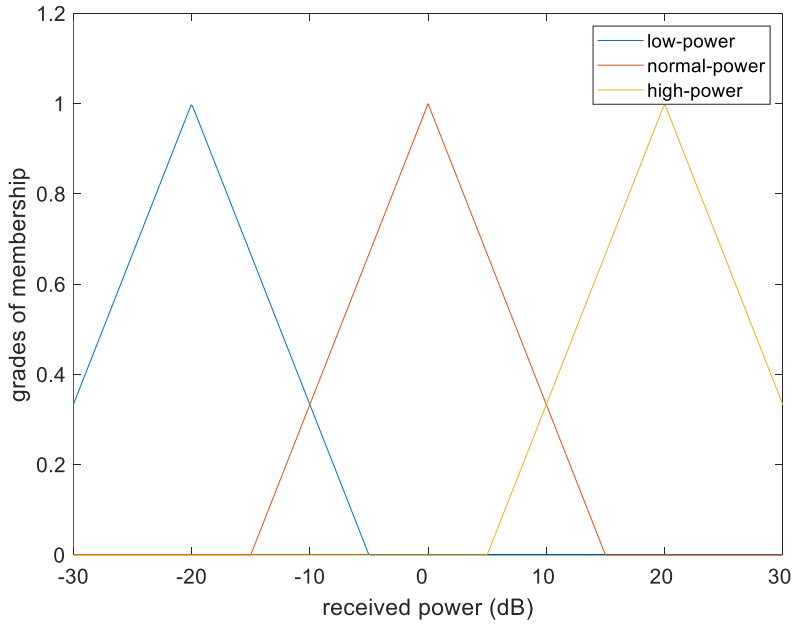
low-power
normal-power
high-power
grades of membership
received power (dB)
0
0.2
0.4
0.6
0.8
1
1.2
-30
-20
-10
0
10
20
30

(c)

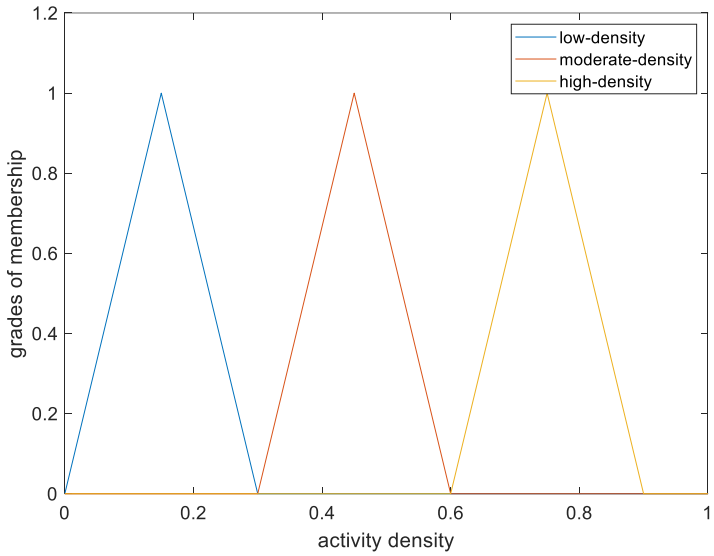

(d)

Fig.51 The fuzzy rule system (a) the flow diagram for the fuzzy rule system, (b) the membership function of velocity (c) the membership function of received power, (d) the membership function of activity density

Due to the distance from the target to radar and the wall attenuation, the received power is higher or moderate if the motion is in the offices (A, B); however, the received power is lower or moderate if the motion is in the meeting room (C). Therefore, the fuzzy rule system used two antecedents: the received power and the velocity, and implemented the cylindrical closure operation. Fig. 40 (a) shows the activity level of meeting room is 65% moderate motion and the high motion is less than 1%. Fig.40 (b) shows the activity level of the office (A) is 48% moderate motion and the high motion in the office is less than 1%. Fig. 40 (c) shows the activity level of the office (b) is 52 % of moderate motion (Table X).

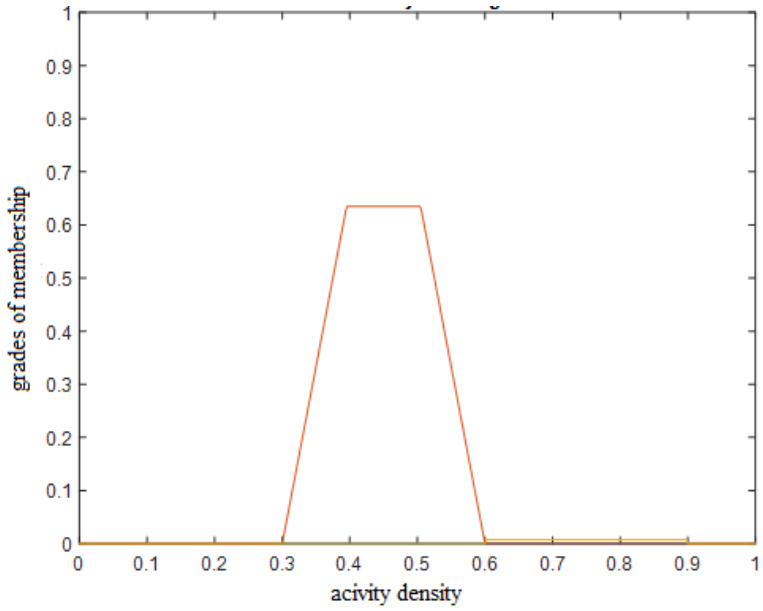
grades of membership
acivity density
0
0.1
0.2
0.3
0.4
0.5
0.6
0.7
0.8
0.9
1

(a)

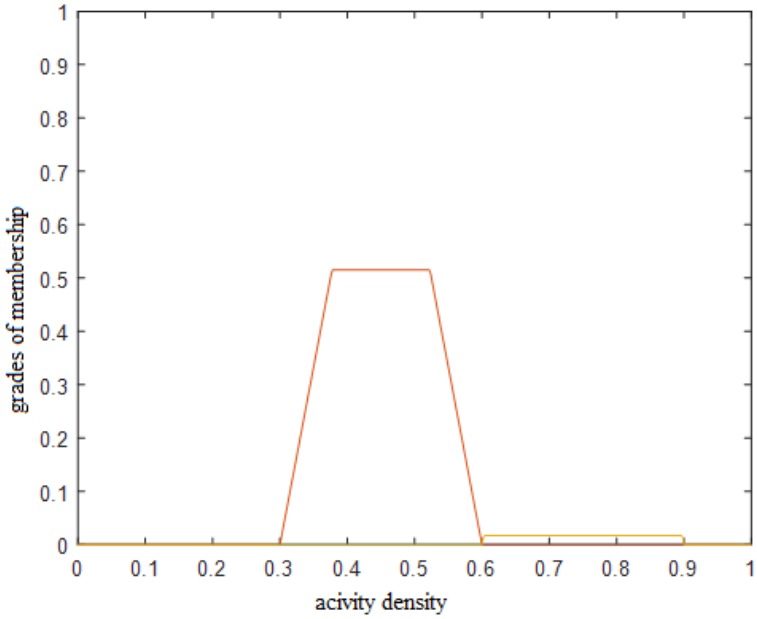
grades of membership
acivity density
0
0.1
0.2
0.3
0.4
0.5
0.6
0.7
0.8
0.9
1

(b)

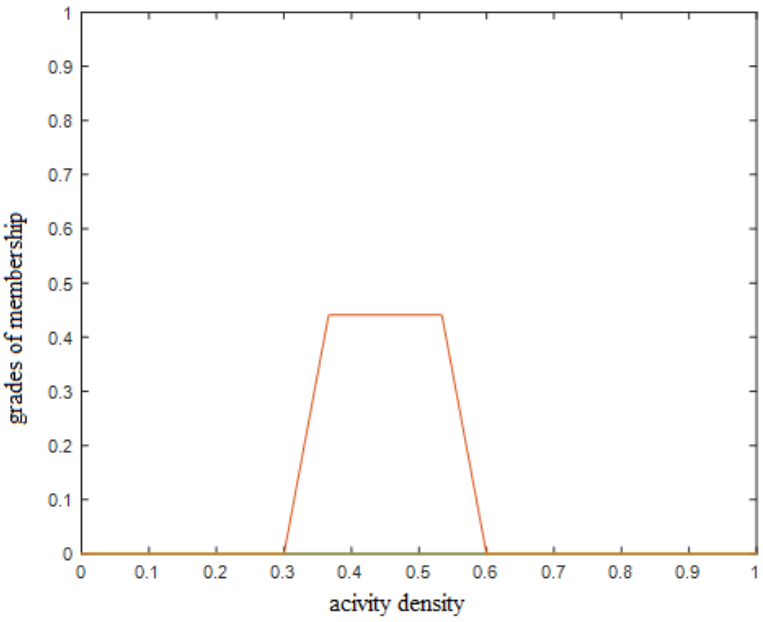

(c)

Fig.52 The output of fuzzy rule system (a) the activity density of meeting room C, (b) the activity density of office A, (c) the activity density of office B

Table.XIV The A-B wall position

Location	Motion density (%)	Activity level
Office room A	48%	Moderate
Office room B	52%	Moderate
Meeting room C	65%	moderate

8.6 Conclusion

In this chapter, we present work on using an RF sensor for learning the room structure and the activity level estimation for in-home monitoring of older adults. We first investigate two different methods for the wall position estimation, which include learning room structure from RF clutter patterns and learning room structure from active movement patterns. The RF clutter pattern is more accurate in estimating wall position in the room without any target, but the movement pattern estimate confirms the wall location by observing moving targets. Comparing the results from the two different methods enables us to get a more accurate wall location in the case of unexpected noise. We also designed a background filter to remove the wall reflection in the received signal for calculating the activity level of older adults over time. In addition, we implemented a system of fuzzy rules using the filtered motion data captured over time, for activity level estimation of older adults in different rooms

IX. Conclusion and Future Work

9.1 Conclusion

This dissertation concentrates on methods for helping two groups of vulnerable populations, namely, frail older adults and psychiatric hospital patients, to monitor their activity level, respiration rate, sleeping quality, and restless time in bed.

In the first part of our work, we have investigated a contactless monitoring system for Psych Center patients in a naturalistic hospital setting. A depth camera and a thermal camera have also been installed and are used as the ground truth.

Chapter 3 provided the list of datasets that we collected for this study, including Psychiatric date set (2019), Eldercare and Rehabilitation Technology Lab Data Set (2021), Contactless Extraction of Heart and Respiratory Rate with Depth, Thermal and Radar Sensing Devices Lab Data Set (2018).

In Chapter 4, I designed a FMCW simulation App, where we can set radar parameters, such as the number of TX/ RX antennas, the samples of per chirp, the number of chirps in per frame, the center frequency, bandwidth, the sample frequency of radar system, and got the important performance parameters of radar, including the range resolution, the velocity resolution, the maximum range, the maximum velocity, and the angle resolution. FMCW simulation App help us to better understand the performance of the FMCW radar system in the Psychiatric center contactless monitoring system and the FMCW system for the learning the room structure via radio wave reflections for longitudinal health monitoring of older adults in a naturalistic home setting.

The RF signal processing was presented in Chapter 5, which was included in frame data processing, beamforming, angle of arrival, matched filter design, and target detection. Compared to variable data frame processing, the constant data frame processing is more accurate. Therefore, we decided to use the constant data frame processing for all radar data signal processing. We used two different methods for detecting target in RF signal processing: Constant false alarm rate (CFAR) detection method, and Cross correlation detection method. Compared to the results from two methods, we could get a more accurate target position.

Chapter 6 presented the out of bed vs. in bed classification algorithm, which was included in data preprocessing, single patient's balanced data classification, and imbalanced data set classification. We designed an SVM classifier, and used six patient data to train the classifier, and out of one patient data for testing the classifier. The classifier has 97% accuracy and 96% recall to the imbalanced data set from Psych Center.

Chapter 7 presented the work on respiration rate estimation with different sleep postures, with the aim of investigating a contactless monitoring system for psychiatric patients in the hospital that can estimate the breathing rate of patients during more typical sleeping postures and find the torso area when the patients use other postures, such as reading books in bed or reversing the body on the bed. I used three different data sets in Chapter 3 to test the respiration rate estimation algorithm. For the 2018 Lab Data Set, the average respiration estimation accuracy on the back sleeping postures is 92%. The average respiration estimation accuracy on the side sleeping postures is 84%, and the respiration estimation accuracy on the stomach sleeping position is 82%. For the 2021 Lab Data Set, the average respiration estimation accuracy on the back sleeping postures is 90%. The

average respiration estimation accuracy when the subjects flipped their head on the other side of bed is 87%, the respiration estimation accuracy on the reading position is 86%. Our respiration estimation algorithm was tested by those two data sets and shown to have a high accuracy. Therefore, we applied the same algorithm to the 2019 Psychiatric data set to estimate the patient's respiration rate in a naturalistic hospital setting. The restless time of a psych center patient is calculated by the number of motion events in the total event.

The aim of investigating a contactless monitoring system for psychiatric patients in the hospital is to detect life signs, such as movement patterns and breathing patterns, in naturalistic hospital settings, which can be achieved in this dissertation. However, there are two limitations in our research: first, our respiration algorithm was tested by the subjects with normal BMI in lab experiments, then was applied to estimate the respiration rate of patients in the psych center hospital, in which the BMI was greater than 26, indicating an overweight condition. An overweight condition can significantly interfere with respiration function by decreasing lung volume and may result in rapid shallow breathing that could be harder to detect with the radar system. Thus, the patients in the psych center may have had a higher breathing rate than the rate estimated by the algorithm. Second, depth camera data are used as ground truth for the radar data, and patients' movement patterns for estimating restless time in depth data were manually labeled. The labeling of depth camera data was subjective, and there were times in which it was hard to see the movement, such as when the patient was under the blanket.

In the second part of our work, we investigate two methods for learning the room structure via radio wave reflections for longitudinal health monitoring of older adults in a naturalistic home setting. We first investigate two different methods for the wall position

estimation, which include learning room structure from RF clutter patterns and learning room structure from active movement patterns. The RF clutter pattern is more accurate in estimating wall position in the room without any target, but the movement pattern estimate confirms the wall location by observing moving targets. Comparing the results from the two different methods enables us to get a more accurate wall location in the case of unexpected noise. The wall position estimation between the offices (A, B) and the meeting room (C) is 3.49m based on the RF clutter patterns; the accuracy of this method is 91% compared to the actual distance as measured manually using a tape measure. Meanwhile, the method using active movement indicates there is no motion between the range of 3.5m to 4.4 m. Therefore, we estimate the final wall position between the offices and the meeting is 3.49 m. The wall position between office (A) and office (B) is 3.62m based on the RF clutter patterns; the accuracy of this method is 98% compared to the manually measured distance. Next, a background filter is designed based on the estimated wall position and remove the wall reflection in the received signal for calculating the activity level of older adults over time. In addition, we implemented a system of fuzzy rules using the filtered motion data captured over time, for activity level estimation of older adults in different rooms.

9.2 Future work

In the first part of our work, we designed a classifier to identify the out of bed vs. in bed and got high accuracy and recall. Meanwhile, we estimate the psych center patient's restless time, and the patient's respiration estimation algorithm with different sleep postures during a peaceful sleeping period. In the future, more work could be done to improve the results:

- Identify the patient's motion from the nurse's motion and get more accurate restless time estimation.
- Identify the empty bed case from the person in bed without breathing.
- Recover the small torso area motion from the body motion signal.
- Improve our radar system. It will be more helpful for the radar signal processing if we know more information about the radar design parameters. The Vayyar radar system has swept bandwidth, 1.75GHz, and the range resolution is 8.6cm. If the RF system with higher bandwidth and higher frequency is used in Psych Center project, the range resolution and velocity resolution can be improved which will help in getting a higher respiration rate estimation accuracy.

In the second part of our work, we investigated two methods for learning the room structure via radio wave reflections for longitudinal health monitoring of older adults in a naturalistic home setting. This is a great research topic. Future work in this area should include the following:

- Change the radar system to the FMCW radar system with a higher bandwidth and multiple antennas.
- Identifying the static object without any doppler shift is a big challenge for the FMCW radar system. A more advanced radar system and more data collection would help in learning the environment structure.

Table.XV List of My Posters and Papers

Posters
Nuerzati Resuli, Marjorie Skubic, Scott Kovaleski. Learning Room Structure via Radio Reflection Patterns for In-Home Monitoring of Older Adults. E-week, University of Missouri, 2019.
Nuerzati Resuli, Nader Rohani, Youssef Atris. FMCW Radar Signal Processing via Data Compression for Automotive Application. On Semiconductor Summer Internship, Phoenix, AZ, USA, 2019.
Papers
Nuerzati Resuli, Marjorie Skubic, Scott Kovaleski. Learning Room Structure and Activity Patterns Using RF Sensing for In-Home Monitoring of Older Adults. 2020 IEEE International Conference on Bioinformatics and Biomedicine (BIBM), 2020.
Nuerzati Resuli, Marjorie Skubic, Jung Myungki. Noninvasive Respiration Monitoring Using an RF Sensor in Different Sleeping Postures. IEEE International Conference on Bioinformatics and Biomedicine 2021 (IEEE BIBM 2021)

References

[1]. National alliance on mental illness: https://www.nami.org/mhstats

[2]. Department of Economic and Social Affairs Population Division, 2017. World Population Ageing 2017. United Nations, New York.

[3]. Merrill I. Skolnok, Introduction to Radar Systems, New York: McGraw-Hill, 1962.

[4]. Mark A.Richards, Fundamentals of Radar Signal Processing, New York: McGraw-Hill, 2005.

[5]. Theodore S. Rappaport, Wireless Communication Principles and Practice, Prentice Hall, 2001

[6]. Sebastián Torres, Ric Adams, Christopher Curtis, Eddie Forren, Douglas Forsyth, Igor Ivić, David Priegnitz, John Thompson, and David Warde, "A Demonstration of Adaptive Weather Surveillance and Multifunction Capabilities on the National Weather Radar Testbed Phased Array Radar," 2014 International Radar Conference, 2014

[7]. M. Yeary, G. Crain, A. Zahrai, R. Kelley, J. Meier, Y. Zhang, I. Ivic, C. Curtis, R. Palmer, T.-Y. Yu, R. Doviak, "An Update on the Multi-Channel Phased Array Weather Radar at the National Weather Radar Testbed," 2011 IEEE RadarCon, 2011

[8]. J.M. Muñoz-Ferreras, J. Calvo-Gallego, and F. Pérez-Martínez, "Monitoring Road Traffic with a High Resolution LFMCW Radar," 2008 IEEE Radar Conference. 2018

[9]. J. M. Muñoz-Ferreras, F. Pérez-Martínez, J. Calvo-Gallego, A. Asensio-López, B. P. Dorta-Naranjo, and A. Blanco-del-Campo, "Traffic Surveillance System Based on a High-Resolution Radar, IEEE Transcations on Geoscience and Remote Sensing," vol.46, No.6, June 2008

[10]. Alessio Balleri, Allann AI-Armaghany, Hugh Griffiths, Kinfai Tong, Takashi Matsuura, Takashi Karasudani, Yuji Ohya, “Measurements and Analysis of the Radar Signature of a New Wind Turbine Design at X-band,” IET Radar Sonar Navig. , 2013, 7(2), pp.170-177.

[11]. Gallardo-Hermando, B., Perez-Martinez, F., Aguado-Encabo, “Detection and Mitigation of Wind Turbine Clutter in C-Band Meteorological Radar,” IET Radar Sonar Navig. , 2010, 4(4), pp.520-527.

[12]. Meftah Mohamed, Qamar Zaman, Travis Esau, Aitazaz Farooque, “Design of Ground Surface using Radar,” Proceedings of the 14th International Conference on Precision Agriculture, 2018.

[13]. Xiaoya Wang, Weiguo Jiang, Jing Li, Jianjun Wu, Yunhao Chen, Adu Gong, Hong Tang, Jianwei Yue, “Using remote sensing to monitor the water change of Xiong’An new area,” IGARSS 2019-2019 IEEE International Geoscience and Remote Sensing Symposium, 2019.

[14]. Zongbo Wang, Sivaprasad Gogineni, Fernando Rodrigues-Morales, Jie-Bang Yan, Richard Hale, John Paden, Carl Leuschen, Calen Carabajal, Daniel Gomez-Garcia, Bryan Townley, “Wideband imaging radar for cryospheric remote sensing,” 2014 IEEE Geoscience and Remote Sensing Symposium, 2014.

[15]. E. Staderini, “UWB radars in medicine,” IEEE Aerosp. Electron. Syst. Mag., vol.17, no.1, pp. 13-18, Jan. 2002.

[16]. D. Zito, D. Pepe, B. Neri, D. D. Rossi, A. Lanata, A. Tognetti, and E. Scilingo, “Wearable system-on-a-chip UWB radar for health care and its application to the safety

improvement of emergency operators," in Proc. 29th Annu. Int. Conf. Eng. Med. Biol. Soc., Aug. 2007, pp. 2651-2654

[17]. Ming-Hua Tsai, Chieh-Ling Huang, Pau-Choo Chung, "A Psychiatric Patients Tracking System," 2006 IEEE International Symposium on Circuits and Systems, 2006

[18]. Fatin Nadhirah Hj Ariffin, Au Thien Wan, Wida Susanty Hj Suhaili, "Psychiatric Patients Monitoring Using RFID," 2015 IEEE International Conference on Computer and Communication, 2015

[19]. Marco B.; Núria C.; Teresa F.; Mercedes G.; Daniel A.; Pere J. R.; Pere C., "Measuring Breathing Pattern in Patients With Chronic Obstructive Pulmonary Disease by Electrical Impedance Tomography," Archivos de Bronconeumologia 2009.

[20]. Noah, J. A.; Boliek, C.; Lam, T.; Yang, J. F., "Breathing Frequency Changes at the Onset of Stepping in Human," Journal of Neurophysiology 2008, Published 1 March pp.1224-1234.

[21]. Hung P.D.; Bonnet S.; Guillemaud R.;Castelli e.; Yen P.T.N., "Estimation Of Respirtaory Waveform Using an Accelerometer, Biomedical Imaging: From Nano to Macro," 2008. ISBI 2008. 5th IEEE International Symposium on, pp 1493 – 1496.

[22]. Kawamoto K.;, Tanaka T.; Kuriyama H., "Your Activity Tracker Knows When You Quit Smoking," UbiComp 2014.

[23]. Heise D.; Skubic M., "Monitoring Pulse and Respiration with a Non-Invasive Hydraulic Bed Sensor," 32nd Annual International Conference of the IEEE EMBS. 2010.

[24]. Su B-Y, Enayati M, Ho K-C, Skubic M, Despins D, Keller J, Popescu M, Guidoboni G & Rantz M, "Monitoring the Relative Blood Pressure Using a Hydraulic

Bed Sensor System," IEEE Trans. on Biomedical Engineering, 66(3): 740-748, March, 2019.

[25]. Rosales L, Su B-Y, M., Skubic M & Ho KC, "Heart Rate Monitoring Using Hydraulic Bed Sensor Ballistocardiogram," Journal of Ambient Intelligence and Smart Environments, Vol. 9, pp. 193-207, 2017

[26]. Griffiths E.; Saponas T.S.;Brush A.J.B., "Health Chair: Implicitly Sensing Heart and Respiratory Rate," UbiComp 2014.

[27]. Rinanda Febriani, Aciek Ida Wuryandari, Tunggal Mardiono, "Design Interaction of Smart Health Chair Approach the Usability Aspect on SHESOP Health Care," 2015 4th International Conference on Interactive Digital Media, December 2015

[28]. Anran Wang, Jacob E.Sunshine, Shyamnath Gollakota, "Contactless Infant Monitoring using White Noise," MobiCom 19: The 25th Annual International Conference on Mobile Computing and Networking, 2019

[29]. Olga Boric-Lubecke, Geert Awater, and Victor M. Lubecke, "Wireless LAN PC Card Sensing of Vital Signs," 2003 IEEE Topical Conference on Wireless Communication Technology, 2003

[30]. V.Vasu, N.Fox, C.Heneghan and S.Sezer, "Using the Lomb Periodogram for Non-Contact Estimation of Respiration Rate," 2010 Annual International Conference of the IEEE Engineering in Medicine and Biology, 2010

[31]. Øyvind Aardal, Yoann Paichard, Member, Tor Berger, Tor Sverre Lande, and Svein-Erik Hamran, "Physical Working Principles of Medical Radar," IEEE Transactions on Biomedical Engineering, Vol.60, No.4, 2013

[32]. K. Mostov, E. Liptsen, and R. Boutchko, “Medical applications of shortwave FM radar: Remote monitoring of cardiac and respiratory motion,” Med. Phys., vol. 37, pp. 1332–1338, 2010.

[33]. D. R. Morgan and M. G. Zierdt, “Novel signal processing techniques for Doppler radar cardiopulmonary sensing,” Signal Process., vol. 89, no. 1, pp. 45–66, 2009.

[34]. Yee Siong Lee, Pubudu N. Pathirana, Christopher Louis Steinfort, and Terry Caelli, “Monitoring and Analysis of Respiratory Patterns Using Microwave Doppler Radar,” Medical Imaging and Diagnostic Radiology, 2014

[35]. N.Du, K.Liu, L.Ge, and J.Zhang, “Apnea Radar: A 24GHz Radar-based Contactless Sleep Apnea Detection System,” in Proc. 2nd Int. Conf. Frontiers Sensor Technol, Apr.2017

[36]. Mostafa Alizadeh, George Shaker, Joao Carlos Martins De Almeida, Plinio Pelegrini Morita, and Safeddin Safavi-Naeini, “ Remote Monitoring of Human Vital Signs Using mm-Wave FMCW,” IEEE Access: Special Section on Advanced Information Sensing and Learning Technologies for Data-Centric Smart Health Application, March 2019

[37]. Adeel Ahmad, June Chul Roh, Dan Wang, Aish Dubey, “Vital Signs Monitoring of Multiple People using a FMCW Millimeter-Wave Sensor,” 2018 IEEE Radar Conference, April 2018

[38]. Shekh M M Islam, Ashikur Rahman, Narayana Prasad, Olga Boric-Lubecke1 and Victor M Lubeck, “Identity Authentication System using a Support Vector Machine (SVM) on Radar Respiration Measurements,”, 2019 93rd ARFTG Microwave Measurement Conference, June 2019

[39]. Shekh M M Islam, Ehsan Yavari, Member, Ashikur Rahman, Victor M. Lubecke, and Olga Boric-Lubecke, " Separation of Respiratory Signatures for Multiple Subjects Using Independent Component Analysis with JADE Algorithm," 2018 40th Annual International Conference of the IEEE Engineering in Medicine and Biology Society, July 2018

[40]. Ruth Ravichandran, Elliot Saba1, Ke-Yu Chen, Mayank Goel, Sidhant Gupta, Shwetak N. Patel, " WiBreathe: Estimating Respiration Rate Using Wireless Signals in Natural Settings in the Home," 2015 IEEE International Conference Pervasive Computing and Communications, March, 2015

[41]. Fadel Adib, Hongzi Mao, Zachary Kabelac, Dina Katabi, Robert C. Miller, "Smart Homes that Monitor Breathing and Heart Rate", CHI 2015, April 2015.

[42]. Shichao Yue, Hao He, Hao Wang, Hariharan Rahul, Dina Katabi, "Extracting Multi-Person Respiration from Entangled RF Signals," Proc. ACM interact. Mob. Wearable Ubiquitous Techol. Vol.2, No.2, June 2018

[43]. W. Hu, Z. Zhao, Y.Wang, H.Zhang, F. Lin, 2014. "Noncontact accurate measurement of cardiopulmonary activity using a compact quadrature doppler radar sensor," IEEE Trans. Biomed. Eng. vol.61, pp.725-735.

[44]. Y. Xiao, J. Lin, O. Boric-Lubecke, V.M. Lubecke, 2006. "Frequency-tuning technique for remote detection of heartbeat and respiration using low-power double-sideband transmission in the Ka-band," IEEE Transactions on Microwave Theory and Techniques, vol.54, pp.2023-2032.

[45]. J.E. Kiriazi, O. Boric-Lubecke, V.M. Lubecke, 2012. “Dual-frequency technique for assessment of cardiopulmonary effective RCS and displacement,” IEEE Sensors Journal, vol.12, pp. 574-582.

[46]. M. He, Y. Nian, B. Liu, “Noncontact hear beat signal extraction based on wavelet transform,” International conference on Biomedical Engineering and Information, 2015.

[47]. D.R. Morgan, M.G Zierdt, 2009. “Novel signal processing techniques for doppler radar cardiopulmonary sensing,” Signal Processing, vol.89, pp.45-66.

[48]. Mi He, YongJian Nian, Yushun Gong, 2017. “Novel signal processing method for vital sign monitoring using FMCW,” Biomedical Signal Processing and Control, vol. 33, pp. 335-345.

[49]. K. Z. Haigh, L. M. Kiff, and G. Ho, 2006. “Independent lifestyle assistant: Lessons learned,” Assistive Technology, vol.18, pp.87–106.

[50]. P. Glascock and D. M. Kutzik, 2000. “Behavioral telemedicine: A new approach to continuous nonintrusive monitoring of activities of daily living,” Telemedicine Journal, vol.6, no.1, pp.33–44.

[51]. J. A. Kayeetal, 2011. “Intelligent systems for assessing aging changes: Homebased, unobtrusive, and continuous assessment of aging,” Journal of Gerontology, Psychological Sciences and Social Sciences, vol. 66B, no. 1, pp. i180–i190.

[52]. M. Skubic, G. Alexander, M. Popescu, M. Rantz, and J. Keller, 2009. “A smart home application to eldercare: current status and lessons learned,” Technology and Health Care, vol. 17, no. 3, pp. 183–201.

[53]. P. Cuddihy, 2004. Successful aging. IEEE Pervasive Computing. vol. 3, no. 2, pp. 48–50.

[54]. S. Wang, M. Skubic, and Y. Zhu, 2012. "Activity density map visualization and dissimilarity comparison for eldercare monitoring," IEEE Transactions on Information Technology in Biomedicine, vol. 16, no. 4, pp. 607–614.

[55]. C. Galambos, M. Skubic, S. Wang, and M. Rantz, 2013. "Management of dementia and depression utilizing in-home passive sensor data," Gerontechnology, vol. 11, no. 3, pp. 457–468.

[56]. R. Beckwith, 2003. "Designing for Ubiquity: The perception of privacy," Pervasive Computing, pp.40–46.

[57]. T. S. Barger, D. E. Brown, and M. Alwan, 2005. "Health-status monitoring through analysis of behavioral patterns," IEEE Transactions on System, Man, and Cybernetics, vol.35, no.1, pp.22–27.

[58]. Y. Barak, R. C. Wagenaar, and K. G. Holt, 2006. "Gait characteristics of elderly people with a history of falls: A dynamic approach," Physical Therapy, vol. 86, no. 11, pp. 1501–1510.

[59]. M. Montero-Odasso, Schapira M, 2005. "Gait velocity as a single predictor of adverse events in healthy seniors aged 75 years and older," Journal Gerontology: Medical Sciences, vol. 60, no. 10, pp. 1304–1309.

[60]. R. Camicioli, D. Howieson, B. Oken, G. Sexton, and J. Kaye, 1998. "Motor slowing precedes cognitive impairment in the oldest old," Neurology, vol. 50, no. 5, pp. 1496–1498.

[61]. Kaye J, Mattek N, 2012. “One walk a year to 1000 within a year: continuous in-home unobtrusive gait assessment of older adults,” Gait Posture, vol. 35, no. 2, pp. 197–202.

[62]. Chen-Yu Hsu, Yunchen Liu, Zach Kabelac, Rumen Hristove, Dina Katabi, 2017. Extracting gait velocity and stride length from surrounding radio signals. ACM CHI 2017.

[63]. H. Pigot, B. Lefebvre, J. G. Meunier, B. Kerherv´e, A. Mayers, and S. Giroux, 2003. “The role of intelligent habitats in upholding elders in residence,” Transactions on Biomedicine and Health, vol. 6, pp. 497-506.

[64]. I.Korhonen, J.Parkka, and M.VanGils, 2003. “Health monitoring in the home of the future,” IEEE Engineering Medicine and Biology Magazine, vol.22, no.3, pp.66–73.

[65]. P. Paavilainen, I. Korhonen, and M. Partinen, 2005. “Telemetric activity monitoring as an indicator of long-term changes in health and well-being of the elderly,” Gerontechnology, vol.4, pp.77–85.

[66]. J. Howell, B. M. Strong, J. Weisenberg, A. Kakade, Q. Gao, P. Cuddihy, S.Delisle, S.Kachnowski, and M.S.Maurer, 2010. “Maximum daily 6 minutes of activity: an index of functional capacity derived from actigraphy and its application to older adults with heart failure,” Journal of American Geriatrics Society, vol.58, no.5, pp.931–936.

[67]. M. Philipose, K. P. Fishkin, M. Perkowitz, D. J. Patterson, D. Fox, H. Kautz, and D. Hhnel, 2004. “Inferring activities from interactions with objects,” Pervasive Computing, vol.3, pp.50–57.

[68]. N. Marques, F. Meneses, and A. Moreira, 2012. "Combining similarity function and majority rules for multi-building, multi-floor, Wi-Fi positioning," 2012 International Conference on Indoor Positioning and Indoor Navigation (IPIN'2012).

[69]. K. Kaemarungsi and P. Krishnamurthy, 2004. "Properties of indoor received signal strength for WLAN location fingerprinting," The 1th Annual International Conference on Mobile and Ubiquitous Systems: Networking and Services, pp. 14-23, 2004.

[70]. Chi Zhang, Xinyu Zhang, 2016. "LiTell: Robust indoor localization Using Unmodified light fixtures," In Proceedings of the 22nd Annual International Conferernce on Mobile Computing and Networking

[71]. H.Liu,Y.Gan, J.Yang, S.Sidhome,2012. "Push the limit of WiFi based localization for Smartphones," ACM Mobicom.

[72]. Kevin Chetty, Graeme E. Smith, and Karl Woodbridge. "Through-the-Wall Sensing of Personnel Using Passive Bistatic WiFi Radar at Standoff Distances," IEEE Transactions on Geoscience and Remote Sensing, Vol.50, No.4, 2012

[73]. Fabiola Colone, Paolo Falcone, Carlo Bongioanni, and Pierfrancesco Lombardo. "WiFi-Based Passive Bistatic Radar: Data Processing Schemes and Experimental Results," IEEE Transactions on Aerospace and Electronic System, Vol.48, No.2, 2012

[74]. S. Ram, C. Christianson, Y. Kim, and H. Ling. "Simulation and Analysis of Human Micro-Doppler in through-Wall Environments," IEEE Trans. Geoscience and Remote Sensing, 2010

[75]. S. Ram, Y. Li, and H. Ling. "Doppler-based Detection and Tracking of Humans in Indoor Environment," Journal of the Franklin Institute, 2008

[76]. S. Ram, and H. Ling. “Through-wall Tracking of Human Movers using Joint Doppler and Array Processing,” IEEE Trans. Geoscience and Remote Sensing, 2008

[77]. F. Soldovieri, and R. Solimene. “Through-wall Imaging via Linear Inverse Scattering Algorithm,” Geoscience and Remote Sensing, 2007

[78]. Radar Vision. http:// www.timedomain.com. Time Domain Corporation

[79]. Y. Yang and A. Fathy. “See-through-wall Imaging using Ultra Wideband Short-pulse Radar System,” IEEE Antennas and Propagation Society International Symposium, 2005

[80]. G. Charvat, L. Kempel, E. Rothwell, C. Coleman, and E. Mokole. “A Through-dielectric Radar Imaging System,” IEEE Trans. Antennas and Propagation, 2010

[81]. T. Ralston, G. Charvat, and J. Peabody. “Real-time Through-wall Imaging using an Ultra Wide Band Multiple-input Multiple-output (MIMO) Phase Array Radar System,” IEEE ARRAY, 2010

[82]. Gregory L. Charvat, Alan J. Fenn, and Bradley T. Perry, 2012. “The MIT IAP radar course: build a small radar system capable of sensing range, Doppler, and synthetic aperture imaging,” IEEE Radar Conference, pp. 138-144, 2012.

[83]. Fadel Adib, and Dina Katabi, 2013. “See through walls with Wi-Fi,” ACM Special Interest Group on Data Communication (SIGCOMM), Hong Kong.

[84]. Fadel Adib, Zachary Kabelac, and Dina Katabi, 2015. “Multi-person localization via RF body Reflections,” Usenix Symposium on Networked Systems Design and Implementation, Oakland, CA.

[85]. Shawn Fernandes, “Contactless Extraction of Respiration Rate from Depth and Thermal Sensors,”, Master Thesis, University of Missouri-Columbia, 2018.

[86]. Tse, D., and Vishwanath, P. Fundamentals of Wireless Communications. Cambridge University Press, 2005.

[87]. Texas Instrument online training: https://training.ti.com/intro-mmwave-sensing-fmcw-radars-module-1-range-estimation.

[88]. Gregory L. Charvat. Small and Short-Range Radar System. New York: CRC Press, 2014

[89]. Vayyar radar: https://vayyar.com

[90]. John G. Proakis and Dimitris G. Manolakis. Digital Signal Processing. Pearson Education, 2007

[91]. Approaches for Angle of Arrival Estimation: https://www.cs.utexas.edu/~swadhin/reading_group/slides/AoA.pdf

[92]. Yang Zhang, Fuming Chen, Huijun Xue, Zhao Li, Qiang An, Jianqi Wang, and Yang Zhang. "Detection and Identification of Multiple Stationary Human Target via Bio-Radar Based on the Cross- Correlation Method," Sensor, 2016

[93]. Yan S. Kong L. J, Yang X. B, Zhou Y. S. "Life Detection Based on Cross Correlation Analysis," In Proceedings of the 2011 IEEE CIE International Conference on Radar, Chendu, China, 2011

[94]. Zaikov E. "UWB Radar for Detection and Localization of Trapped People," In Proceeding of the International Radar Symposium. Vilnius, Lithuania, 2010

[95]. Sergios Theodoridis and Konstanions Koutroumbas. Pattern Recognition. Burlington: Elsevier Press, 2009

[96]. Richard O. Duda, Peter E. Hart, and David G. Stork. Pattern Classification. Wiley, 2006

[97]. Christopher M. Bishop. Pattern Recognition and Machine Learning. Cambridge, 2006

[98]. Mateusz Buda, Atsuto Maki, and Maciej A. Mazurowski, A Systematic Study of the Class Imbalance Problem in Convolutional Neural Networks, Neural Networks, 2016

[99]. Timothy C. Havens, James C. Bezdek, 2012. "An Efficient Formulation of the Improved Visual Assessment of Cluster Tendency (iVAT) Algorithm," IEEE Transactions on Knowledge and Data Engineering, Vol 24, NO.5.

[100]. Jacalyn M. Hubanda, James C. Bezdeka, Richard J. Hathawayb. "BigVAT:Visual Assessment of Cluster Tendency for Large Data Sets," 2005 Pattern Recognition Society. Published by Elsevier Ltd., 2005

[101]. James M. Keller, Derong Liu, David B.Fogel, 2016. Fundamental of Computational Intelligence: Neural Networks, Fuzzy System, and Evolutionary Computation. Piscataway, NJ

[102]. L. A. ZADEH. Fuzzy Set. Information and Control, 1965

[103]. George J.Klir, Bo Yuan. Fuzzy Sets and Fuzzy Logic Theory and Application. New Jersey: Prentice Hall, 1995

Appendix A. Nursing Notes

1. Subject: 001

Time: 09/10/2019 AT 19:59 – 09/11/2019 AT 06:51

CLINICAL PATIENT INFO		
09/11/2019 06:51 CDT	Patient Room	Lying in Bed
09/11/2019 06:41 CDT	Day/Dining Room	Interacting with othe
09/11/2019 06:25 CDT	Patient Room	Sleeping
09/11/2019 06:04 CDT	Patient Room	Sleeping
09/11/2019 05:48 CDT	Patient Room	Sleeping
09/11/2019 05:30 CDT	Patient Room	Sleeping
09/11/2019 05:24 CDT	Patient Room	Sleeping
09/11/2019 05:08 CDT	Patient Room	Sleeping
09/11/2019 04:56 CDT	Patient Room	Sleeping
09/11/2019 04:35 CDT	Patient Room	Sleeping
09/11/2019 04:23 CDT	Patient Room	Sleeping
09/11/2019 04:06 CDT	Patient Room	Sleeping
09/11/2019 03:51 CDT	Patient Room	Sleeping
09/11/2019 03:33 CDT	Patient Room	Sleeping
09/11/2019 03:27 CDT	Patient Room	Sleeping
09/11/2019 03:07 CDT	Patient Room	Sleeping
09/11/2019 02:50 CDT	Patient Room	Sleeping
09/11/2019 02:32 CDT	Patient Room	Sleeping
09/11/2019 02:15 CDT	Patient Room	Sleeping
09/11/2019 02:01 CDT	Patient Room	Sleeping
09/11/2019 01:46 CDT	Patient Room	Sleeping
09/11/2019 01:30 CDT	Patient Room	Sleeping
09/11/2019 01:18 CDT	Patient Room	Sleeping
09/11/2019 01:00 CDT	Patient Room	Sleeping
09/11/2019 00:47 CDT	Patient Room	Sleeping
09/11/2019 00:30 CDT	Patient Room	Sleeping
09/11/2019 00:20 CDT	Patient Room	Sleeping
09/11/2019 00:07 CDT	Patient Room	Sleeping
09/10/2019 23:54 CDT	Patient Room	Sleeping
09/10/2019 23:40 CDT	Patient Room	Sleeping
09/10/2019 23:19 CDT	Patient Room	Sleeping
09/10/2019 23:07 CDT	Patient Room	Sleeping
09/10/2019 22:50 CDT	Patient Room	Sleeping
09/10/2019 22:37 CDT	Patient Room	Sleeping
09/10/2019 22:20 CDT	Patient Room	Sleeping
09/10/2019 22:04 CDT	Patient Room	Sleeping
09/10/2019 21:49 CDT	Patient Room	Sleeping
09/10/2019 21:41 CDT	Patient Room	Sleeping
09/10/2019 21:18 CDT	Day/Dining Room	Sitting/Standing
09/10/2019 21:09 CDT	Day/Dining Room	Sitting/Standing
09/10/2019 20:50 CDT	Day/Dining Room	Interacting with othe
09/10/2019 20:44 CDT	Day/Dining Room	Interacting with othe
09/10/2019 20:22 CDT	Day/Dining Room	Sitting/Standing
09/10/2019 20:14 CDT	Day/Dining Room	Interacting with othe
09/10/2019 19:59 CDT	Day/Dining Room	Interacting with othe

2. Subject: 001

Time: 09/11/2019 AT 19:50 – 09/12/2019 AT 06:48

CLINICAL PATIENT INFO		
09/12/2019 06:48 CDT	Patient Room	Sleeping
09/12/2019 06:32 CDT	Patient Room	Sleeping
09/12/2019 06:16 CDT	Patient Room	Sleeping
09/12/2019 06:00 CDT	Patient Room	Lying in Bed
09/12/2019 05:46 CDT	Day/Dining Room	Sitting/Standing
09/12/2019 05:30 CDT	Patient Room	Sleeping
09/12/2019 05:17 CDT	Patient Room	Sleeping
09/12/2019 05:03 CDT	Patient Room	Sleeping
09/12/2019 04:45 CDT	Patient Room	Sleeping
09/12/2019 04:30 CDT	Patient Room	Sleeping
09/12/2019 04:20 CDT	Patient Room	Sleeping
09/12/2019 04:07 CDT	Patient Room	Sleeping
09/12/2019 03:45 CDT	Patient Room	Sleeping
09/12/2019 03:32 CDT	Patient Room	Sleeping
09/12/2019 03:15 CDT	Patient Room	Lying in Bed
09/12/2019 03:00 CDT	Patient Room	Sleeping
09/12/2019 02:45 CDT	Patient Room	Lying in Bed
09/12/2019 02:44 CDT	Patient Room	Sleeping
09/12/2019 02:22 CDT	Patient Room	Sleeping
09/12/2019 02:06 CDT	Patient Room	Sleeping
09/12/2019 01:48 CDT	Patient Room	Sleeping
09/12/2019 01:41 CDT	Patient Room	Sleeping
09/12/2019 01:15 CDT	Patient Room	Sleeping
09/12/2019 01:00 CDT	Patient Room	Sleeping
09/12/2019 00:45 CDT	Patient Room	Sleeping
09/12/2019 00:44 CDT	Patient Room	Sleeping
09/12/2019 00:21 CDT	Patient Room	Sleeping
09/12/2019 00:05 CDT	Patient Room	Sleeping
09/11/2019 23:50 CDT	Patient Room	Sleeping
09/11/2019 23:30 CDT	Patient Room	Interacting with oth
09/11/2019 23:19 CDT	Patient Room	Interacting with oth
09/11/2019 23:05 CDT	Patient Room	Interacting with oth
09/11/2019 22:59 CDT	Day/Dining Room	Engaged in activity
09/11/2019 22:35 CDT	Day/Dining Room	Engaged in activity
09/11/2019 22:21 CDT	Day/Dining Room	Engaged in activity, I
09/11/2019 22:09 CDT	Day/Dining Room	Engaged in activity, I
09/11/2019 21:54 CDT	Day/Dining Room	Engaged in activity, I
09/11/2019 21:42 CDT	Day/Dining Room	Engaged in activity, I
09/11/2019 21:21 CDT	Day/Dining Room	Engaged in activity, I
09/11/2019 21:05 CDT	Day/Dining Room	Engaged in activity, I
09/11/2019 20:52 CDT	Day/Dining Room	Engaged in activity, I
09/11/2019 20:44 CDT	Day/Dining Room	Engaged in activity, I
09/11/2019 20:20 CDT	Day/Dining Room	Sitting/Standing
09/11/2019 20:07 CDT	Day/Dining Room	Sitting/Standing
09/11/2019 19:50 CDT	group; Off Unit	Engaged in activity

3. Subject: 001

Time: 09/12/2019 AT 19:51 – 09/13/2019 AT 06:46

CLINICAL PATIENT INFO		
09/13/2019 06:46 CDT	Exam	ketamine
09/13/2019 06:30 CDT	Patient Room	Sleeping
09/13/2019 06:21 CDT	Patient Room	Sleeping
09/13/2019 06:14 CDT	Patient Room	Sleeping
09/13/2019 05:53 CDT	Patient Room	Sleeping
09/13/2019 05:32 CDT	Patient Room	Sleeping
09/13/2019 05:17 CDT	Patient Room	Sleeping
09/13/2019 05:03 CDT	Patient Room	Sleeping
09/13/2019 04:46 CDT	Patient Room	Sleeping
09/13/2019 04:33 CDT	Patient Room	Sleeping
09/13/2019 04:16 CDT	Patient Room	Sleeping
09/13/2019 04:01 CDT	Patient Room	Sleeping
09/13/2019 03:45 CDT	Patient Room	Lying in Bed
09/13/2019 03:34 CDT	Patient Room	Sleeping
09/13/2019 03:17 CDT	Patient Room	Sleeping
09/13/2019 03:02 CDT	Patient Room	Sleeping
09/13/2019 02:47 CDT	Bathroom	Toileting/showering
09/13/2019 02:30 CDT	Patient Room	Sleeping
09/13/2019 02:20 CDT	Patient Room	Sleeping
09/13/2019 02:01 CDT	Patient Room	Sleeping
09/13/2019 01:46 CDT	Patient Room	Sleeping
09/13/2019 01:32 CDT	Patient Room	Sleeping
09/13/2019 01:15 CDT	Patient Room	Sleeping
09/13/2019 01:02 CDT	Patient Room	Sleeping
09/13/2019 00:47 CDT	Patient Room	Sleeping
09/13/2019 00:37 CDT	Patient Room	Sleeping
09/13/2019 00:20 CDT	Patient Room	Sleeping
09/13/2019 00:07 CDT	Patient Room	Sleeping
09/12/2019 23:53 CDT	Patient Room	Sleeping
09/12/2019 23:38 CDT	Patient Room	Sleeping
09/12/2019 23:17 CDT	Patient Room	Sleeping
09/12/2019 23:06 CDT	Patient Room	Sleeping
09/12/2019 22:48 CDT	Patient Room	Sleeping
09/12/2019 22:36 CDT	Patient Room	Sleeping
09/12/2019 22:18 CDT	Patient Room	Sleeping
09/12/2019 22:04 CDT	Patient Room	Sleeping
09/12/2019 21:48 CDT	Patient Room	Sleeping
09/12/2019 21:33 CDT	Patient Room	Sleeping
09/12/2019 21:22 CDT	Day/Dining Room	on the phone
09/12/2019 21:11 CDT	Day/Dining Room	on the phone
09/12/2019 20:56 CDT	Medication Window	Taking Meds
09/12/2019 20:40 CDT	Patient Room	Sleeping
09/12/2019 20:21 CDT	Patient Room	Sleeping
09/12/2019 20:05 CDT	Patient Room	Sitting/Standing
09/12/2019 19:51 CDT	TR	therapy room

4. Subject: 002

Time: 09/10/2019 AT 19:52 – 09/11/2019 AT 06:46

CLINICAL PATIENT INFO		
09/11/2019 06:46 CDT	Patient Room	Sleeping
09/11/2019 06:41 CDT	Patient Room	Sleeping
09/11/2019 06:25 CDT	Patient Room	Sleeping
09/11/2019 06:04 CDT	Patient Room	Sleeping
09/11/2019 05:48 CDT	Patient Room	Sleeping
09/11/2019 05:30 CDT	Patient Room	Sleeping
09/11/2019 05:24 CDT	Patient Room	Sleeping
09/11/2019 05:08 CDT	Patient Room	Sleeping
09/11/2019 04:56 CDT	Patient Room	Sleeping
09/11/2019 04:35 CDT	Patient Room	Sleeping
09/11/2019 04:23 CDT	Patient Room	Sleeping
09/11/2019 04:06 CDT	Patient Room	Sleeping
09/11/2019 03:51 CDT	Patient Room	Sleeping
09/11/2019 03:33 CDT	Patient Room	Sleeping
09/11/2019 03:27 CDT	Patient Room	Sleeping
09/11/2019 03:07 CDT	Patient Room	Sleeping
09/11/2019 02:50 CDT	Patient Room	Sleeping
09/11/2019 02:32 CDT	Patient Room	Sleeping
09/11/2019 02:15 CDT	Patient Room	Lying in Bed
09/11/2019 02:01 CDT	Patient Room	Sleeping
09/11/2019 01:46 CDT	Patient Room	Lying in Bed
09/11/2019 01:30 CDT	Patient Room	Sleeping
09/11/2019 01:18 CDT	Patient Room	Sleeping
09/11/2019 01:00 CDT	Patient Room	Sleeping
09/11/2019 00:47 CDT	Patient Room	Sleeping
09/11/2019 00:30 CDT	Patient Room	Sleeping
09/11/2019 00:18 CDT	Patient Room	Lying in Bed
09/11/2019 00:05 CDT	Bathroom	Toileting/showering
09/10/2019 23:50 CDT	Patient Room	Lying in Bed
09/10/2019 23:38 CDT	Patient Room	Sitting/Standing
09/10/2019 23:19 CDT	Hallway	Pacing
09/10/2019 23:07 CDT	Day/Dining Room	Interacting with othe
09/10/2019 22:50 CDT	Day/Dining Room	Interacting with othe
09/10/2019 22:37 CDT	Day/Dining Room	Pacing
09/10/2019 22:19 CDT	Day/Dining Room	Interacting with othe
09/10/2019 22:04 CDT	Day/Dining Room	Pacing
09/10/2019 21:50 CDT	Nurses Desk	Speaking with Staff
09/10/2019 21:35 CDT	Nurses Desk	Speaking with Staff
09/10/2019 21:18 CDT	Patient Room	Sitting/Standing
09/10/2019 21:07 CDT	Day/Dining Room	Engaged in activity
09/10/2019 20:51 CDT	Patient Room	Sleeping
09/10/2019 20:44 CDT	Patient Room	Sleeping
09/10/2019 20:20 CDT	Patient Room	Sleeping
09/10/2019 20:14 CDT	Patient Room	Sleeping
09/10/2019 19:52 CDT	Patient Room	Sleeping

5. Subject: 002

Time: 09/11/2019 AT 19:50 – 09/12/2019 AT 06:48

CLINICAL PATIENT INFO		
09/12/2019 06:48 CDT	Patient Room	Lying in Bed
09/12/2019 06:32 CDT	Patient Room	Sleeping
09/12/2019 06:16 CDT	Patient Room	Lying in Bed
09/12/2019 06:00 CDT	Patient Room	Lying in Bed
09/12/2019 05:46 CDT	Patient Room	Sleeping
09/12/2019 05:30 CDT	Patient Room	Sleeping
09/12/2019 05:17 CDT	Patient Room	Sleeping
09/12/2019 05:03 CDT	Patient Room	Sleeping
09/12/2019 04:45 CDT	Patient Room	Sleeping
09/12/2019 04:30 CDT	Patient Room	Sleeping
09/12/2019 04:20 CDT	Patient Room	Sleeping
09/12/2019 04:07 CDT	Patient Room	Sleeping
09/12/2019 03:45 CDT	Day/Dining Room	Sitting/Standing
09/12/2019 03:32 CDT	Patient Room	Sleeping
09/12/2019 03:15 CDT	Patient Room	Sleeping
09/12/2019 03:00 CDT	Patient Room	Lying in Bed
09/12/2019 02:45 CDT	Patient Room	Sleeping
09/12/2019 02:44 CDT	Patient Room	Sleeping
09/12/2019 02:22 CDT	Patient Room	Sleeping
09/12/2019 02:06 CDT	Patient Room	Sleeping
09/12/2019 01:48 CDT	Patient Room	Sleeping
09/12/2019 01:41 CDT	Patient Room	Sleeping
09/12/2019 01:15 CDT	Patient Room	Sleeping
09/12/2019 01:00 CDT	Patient Room	Sleeping
09/12/2019 00:45 CDT	Patient Room	Sleeping
09/12/2019 00:44 CDT	Patient Room	Sleeping
09/12/2019 00:21 CDT	Patient Room	Sleeping
09/12/2019 00:05 CDT	Patient Room	Sleeping
09/11/2019 23:50 CDT	Patient Room	Sleeping
09/11/2019 23:30 CDT	Patient Room	Interacting with othe
09/11/2019 23:19 CDT	Patient Room	Interacting with othe
09/11/2019 23:05 CDT	Patient Room	Interacting with othe
09/11/2019 22:59 CDT	Day/Dining Room	Engaged in activity
09/11/2019 22:35 CDT	Day/Dining Room	Engaged in activity
09/11/2019 22:20 CDT	Day/Dining Room	interacting with staff
09/11/2019 22:08 CDT	Hallway	Interacting with othe
09/11/2019 21:54 CDT	Hallway	Pacing
09/11/2019 21:42 CDT	TV room	Watching TV
09/11/2019 21:24 CDT	Day/Dining Room	Interacting with othe
09/11/2019 21:05 CDT	Day/Dining Room	Interacting with othe
09/11/2019 20:51 CDT	Day/Dining Room	Interacting with othe
09/11/2019 20:44 CDT	Day/Dining Room	Watching Tv
09/11/2019 20:19 CDT	Day/Dining Room	Sitting/Standing
09/11/2019 20:06 CDT	Day/Dining Room	Sitting/Standing
09/11/2019 19:50 CDT	group; Off Unit	Engaged in activity

6. Subject: 002

Time: 09/12/2019 AT 19:51 – 09/13/2019 AT 06:46

CLINICAL PATIENT INFO		
09/13/2019 06:46 CDT	Patient Room	Sleeping
09/13/2019 06:30 CDT	Patient Room	Sleeping
09/13/2019 06:21 CDT	Patient Room	Sleeping
09/13/2019 06:14 CDT	Patient Room	Sleeping
09/13/2019 05:53 CDT	Patient Room	Sleeping
09/13/2019 05:32 CDT	Day/Dining Room	Sitting/Standing
09/13/2019 05:17 CDT	Day/Dining Room	Sitting/Standing
09/13/2019 05:03 CDT	Patient Room	Sleeping
09/13/2019 04:46 CDT	Patient Room	Sleeping
09/13/2019 04:33 CDT	Patient Room	Sleeping
09/13/2019 04:16 CDT	Patient Room	Sleeping
09/13/2019 04:01 CDT	Patient Room	Sleeping
09/13/2019 03:45 CDT	Patient Room	Sleeping
09/13/2019 03:34 CDT	Patient Room	Sleeping
09/13/2019 03:17 CDT	Patient Room	Sleeping
09/13/2019 03:02 CDT	Patient Room	Sleeping
09/13/2019 02:46 CDT	Patient Room	Sleeping
09/13/2019 02:30 CDT	Patient Room	Sleeping
09/13/2019 02:20 CDT	Patient Room	Sleeping
09/13/2019 02:01 CDT	Patient Room	Sleeping
09/13/2019 01:46 CDT	Patient Room	Sleeping
09/13/2019 01:32 CDT	Patient Room	Sleeping
09/13/2019 01:15 CDT	Patient Room	Sleeping
09/13/2019 01:02 CDT	Patient Room	Sleeping
09/13/2019 00:47 CDT	Patient Room	Sleeping
09/13/2019 00:37 CDT	Patient Room	Sleeping
09/13/2019 00:20 CDT	Patient Room	Sitting/Standing
09/13/2019 00:07 CDT	Day/Dining Room	Walking around
09/12/2019 23:53 CDT	Day/Dining Room	Walking around
09/12/2019 23:38 CDT	Day/Dining Room	Walking around
09/12/2019 23:17 CDT	Day/Dining Room	Sitting/Standing
09/12/2019 23:05 CDT	Day/Dining Room	Sitting/Standing
09/12/2019 22:48 CDT	Day/Dining Room	watching tv
09/12/2019 22:36 CDT	Day/Dining Room	Engaged in activity
09/12/2019 22:18 CDT	Day/Dining Room	Engaged in activity
09/12/2019 22:04 CDT	Day/Dining Room	Engaged in activity
09/12/2019 21:48 CDT	Day/Dining Room	Engaged in activity
09/12/2019 21:33 CDT	Day/Dining Room	Engaged in activity
09/12/2019 21:22 CDT	Day/Dining Room	Engaged in activity
09/12/2019 21:11 CDT	Day/Dining Room	on the phone
09/12/2019 20:54 CDT	Day/Dining Room	on the phone
09/12/2019 20:31 CDT	Day/Dining Room	Interacting with othe
09/12/2019 20:21 CDT	Bathroom	Toileting/showering
09/12/2019 20:04 CDT	Day/Dining Room	Sitting/Standing
09/12/2019 19:51 CDT	TR	therapy room

7. Subject: 003

Time: 09/17/2019 AT 19:05 – 09/18/2019 AT 06:51

CLINICAL PATIENT INFO		
09/18/2019 06:51 CDT	Patient Room	Sleeping
09/18/2019 06:15 CDT	Patient Room	Sleeping
09/18/2019 06:00 CDT	Patient Room	Sleeping
09/18/2019 05:45 CDT	Patient Room	Sleeping
09/18/2019 05:39 CDT	Patient Room	Sleeping
09/18/2019 05:15 CDT	Patient Room	Sleeping
09/18/2019 05:03 CDT	Patient Room	Sleeping
09/18/2019 04:51 CDT	Patient Room	Sleeping
09/18/2019 04:35 CDT	Patient Room	Sleeping
09/18/2019 04:20 CDT	Patient Room	Sleeping
09/18/2019 04:05 CDT	Patient Room	Sleeping
09/18/2019 03:51 CDT	Patient Room	Sleeping
09/18/2019 03:36 CDT	Patient Room	Sleeping
09/18/2019 03:17 CDT	Patient Room	Sleeping
09/18/2019 03:00 CDT	Patient Room	Sleeping
09/18/2019 02:45 CDT	Patient Room	Sleeping
09/18/2019 02:32 CDT	Patient Room	Sleeping
09/18/2019 02:19 CDT	Patient Room	Sleeping
09/18/2019 02:05 CDT	Patient Room	Sleeping
09/18/2019 01:50 CDT	Patient Room	Sleeping
09/18/2019 01:37 CDT	Patient Room	Sleeping
09/18/2019 01:15 CDT	Patient Room	Sleeping
09/18/2019 01:02 CDT	Patient Room	Sleeping
09/18/2019 00:45 CDT	Patient Room	Sleeping
09/18/2019 00:34 CDT	Patient Room	Sleeping
09/18/2019 00:23 CDT	Patient Room	Sleeping
09/18/2019 00:03 CDT	Patient Room	Sleeping
09/17/2019 23:48 CDT	Patient Room	Sleeping
09/17/2019 23:23 CDT	Patient Room	Sleeping
09/17/2019 23:06 CDT	Day/Dining Room	Sitting/Standing
09/17/2019 22:55 CDT	Day/Dining Room	tv
09/17/2019 22:35 CDT	Day/Dining Room	Interacting with othe
09/17/2019 22:18 CDT	front desk	Interacting with othe
09/17/2019 22:02 CDT	Day/Dining Room	watching tv
09/17/2019 21:45 CDT	Day/Dining Room	watching tv
09/17/2019 21:43 CDT	TV room	Watching TV
09/17/2019 21:19 CDT	Day/Dining Room	Sitting/Standing
09/17/2019 21:03 CDT	Day/Dining Room	Sitting/Standing
09/17/2019 20:54 CDT	Day/Dining Room	Sitting/Standing
09/17/2019 20:44 CDT	Day/Dining Room; Re	Interacting with othe
09/17/2019 20:24 CDT	Day/Dining Room	Sitting/Standing
09/17/2019 20:12 CDT	Day/Dining Room	Sitting/Standing
09/17/2019 19:59 CDT	Day/Dining Room; Da	Sitting/Standing; Inte
09/17/2019 19:42 CDT	Day/Dining Room	Sitting/Standing
09/17/2019 19:05 CDT	Off Unit	group

8. Subject: 004

Time: 09/17/2019 AT 19:05 – 09/18/2019 AT 06:50

CLINICAL PATIENT INFO		
09/18/2019 06:50 CDT	Patient Room	Sleeping
09/18/2019 06:15 CDT	Patient Room	Sleeping
09/18/2019 06:00 CDT	Patient Room	Sleeping
09/18/2019 05:45 CDT	Patient Room	Sleeping
09/18/2019 05:39 CDT	Patient Room	Sleeping
09/18/2019 05:15 CDT	Patient Room	Sleeping
09/18/2019 05:03 CDT	Patient Room	Sleeping
09/18/2019 04:51 CDT	Patient Room	Sleeping
09/18/2019 04:35 CDT	Patient Room	Sleeping
09/18/2019 04:20 CDT	Patient Room	Sleeping
09/18/2019 04:05 CDT	Patient Room	Sleeping
09/18/2019 03:51 CDT	Patient Room	Sleeping
09/18/2019 03:36 CDT	Patient Room	Sleeping
09/18/2019 03:17 CDT	Patient Room	Sleeping
09/18/2019 03:00 CDT	Patient Room	Sleeping
09/18/2019 02:45 CDT	Patient Room	Sleeping
09/18/2019 02:32 CDT	Patient Room	Sleeping
09/18/2019 02:19 CDT	Patient Room	Sleeping
09/18/2019 02:05 CDT	Patient Room	Sleeping
09/18/2019 01:50 CDT	Patient Room	Sleeping
09/18/2019 01:37 CDT	Patient Room	Sleeping
09/18/2019 01:15 CDT	Patient Room	Lying in Bed
09/18/2019 01:02 CDT	Patient Room	Sleeping
09/18/2019 00:45 CDT	Patient Room	Sleeping
09/18/2019 00:34 CDT	Patient Room	Sleeping
09/18/2019 00:23 CDT	Patient Room	Sleeping
09/18/2019 00:03 CDT	Patient Room	Sleeping
09/17/2019 23:48 CDT	Patient Room	Sleeping
09/17/2019 23:23 CDT	Patient Room	Sleeping
09/17/2019 23:05 CDT	Patient Room	Sleeping
09/17/2019 22:54 CDT	Patient Room	Sleeping
09/17/2019 22:34 CDT	Patient Room	Sleeping
09/17/2019 22:18 CDT	Patient Room	Sleeping
09/17/2019 22:03 CDT	Patient Room	Sleeping
09/17/2019 21:50 CDT	Patient Room	Sleeping
09/17/2019 21:43 CDT	Patient Room	Sleeping
09/17/2019 21:19 CDT	Day/Dining Room	Sitting/Standing
09/17/2019 21:03 CDT	Day/Dining Room	Sitting/Standing
09/17/2019 20:54 CDT	Day/Dining Room	Sitting/Standing
09/17/2019 20:44 CDT	Day/Dining Room; Re	Interacting with othe
09/17/2019 20:22 CDT	Day/Dining Room	Sitting/Standing
09/17/2019 20:12 CDT	Day/Dining Room	Sitting/Standing
09/17/2019 19:59 CDT	Day/Dining Room; Da	Sitting/Standing; Inte
09/17/2019 19:42 CDT	Day/Dining Room	Sitting/Standing
09/17/2019 19:05 CDT	Off Unit	group

9. Subject: 005

Time: 09/18/2019 AT 19:04 – 09/19/2019 AT 06:09

CLINICAL PATIENT INFO		
09/19/2019 06:09 CDT	Exam	Labs
09/19/2019 05:51 CDT	Patient Room	Sleeping
09/19/2019 05:40 CDT	Patient Room	Sleeping
09/19/2019 05:16 CDT	Patient Room	Sleeping
09/19/2019 05:02 CDT	Patient Room	Sleeping
09/19/2019 04:46 CDT	Patient Room	Sleeping
09/19/2019 04:32 CDT	Patient Room	Sleeping
09/19/2019 04:22 CDT	Patient Room	Sleeping
09/19/2019 04:04 CDT	Patient Room	Sleeping
09/19/2019 03:51 CDT	Patient Room	Sleeping
09/19/2019 03:44 CDT	Patient Room	Sleeping
09/19/2019 03:17 CDT	Patient Room	Sleeping
09/19/2019 03:00 CDT	Patient Room	Sleeping
09/19/2019 02:47 CDT	Patient Room	Sleeping
09/19/2019 02:39 CDT	Patient Room	Sleeping
09/19/2019 02:22 CDT	Patient Room	Sleeping
09/19/2019 02:01 CDT	Patient Room	Sleeping
09/19/2019 01:46 CDT	Patient Room	Sleeping
09/19/2019 01:31 CDT	Patient Room	Sleeping
09/19/2019 01:27 CDT	Patient Room	Sleeping
09/19/2019 01:05 CDT	Patient Room	Sleeping
09/19/2019 00:51 CDT	Patient Room	Sleeping
09/19/2019 00:35 CDT	Patient Room	Sleeping
09/19/2019 00:17 CDT	Patient Room	Sleeping
09/19/2019 00:01 CDT	Patient Room	Sleeping
09/18/2019 23:45 CDT	Patient Room	Sleeping
09/18/2019 23:30 CDT	Patient Room	Sleeping
09/18/2019 23:18 CDT	Patient Room	Sleeping
09/18/2019 23:02 CDT	Patient Room	Sleeping
09/18/2019 22:52 CDT	Patient Room	Sleeping
09/18/2019 22:42 CDT	Patient Room	Sleeping
09/18/2019 22:21 CDT	Medication Window	Taking Meds
09/18/2019 22:03 CDT	Patient Room	Sleeping
09/18/2019 21:48 CDT	Patient Room	Sleeping
09/18/2019 21:40 CDT	Patient Room	Sleeping
09/18/2019 21:18 CDT	Patient Room	Sleeping
09/18/2019 21:03 CDT	Patient Room	Sleeping
09/18/2019 20:53 CDT	Patient Room	Sleeping
09/18/2019 20:40 CDT	Patient Room	Sleeping
09/18/2019 20:18 CDT	Patient Room	Lying in Bed
09/18/2019 20:08 CDT	Patient Room	Lying in Bed
09/18/2019 19:50 CDT	Patient Room	Lying in Bed
09/18/2019 19:43 CDT	Patient Room	Lying in Bed
09/18/2019 19:21 CDT	Patient Room	Sleeping
09/18/2019 19:04 CDT	Patient Room	Sleeping

10. Subject: 007

Time: 09/24/2019 AT 19:20 – 09/25/2019 AT 06:19

CLINICAL PATIENT INFO		
09/25/2019 06:19 CDT	Patient Room	Sleeping
09/25/2019 06:00 CDT	Patient Room	Sleeping
09/25/2019 05:45 CDT	Patient Room	Sleeping
09/25/2019 05:36 CDT	Patient Room	Sleeping
09/25/2019 05:16 CDT	Patient Room	Sleeping
09/25/2019 05:01 CDT	Patient Room	Sleeping
09/25/2019 04:48 CDT	Patient Room	Sleeping
09/25/2019 04:36 CDT	Patient Room	Lying in Bed
09/25/2019 04:16 CDT	Patient Room	Sleeping
09/25/2019 04:03 CDT	Patient Room	Sleeping
09/25/2019 03:45 CDT	Patient Room	Sleeping
09/25/2019 03:37 CDT	Patient Room	Sleeping
09/25/2019 03:18 CDT	Patient Room	Sleeping
09/25/2019 03:04 CDT	Patient Room	Sleeping
09/25/2019 02:45 CDT	Patient Room	Lying in Bed
09/25/2019 02:30 CDT	Patient Room	Sleeping
09/25/2019 02:15 CDT	Patient Room	Sleeping
09/25/2019 02:05 CDT	Patient Room	Sleeping
09/25/2019 01:47 CDT	Patient Room	Sleeping
09/25/2019 01:33 CDT	Patient Room	Sleeping
09/25/2019 01:18 CDT	Patient Room	Sleeping
09/25/2019 01:04 CDT	Patient Room	Sleeping
09/25/2019 00:48 CDT	Patient Room	Sleeping
09/25/2019 00:35 CDT	Patient Room	Sleeping
09/25/2019 00:16 CDT	Patient Room	Sleeping
09/25/2019 00:00 CDT	Patient Room	Sleeping
09/24/2019 23:45 CDT	Patient Room	Sleeping
09/24/2019 23:30 CDT	Patient Room	Sleeping
09/24/2019 23:16 CDT	Patient Room	Sleeping
09/24/2019 23:03 CDT	Patient Room	Sleeping
09/24/2019 22:52 CDT	Patient Room	Sleeping
09/24/2019 22:36 CDT	Patient Room	Sleeping
09/24/2019 22:19 CDT	Patient Room	Sleeping
09/24/2019 22:03 CDT	Patient Room	Sleeping
09/24/2019 21:49 CDT	Patient Room	Sleeping
09/24/2019 21:42 CDT	Patient Room	Sleeping
09/24/2019 21:23 CDT	Patient Room	Sleeping
09/24/2019 21:07 CDT	Patient Room	Sleeping
09/24/2019 20:49 CDT	Patient Room	Sleeping
09/24/2019 20:44 CDT	Patient Room	Sleeping
09/24/2019 20:21 CDT	Patient Room	Sleeping
09/24/2019 20:07 CDT	Patient Room	Sleeping
09/24/2019 19:49 CDT	Patient Room	Sleeping
09/24/2019 19:41 CDT	Patient Room	Sleeping
09/24/2019 19:20 CDT	Patient Room	Lying in Bed

11. Subject: 010

Time: 10/02/2019 AT 19:44 – 10/03/2019 AT 06:46

CLINICAL PATIENT INFO		
10/03/2019 06:46 CDT	Patient Room	Sleeping
10/03/2019 06:24 CDT	Patient Room	Sleeping
10/03/2019 06:05 CDT	Patient Room	Sleeping
10/03/2019 05:50 CDT	Patient Room	Sleeping
10/03/2019 05:36 CDT	Patient Room	Sleeping
10/03/2019 05:20 CDT	Patient Room	Sleeping
10/03/2019 05:06 CDT	Patient Room	Sleeping
10/03/2019 04:55 CDT	Patient Room	Sleeping
10/03/2019 04:33 CDT	Patient Room	Sleeping
10/03/2019 04:15 CDT	Patient Room	Sleeping
10/03/2019 04:02 CDT	Patient Room	Sleeping
10/03/2019 03:46 CDT	Patient Room	Sleeping
10/03/2019 03:35 CDT	Patient Room	Sleeping
10/03/2019 03:17 CDT	Patient Room	Sleeping
10/03/2019 03:02 CDT	Patient Room	Sleeping
10/03/2019 02:49 CDT	Patient Room	Sleeping
10/03/2019 02:42 CDT	Patient Room	Sleeping
10/03/2019 02:16 CDT	Patient Room	Sleeping
10/03/2019 02:03 CDT	Patient Room	Sleeping
10/03/2019 01:48 CDT	Patient Room	Sleeping
10/03/2019 01:33 CDT	Patient Room	Sleeping
10/03/2019 01:19 CDT	Patient Room	Sleeping
10/03/2019 01:05 CDT	Patient Room	Sleeping
10/03/2019 00:51 CDT	Patient Room	Sleeping
10/03/2019 00:34 CDT	Patient Room	Sleeping
10/03/2019 00:18 CDT	Patient Room	Sleeping
10/03/2019 00:00 CDT	Patient Room	Sleeping
10/02/2019 23:50 CDT	Patient Room	Sleeping
10/02/2019 23:37 CDT	Patient Room	Sleeping
10/02/2019 23:17 CDT	Patient Room	Sleeping
10/02/2019 23:05 CDT	Patient Room	Sleeping
10/02/2019 22:49 CDT	Patient Room	Sleeping
10/02/2019 22:34 CDT	Patient Room	Sleeping
10/02/2019 22:22 CDT	Patient Room	Sleeping
10/02/2019 22:05 CDT	Patient Room	Sleeping
10/02/2019 21:56 CDT	Patient Room	Sleeping
10/02/2019 21:34 CDT	Patient Room	Sleeping
10/02/2019 21:23 CDT	Patient Room	Lying in Bed
10/02/2019 21:05 CDT	Day/Dining Room	tv
10/02/2019 20:51 CDT	Day/Dining Room	tv
10/02/2019 20:34 CDT	Day/Dining Room	Interacting with othe
10/02/2019 20:17 CDT	Medication Window	Taking Meds
10/02/2019 20:05 CDT	Day/Dining Room	watching tv
10/02/2019 19:51 CDT	Day/Dining Room	watching tv
10/02/2019 19:44 CDT	Day/Dining Room	watching tv

12. Subject: 010

Time: 10/03/2019 AT 19:16 – 10/04/2019 AT 06:16

CLINICAL PATIENT INFO		
10/04/2019 06:16 CDT	Patient Room	Sleeping
10/04/2019 06:00 CDT	Patient Room	Sleeping
10/04/2019 05:45 CDT	Patient Room	Sleeping
10/04/2019 05:33 CDT	Patient Room	Sleeping
10/04/2019 05:20 CDT	Patient Room	Sleeping
10/04/2019 05:08 CDT	Patient Room	Sleeping
10/04/2019 04:47 CDT	Patient Room	Sleeping
10/04/2019 04:38 CDT	Patient Room	Sleeping
10/04/2019 04:17 CDT	Patient Room	Sleeping
10/04/2019 04:01 CDT	Patient Room	Sleeping
10/04/2019 03:45 CDT	Patient Room	Sleeping
10/04/2019 03:34 CDT	Patient Room	Sleeping
10/04/2019 03:16 CDT	Patient Room	Sleeping
10/04/2019 03:03 CDT	Patient Room	Sleeping
10/04/2019 02:49 CDT	Patient Room	Sleeping
10/04/2019 02:41 CDT	Patient Room	Sleeping
10/04/2019 02:16 CDT	Patient Room	Sleeping
10/04/2019 02:02 CDT	Patient Room	Sleeping
10/04/2019 01:46 CDT	Patient Room	Sleeping
10/04/2019 01:30 CDT	Patient Room	Sleeping
10/04/2019 01:16 CDT	Patient Room	Sleeping
10/04/2019 01:04 CDT	Patient Room	Sleeping
10/04/2019 00:47 CDT	Patient Room	Sleeping
10/04/2019 00:38 CDT	Patient Room	Sleeping
10/04/2019 00:23 CDT	Patient Room	Sleeping
10/04/2019 00:03 CDT	Patient Room	Sleeping
10/03/2019 23:59 CDT	Patient Room; Result	Sleeping; Result In
10/03/2019 23:44 CDT	Patient Room	Sleeping
10/03/2019 23:16 CDT	Patient Room	Sleeping
10/03/2019 23:01 CDT	Patient Room	Sleeping
10/03/2019 22:48 CDT	Patient Room	Sleeping
10/03/2019 22:43 CDT	Patient Room	Sleeping
10/03/2019 22:18 CDT	Patient Room	Sleeping
10/03/2019 22:03 CDT	Patient Room	Sleeping
10/03/2019 21:49 CDT	Patient Room	Sleeping
10/03/2019 21:34 CDT	Patient Room	Sleeping
10/03/2019 21:21 CDT	Patient Room	Sleeping
10/03/2019 21:09 CDT	Patient Room	Sleeping
10/03/2019 20:49 CDT	Patient Room	Sleeping
10/03/2019 20:33 CDT	Patient Room	Sleeping
10/03/2019 20:18 CDT	Day/Dining Room	Sitting/Standing
10/03/2019 20:10 CDT	Patient Room	Sitting/Standing
10/03/2019 19:45 CDT	TR	game room
10/03/2019 19:41 CDT	TR	game room
10/03/2019 19:16 CDT	TR	game room

VITA

Nuerzati Resuli received the Bachelor of Science Degree and Master of Science Degree in Electrical Engineering, both from Xi'an Shiyou University. She was a graduate research assistant in the Center for Eldercare and Rehabilitation Technology, in the EECS department at the University of Missouri – Columbia. She has worked on RF sensing and processing methods for noninvasive health monitoring for the patients in psychiatric hospitals and the older adults. The results were published in the BIBM conference. Her research interests include machine learning, RF sensing, wireless communication, and radar signal processing.